Budapest University of Technology and Economics
Faculty of Mechanical Engineering
Department of Applied Mechanics

Parametric analysis of the admissible control-loop delay during balancing

Author: Tamás Balogh

Supervisor: Tamás Insperger

This dissertation is submitted for the degree of Doctor of Philosophy

Budapest, 2024

Contents

List of Figures

List of Tables

Chapter 1

Introduction

Time delays are inherently present in feedback systems due to control-loop latency, and they are considered to be a source of poor performance and instability [55, 101, 22, 75]. Stabilization of unstable plants by means of delayed state feedback is limited by the admissible size of the feedback delay, which is often described by the concept of *delay margin* or *critical delay*. The delay margin is the maximum admissible delay for a fixed combination of control gains for which the system is still stable [32, 111, 100, 67]. For different control gain combinations the delay margin is different. In contrast, the critical delay is the maximum admissible delay without any constraints on the control gains [97, 99, 102, 18]. Therefore, the critical delay is the maximum of the delay margins over the space of control gains.

The critical delay sets strong limitations on stabilizability, which can be demonstrated through the inverted pendulum paradigm. A short pendulum falls faster and, therefore, requires faster control action than a long pendulum. Nevertheless, the feedback delay cannot be reduced arbitrarily due to physical limits. Extending the admissible delay by employing different control laws is, therefore, an important task. The concept of critical delay is spectacularly manifested in human stick balancing. The typical human reaction time is about 230 ms, and human subjects typically cannot balance a stick shorter than 40 cm on their fingertip [26, 79]. Establishing the relation between human reaction time and the shortest stick length can help in understanding the control mechanism behind human balancing [72, 47, 118].

Finding the critical delay for feedback systems is a challenging task. This typically requires the exploration of multidimensional parameter spaces, which can be implemented by numerical optimization techniques, e.g., direct search technique [60], gradient sampling algorithm [23] or particle swarm optimization [92]. A combined

analytical-graphical technique can be applied if the number of tunable parameters is reasonable. Closed-form formulas can usually be derived only for low-order systems [99, 21, 18]. The dissertation aims at generalizing some of the existing concepts and results while keeping the applications in mind.

Time delay and fractional derivatives are both used to model the memory and hereditary properties of materials and processes. In engineering or biological control systems, different sensory inputs require different processing times, which can be modeled by different discrete delays. If the dynamics of the system depend on the values of a time-dependent variable over a finite or infinite time interval, then usually, a distributed delay term appears in the mathematical model. A similar dependency can also be expressed by fractional derivatives of the time-dependent function since they depend on the time history of the function. In this dissertation, different discrete delays and fractional derivatives will be considered.

The inverted pendulum is the simplest unstable system in Newtonian (second-order) dynamics. Many complex dynamical systems that have one unstable manifold can be reduced to the linearized model equation of the inverted pendulum. Stabilization of objects around unstable periodic orbits, control of walking robots and one-wheeled vehicles, or human balancing tasks can be mentioned as examples.

The dissertation consists of seven chapters. Chapter 1 contains the motivation, the goals and the outline of the dissertation.

Chapter 2 demonstrates the concept of stabilizability through the example of the inverted pendulum subject to delayed proportional-derivative feedback of the pendulum angle. Then, stabilizability is discussed in a more general setting that is applicable in the case of retarded, neutral and fractional-order delay differential equation. This chapter also introduces some other concepts and notations that are used throughout the dissertation.

In Chapter 3, general integer-order single-delay single-input systems are investigated. Sufficient and necessary conditions are derived in order to determine the stabilizable delay intervals. These conditions are applied in the case of real-rooted open-loop systems.

In Chapter 4, the effects of acceleration feedback and multiple delays are investigated. The delays are considered to be the sum of a single delay and some delay detunings.

Chapter 5 explores delayed fractional-order feedback with multiple delays. Special attention is given to the connection between the geometry of the stability boundaries and the roots of the characteristic function at the limit of stabilizability.

In Chapter 6, the inverted pendulum is subjected to fractional-order dynamics. Human control action is modeled as fractional-order delayed proportional-derivative feedback, and the corresponding stabilizability limits are derived. The results of virtual stick balancing measurements are compared with theoretical stabilizibility limits. Nonlinear regression is carried out in order to determine the parameters in the feedback model.

Finally, Chapter 7 summarizes the results of the dissertation.

Chapter 2

Theoretical background

In many engineering applications, such as feedback control systems, regenerative machine tool chatter and dynamics of towed elastic wheels [51], the rate of change of the state depends on past values of the state or past values of the rate of change itself. These systems can usually be described by retarded or neutral delay differential equations. Fractional-order differential equations capture another aspect of the memory effect: the rate of change is replaced by a fractional-order derivative that is defined in a non-local manner such that it gives a transition between (local) integer-order derivatives. Fractional-order differential equations are often used to model viscoelastic materials, acoustic wave propagation and biological controls systems [88], just to mention a few.

The theory of delay differential equations [40, 101, 75] and the theory of fractional-order differential equations [88, 33] are well-established in the literature. The combination of these, that is, the theory of fractional-order delay differential equations, has been started to develop only recently. This chapter introduces those concepts and properties that will be used throughout the dissertation. A complete theoretical formulation will not be presented here; however, the key ingredients for the stability and stabilizability analysis of linear feedback systems are included.

2.1 Benchmark problem: the inverted pendulum

Balancing an inverted pendulum in the presence of feedback delay is a frequently cited example in dynamics and control theory [2, 98]. Different control methods are often implemented in simple inverted pendulum systems [39, 116, 93]. The inverted pendulum is also a basic concept in human balancing models [70, 78, 83, 48]. The equation of

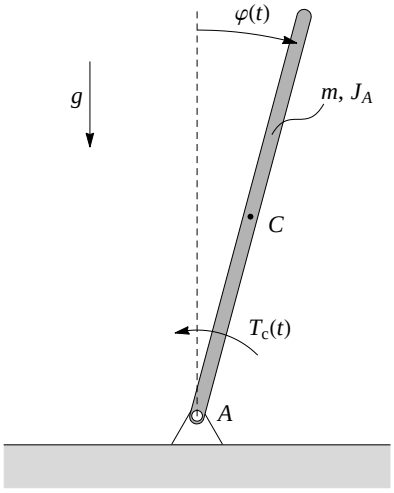

Figure 2.1: Pinned inverted pendulum.

motion of a pinned inverted pendulum subject to torque control (see Figure 2.1) reads

$$J_A\ddot{\varphi}(t) - mgl_{AC}\sin\varphi(t) = -T_{\mathrm{c}}(t)\,, \tag{2.1}$$

where $\varphi(t)$ is the angular displacement of the pendulum measured from the vertically upward position, $\ddot{\varphi}(t)$ is its second derivative, J_A is the moment of inertia about the support axis, m is the mass of the pendulum, g is the gravitational acceleration, l_{AC} is the distance between the support point A and the center of gravity C, and $T_{\mathrm{c}}(t)$ is the control torque. In case of a homogeneous pendulum of length l, $J_A = ml^2/3$ and $l_{AC} = l/2$. After linearization around the upper equilibrium position, the equation of motion can be written as

$$\ddot{\varphi}(t) + a_0\varphi(t) = u(t)\,, \tag{2.2}$$

where $a_0 = -3g/(2l) < 0$ is the plant parameter, and $u(t) = -3T_{\mathrm{c}}(t)/(ml^2)$ is the control action.

In case of a delayed proportional-derivative (PD) controller, $u(t)$ reads

$$u(t) = -b_0\varphi(t-\tau) - b_1\dot{\varphi}(t-\tau)\,, \tag{2.3}$$

where b_0 and b_1 are control gains, and $\tau > 0$ is the closed-loop feedback delay. The characteristic function corresponding to (2.2) and (2.3) is

$$D(s) = s^2 + a_0 + \mathrm{e}^{-s\tau}(b_0 + b_1 s)\,. \tag{2.4}$$

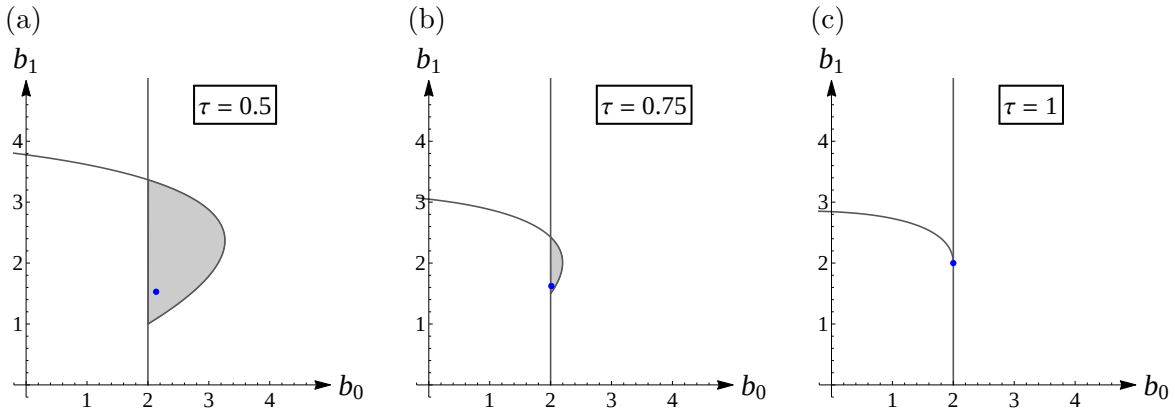

Figure 2.2: Stability charts of (2.4) for different values of τ with $a_0 = -2$.

Note that the open-loop characteristic function $P(s) = s^2 + a_0$ has real roots $\pm\sqrt{-a_0}$ since $a_0 < 0$. This property proves to be useful in Chapter 3.

Stability charts for (2.4) can be determined using the D-subdivision method [86]. Substituting $s = 0$ and $s = \mathrm{i}\omega$ into (2.4) and solving for b_0 and b_1 give the so-called D-curves

$$s = 0 \ : \quad b_0 = -a_0 \ , \quad b_1 \in \mathbb{R} \ , \tag{2.5}$$

$$s = \pm\mathrm{i}\omega, \omega > 0 \ : \quad \begin{cases} b_0 = (\omega^2 - a_0)\cos(\omega\tau) \ , \\ b_1 = \dfrac{(\omega^2 - a_0)\sin(\omega\tau)}{\omega} \ . \end{cases} \tag{2.6}$$

These curves split the parameter plane (b_0, b_1) into domains where the number of unstable roots is constant. The number of unstable roots can be determined, for instance, via root tendency along the D-curves [51], by using the Stépán–Hassard formula [101, 42], or by numerical testing integrals based on the argument principle [112]. Figure 2.2 shows some stability charts. As it can be seen, the stable domain shrinks as the delay is increased. At a critical value τ_{crit}, the stable domain disappears, and the system cannot be stabilized if τ is larger than τ_{crit}.

The critical delay of system (2.4) is well known from the literature [97, 101, 102]:

$$\tau_{\mathrm{crit}} = \sqrt{-\frac{2}{a_0}} \, . \tag{2.7}$$

The trivial solution of system (2.2)–(2.3) can be asymptotically stable if and only if $\tau < \tau_{\mathrm{crit}}$. Next, we will demonstrate that the critical delay (2.7) can be obtained by

studying the multiple roots of the characteristic function $D(s)$.

Assume that $D(s)$ has a real root s_0 with algebraic multiplicity at least $\deg P(s) + 1 = 3$. Then, $D(s_0) = 0$, $D'(s_0) = 0$ and $D''(s_0) = 0$ give the system of equations

$$\left.\begin{aligned} s_0^2 + a_0 + \mathrm{e}^{-s_0\tau}(b_0 + b_1 s_0) &= 0\,, \\ 2s_0 + \mathrm{e}^{-s_0\tau}(-\tau(b_0 + b_1 s_0) + b_1) &= 0\,, \\ 2 + \mathrm{e}^{-s_0\tau}(\tau^2(b_0 + b_1 s_0) - 2\tau b_1) &= 0\,, \end{aligned}\right\} \tag{2.8}$$

which is linear in b_0 and b_1 and nonlinear in s_0 and τ. For a given τ, the solution of (2.8) is

$$\left.\begin{aligned} b_0 &= \mathrm{e}^{s_0\tau}\left(\tau s_0^3 + s_0^2 + a_0\tau s_0 - a_0\right)\,, \\ b_1 &= -\mathrm{e}^{s_0\tau}\left(\tau s_0^2 + 2s_0 + a_0\tau\right)\,, \\ s_0 &= \frac{-2 \pm \sqrt{2 - a_0\tau^2}}{\tau} =: s_{0,\pm}\,. \end{aligned}\right\} \tag{2.9}$$

It can be shown that the triple root $s_{0,+}$ is negative and dominant (rightmost) for every $0 < \tau < \tau_{\mathrm{crit}}$, and therefore system (2.2) with (2.3) is asymptotically stable. Hence, the solution (b_0, b_1) corresponding to $s_{0,+}$ lies inside the stable region (see the blue dots in Figure 2.2). In particular, at the upper bound $\tau = \tau_{\mathrm{crit}}$ the triple root is $s_{0,+} = 0$ and it is the dominant root of (2.4) with control coefficients $b_0 = -a_0$ and $b_1 = -a_0\tau_{\mathrm{crit}}$.

Alternatively, for a given $s_0 = \gamma < 0$, (2.8) can be solved for b_0, b_1 and τ. The smallest positive solution for τ is the critical delay $\tau_{\mathrm{crit}}(\gamma)$ associated with γ-stability. The dominancy of $s_{0,+}$ may be shown by using the argument principle (see, for instance, [17, 19]). In Chapter 3, we use a different method based on an integral representation of the characteristic function.

2.2 Retarded delay differential equations

Let us consider the multiple-input linear time-invariant state equation

$$\dot{\mathbf{x}}(t) = \mathbf{A}\mathbf{x}(t) + \mathbf{B}\mathbf{u}(t)\,, \tag{2.10}$$

where $\mathbf{A} \in \mathbb{R}^{n\times n}$ and $\mathbf{B} \in \mathbb{R}^{n\times m}$ are constant matrices, $\mathbf{x}(t) : \mathbb{R} \mapsto \mathbb{R}^n$ is the state vector and $\mathbf{u}(t) : \mathbb{R} \mapsto \mathbb{R}^m$ is the input (or control) vector. If we apply a multiple-delay state feedback

$$\mathbf{u}(t) = \sum_{i=1}^{r} \mathbf{K}_i \mathbf{x}(t - \tau_i) \tag{2.11}$$

with $\mathbf{K}_i \in \mathbb{R}^{m\times n}$ and $\tau_i > 0$, then we obtain a retarded delay differential equation of the form

$$\dot{\mathbf{x}}(t) = \mathbf{A}\mathbf{x}(t) + \sum_{i=1}^{r} \mathbf{B}\mathbf{K}_i\mathbf{x}(t-\tau_i)\,. \tag{2.12}$$

The matrices $\mathbf{K}_i$ contain the control parameters that are used to achieve the desired dynamics.

Stability of (2.12) can be assessed by investigating its characteristic function

$$D(s) = \det\Big(s\mathbf{I} - \mathbf{A} - \sum_{i=1}^{r} \mathbf{B}\mathbf{K}_i \mathrm{e}^{-s\tau_i}\Big)\,. \tag{2.13}$$

The trivial solution of (2.12) is exponentially stable if and only if all the roots of $D(s)$ have negative real part [75]. In general, (2.13) takes the form

$$D(s) = s^n + d_{n-1}(s)s^{n-1} + ... + d_0(s)\,, \tag{2.14}$$

where each function $d_k(s)$ is a polynomial in $\mathrm{e}^{-s\tau_i}$, $i = 1, 2, ..., r$ [42].

However, if (2.10) is a single-input state equation with $m = 1$, $\mathbf{B} \in \mathbb{R}^{n\times 1}$ and $\mathbf{u}(t) : \mathbb{R} \mapsto \mathbb{R}$ and we apply a single-delay state feedback $\mathbf{u}(t) = \mathbf{K}\mathbf{x}(t-\tau)$ with $\mathbf{K} \in \mathbb{R}^{1\times n}$, then (2.13) can be simplified using the matrix determinant lemma [44, 109] as

$$\begin{aligned} D(s) &= \det\Big(s\mathbf{I} - \mathbf{A} - \mathbf{B}\mathbf{K}\mathrm{e}^{-s\tau}\Big) \\ &= \det\left(s\mathbf{I} - \mathbf{A}\right) - \mathbf{K}\,\mathrm{adj}(s\mathbf{I} - \mathbf{A})\mathbf{B}\mathrm{e}^{-s\tau} \\ &= P(s) + Q(s)\mathrm{e}^{-s\tau}\,, \end{aligned} \tag{2.15}$$

where

$$\begin{aligned} P(s) &= a_n s^n + a_{n-1}s^{n-1} + ... + a_0\,, \\ Q(s) &= b_{n-1}s^{n-1} + b_{n-2}s^{n-2} + ... + b_0 \end{aligned} \tag{2.16}$$

and $a_n = 1$. Furthermore, if the pair $(\mathbf{A}, \mathbf{B})$ is controllable, then the coefficients b_k in $Q(s)$ can be adjusted independently using the feedback matrix $\mathbf{K}$. Characteristic functions of the form (2.15)–(2.16) will be analyzed in Chapter 3.

2.2.1 The concept of stabilizability

With delayed feedback stabilization (2.10)–(2.11) in mind, we may define stabilizability in a more general setting. For any system $\mathcal{S}$ with a real parameter vector $\mathbf{p} \in \mathbb{R}^n$, we may divide $\mathbf{p}$ into system parameters $\mathbf{p}_\mathrm{s} \in \mathbb{R}^{n_\mathrm{s}}$ and control parameters $\mathbf{p}_\mathrm{c} \in \mathbb{R}^{n_\mathrm{c}}$ with

$n = n_\mathrm{s} + n_\mathrm{c}$. With any notion of stability, $\mathcal{S}(\mathbf{p}_\mathrm{s}, \mathbf{p}_\mathrm{c})$ is said to be stabilizable for a given $\mathbf{p}_\mathrm{s}$ if there exist control parameters $\mathbf{p}_\mathrm{c}$ such that $\mathcal{S}(\mathbf{p}_\mathrm{s}, \mathbf{p}_\mathrm{c})$ is stable.

The stable region of $\mathcal{S}$ is a subset of the n-dimensional space $\mathbb{R}^n$, while the stabilizable region is a subset of $\mathbb{R}^{n_\mathrm{s}}$. In fact, if we project the stable region onto the space of the system parameters, we obtain precisely the stabilizable region. This gives the geometric interpretation of stabilizability.

We may also fix some of the system parameters during the analysis and divide $\mathbf{p}_\mathrm{s}$ further into $\widetilde{\mathbf{p}}_\mathrm{s} \in \mathbb{R}^{\widetilde{n}_\mathrm{s}}$ and $\mathbf{p}_\mathrm{s,f} \in \mathbb{R}^{n_\mathrm{s,f}}$ with $n_\mathrm{s} = \widetilde{n}_\mathrm{s} + n_\mathrm{s,f}$. In this case, the stabilizable region of $\mathcal{S}(\widetilde{\mathbf{p}}_\mathrm{s}, \mathbf{p}_\mathrm{c}; \mathbf{p}_\mathrm{s,f})$ can be given while the fixed parameter vector $\mathbf{p}_\mathrm{s,f}$ is held constant. These stabilizable regions are cross-sections of the stabilizable region of $\mathcal{S}(\mathbf{p}_\mathrm{s}, \mathbf{p}_\mathrm{c})$.

On the other hand, the fixed parameter vector can also consist of some of the control parameters $\mathbf{p}_\mathrm{c}$, that is, $\widetilde{\mathbf{p}}_\mathrm{c} \in \mathbb{R}^{\widetilde{n}_\mathrm{c}}$ and $\mathbf{p}_\mathrm{c,f} \in \mathbb{R}^{n_\mathrm{c,f}}$ with $n_\mathrm{c} = \widetilde{n}_\mathrm{c} + n_\mathrm{c,f}$. In this case, we can determine the stabilizable region of $\mathcal{S}(\mathbf{p}_\mathrm{s}, \mathbf{p}_\mathrm{c})$ by taking the union of the stabilizable regions of $\mathcal{S}(\mathbf{p}_\mathrm{s}, \widetilde{\mathbf{p}}_\mathrm{c}; \mathbf{p}_\mathrm{c,f})$ for all possible values of $\mathbf{p}_\mathrm{c,f}$.

In this dissertation, delays are considered system parameters in Chapter 3 and Chapter 6, but they can also be considered control parameters as in Chapter 4 and Chapter 5. In the example of Section 2.1, $\widetilde{\mathbf{p}}_\mathrm{s} = (\tau)$, $\mathbf{p}_\mathrm{s,f} = (a_0)$ and $\mathbf{p}_\mathrm{c} = (b_0, b_1)$, and the upper endpoint of the single stablizable interval is τ_crit.

2.2.2 Multiplicity of characteristic roots

Assume that the stable region is bounded by a (continuously differentiable) function $g(\mathbf{p}_\mathrm{s}, \mathbf{p}_\mathrm{c}) = 0$ and there is only a single control parameter. Figure 2.3 illustrates the projection of the stable region onto the plane of the system parameters if $\mathbf{p}_\mathrm{s} = (p_1, p_2)$ and $\mathbf{p}_\mathrm{c} = (p_3)$. In this case, projections of vertical cross-sections are line segments on the plane (p_1, p_2). As can be seen in Figure 2.3, the partial derivative $\partial g/\partial p_3$ is zero at the points that project to the endpoints of these line segments. Therefore, $\partial g/\partial p_3 = 0$ holds along with $g = 0$ at the boundary of the stabilizable region.

In general, the stabilizable region may be constructed by successive projections. Let $\mathbf{a} \in \mathbb{R}^{n_1}$, $\mathbf{b} \in \mathbb{R}^{n_2}$ and $\mathbf{c} \in \mathbb{R}^{n_3}$. If a region in the space of $\mathbf{a}$ and $\mathbf{b}$ is bounded by a continuously differentiable $\mathbf{g}(\mathbf{a}, \mathbf{b}, \mathbf{c}) = \mathbf{0}$ with $\mathbf{g} : \mathbb{R}^{n_1+n_2+n_3} \mapsto \mathbb{R}^{n_3+1}$, then conditions of the form $\det(\mathbf{J}_{\mathbf{g},(b_i,\mathbf{c})}) = 0$ appear at the boundary of the projection of that region to the space of $\mathbf{a}$. Here, $\mathbf{J}_{\mathbf{g},(b_i,\mathbf{c})}$ denotes the Jacobian matrix of $\mathbf{g}$ with respect to $(b_i, \mathbf{c})$, and b_i is the ith element in the parameter vector $\mathbf{b}$.

In the case of time-delay systems of the form (2.13), the stable region can be

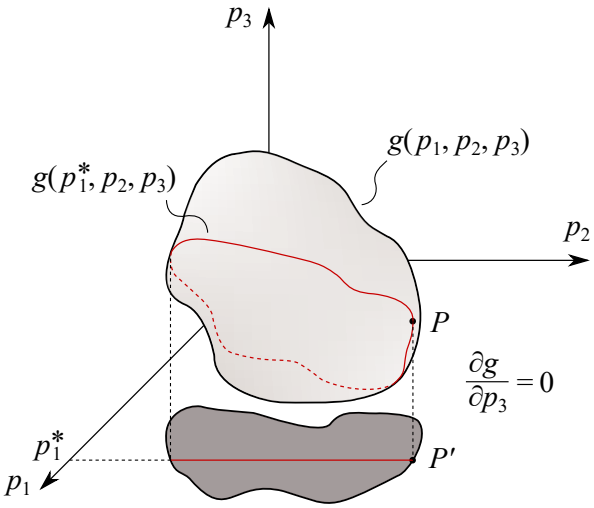

Figure 2.3: Projection of a stable region onto the plane of system parameters (p_1, p_2). The boundary of a cross-section for a fixed p_1 is shown by red line. At the boundary of the projection, $\partial g/\partial p_3 = 0$.

bounded by two different types of stability boundaries according to D-subdivision. At the connections of the boundaries $D(0; \mathbf{p})$ and $D(\mathrm{i}\omega; \mathbf{p})$, the stable region has edges where the boundary is not differentiable. These kinds of edges (or vertices) usually project to the boundary of the stablilizable region, and they correspond to purely imaginary characteristic roots (including the zero root) with higher algebraic multiplicity. However, turning points satisfying equations of the form $\det(\mathbf{J}) = 0$ were also observed in [75].

Even though the characteristic function (2.13) has infinitely many roots, the number of real spectral values (and hence the multiplicity of zero) is limited by the Pólya–Szegő bound [90]. We may rewrite (2.14) as

$$D(s) = \sum_{i=1}^{M} p_i(s) \mathrm{e}^{-\vartheta_i s}, \tag{2.17}$$

where $\vartheta_1 < \vartheta_2 < \ldots < \vartheta_M$ are real numbers, $p_i(s)$ are polynomials of degree n_i, $p_1(s)$ and $p_M(s)$ are not identically zero and $\sum_{i=1}^{M} n_i = N$. Then, the upper bound for the number of real roots of (2.17) is $N + M - 1$, which is equal to the degree of the quasipolynomial (2.17). This is a sharp bound, which can be reached if $p_i(s)$ are general polynomials with arbitrary coefficients. However, if they are polynomials with constraints on the coefficients (such as sparse polynomials with some coefficients equal to zero), then it may not be possible to reach the Pólya–Szegő bound [16].

The characteristic root with the largest real part is usually called the *dominant root* or rightmost root. For some classes of time-delay systems, a real root with maximal multiplicity is necessarily dominant. This so-called *multiplicity-induced dominancy* (MID) was observed and proved in several recent works for low-order time-delay systems [21, 18].

2.2.3 Spectral abscissa and γ-stabilizabilty

The real part of the dominant root is the spectral abscissa, which gives the exponential decay rate of the time-domain solutions. Therefore, if we want to achieve faster-decaying solutions (and better performance), we need to minimize the spectral abscissa with respect to some control parameters. In order to do so, we may consider γ-*stability* instead of stability: a system is said to be γ-stable if the roots of its characteristic equation have real parts smaller than γ. We can also define γ-*stabilizability* following the general concept of Subsection 2.2.1. Then, the system parameters $\mathbf{p}_\mathrm{s}$ are at the boundary of the γ-stabilizable region if and only if the minimum of the spectral abscissa is γ with respect to the control parameters $\mathbf{p}_\mathrm{c}$. Consider the single-input single-delay system (2.15) with varying $\mathbf{K}$ and fixed $\mathbf{A}$, $\mathbf{B}$ and τ. If the spectral abscissa has a local minimum for $\mathbf{K} = \mathbf{K}_0$ and the minimum value is γ_0, then (2.15) has at least $n+1$ characteristic roots with real part equal to γ_0 for $\mathbf{K} = \mathbf{K}_0$ [75].

There is a connection between multiple characteristic roots and the minimum of the spectral abscissa even in the case of delay-free systems. In [37], the damped harmonic oscillator $D(s) = \det\Big(\mathbf{M}s^2 + \mathbf{D}s + \mathbf{S}\Big)$ with n-by-n real symmetric matrices was investigated if $\mathbf{M}$ and $\mathbf{S}$ are positive definite. The matrices $\mathbf{M}$ and $\mathbf{S}$ were considered system parameters and the damping matrix $\mathbf{D}$ was considered control parameter, and it was shown that the spectral abscissa attains its minimum if $D(s)$ has a real root with (algebraic) multiplicity $2n$.

2.3 Neutral delay differential equations

If we consider the state equation (2.10) and apply a multiple-delay state and state derivative feedback

$$\mathbf{u}(t) = \sum_{i=1}^{r} \mathbf{K}_i \mathbf{x}(t-\tau_i) + \sum_{i=1}^{r} \mathbf{L}_i \dot{\mathbf{x}}(t-\tau_i) \tag{2.18}$$

with $\mathbf{K}_i, \mathbf{L}_i \in \mathbb{R}^{m\times n}$ and $\tau_i > 0$, then we obtain a neutral delay differential equation of the form

$$\dot{\mathbf{x}}(t) - \sum_{i=1}^{r} \mathbf{B}\mathbf{L}_i \dot{\mathbf{x}}(t-\tau_i) = \mathbf{A}\mathbf{x}(t) + \sum_{i=1}^{r} \mathbf{B}\mathbf{K}_i \mathbf{x}(t-\tau_i)\,. \tag{2.19}$$

The characteristic function of (2.19) can be written as

$$D(s) = \det\Big(s\Big(\mathbf{I} - \sum_{i=1}^{r} \mathbf{B}\mathbf{L}_i \mathrm{e}^{-s\tau_i}\Big) - \mathbf{A} - \sum_{i=1}^{r} \mathbf{B}\mathbf{K}_i \mathrm{e}^{-s\tau_i}\Big)\,. \tag{2.20}$$

The trivial solution of (2.19) is exponentially stable if and only if all the roots of $D(s)$ have negative real part and are bounded away from the imaginary axis [75]. The latter condition means that there are no chains of roots asymptotic to the imaginary axis. In general, (2.20) takes the form

$$D(s) = d_n(s)s^n + d_{n-1}(s)s^{n-1} + ... + d_0(s)\,, \tag{2.21}$$

where each function $d_k(s)$ is a polynomial in $\mathrm{e}^{-s\tau_i}$, $i = 1, 2, ..., r$. Note that (2.21) is almost identical to (2.14), but in this case $d_n(s) \not\equiv 1$.

Let $\mathbf{H}_i = \mathbf{B}\mathbf{L}_i$. Then, the delay-difference equation associated with (2.19) is

$$\mathbf{x}(t) - \sum_{i=1}^{r} \mathbf{H}_i \mathbf{x}(t-\tau_i) = \mathbf{0}\,. \tag{2.22}$$

The exponential stability of the trivial solution of (2.22) is a necessary condition for the exponential stability of the trivial solution of (2.19) [75].

Exponential stability of (2.22) may be sensitive to small delay perturbations. The trivial solution of (2.22) is said to be *strongly exponentially stable* if it remains exponentially stable when subjected to small variations in the delays [41, 75]. Let us define

$$\rho_0 = \max_{\theta_j \in [0,2\pi]} \rho\Big(\sum_{j=1}^{r} \mathbf{H}_j \mathrm{e}^{\mathrm{i}\theta_j}\Big)\,, \tag{2.23}$$

where $\rho(\mathbf{X})$ is the spectral radius of $\mathbf{X}$. Then, (2.22) is strongly exponentially stable if and only if $\rho_0 < 1$. If $\rho_0 > 1$, then the neutral delay differential equation (2.19) may be exponentially stable, but exponential stability is lost in case of infinitesimal perturbations of the delays [75]. If there is only a single nonzero matrix $\mathbf{H}_i$ in the delay-difference equation (2.22), then strong exponential stability and exponential stability of (2.22) coincide.

An example for neutral delay differential equations is

$$\ddot{\varphi}(t) + a_0\varphi(t) = -b_0\varphi(t-\tau) - b_1\dot{\varphi}(t-\tau) - b_2\ddot{\varphi}(t-\tau)\,, \tag{2.24}$$

which is a model for the inverted pendulum subject to delayed proportional-derivative-acceleration (PDA) feedback. We may rewrite (2.24) in the form of (2.19) as

$$\begin{bmatrix}\dot{x}_1(t)\\ \dot{x}_2(t)\end{bmatrix} - \begin{bmatrix}0\\1\end{bmatrix}\begin{bmatrix}0 & -b_2\end{bmatrix}\begin{bmatrix}\dot{x}_1(t-\tau)\\ \dot{x}_2(t-\tau)\end{bmatrix} = \begin{bmatrix}0 & 1\\ -a_0 & 0\end{bmatrix}\begin{bmatrix}x_1(t)\\ x_2(t)\end{bmatrix} + \begin{bmatrix}0\\1\end{bmatrix}\begin{bmatrix}-b_0 & -b_1\end{bmatrix}\begin{bmatrix}x_1(t-\tau)\\ x_2(t-\tau)\end{bmatrix} \tag{2.25}$$

with $x_1(t) = \varphi(t)$ and $x_2(t) = \dot{\varphi}(t)$. The associated delay-difference equation reads

$$\begin{bmatrix}x_1(t)\\ x_2(t)\end{bmatrix} - \begin{bmatrix}0 & 0\\ 0 & -b_2\end{bmatrix}\begin{bmatrix}x_1(t-\tau)\\ x_2(t-\tau)\end{bmatrix} = \begin{bmatrix}0\\0\end{bmatrix}, \tag{2.26}$$

which is exponentially stable if and only if $|b_2| < 1$. Hence, $|b_2| < 1$ is a necessary condition for the stability of (2.24).

2.4 Fractional-order systems

There are many different definitions for the fractional derivative based on different generalizations of integer-order differentiation and integration. In this dissertation, we usually apply the Caputo fractional derivative defined as

$${}_{t_0}^{t}D_*^{\alpha} f(t) = \frac{1}{\Gamma(\nu-\alpha)}\int_{t_0}^{t}(t-\vartheta)^{\nu-\alpha-1} f^{(\nu)}(\vartheta)\mathrm{d}\vartheta, \quad \nu-1<\alpha<\nu\in\mathbb{N}^+\,, \tag{2.27}$$

where $\Gamma(\cdot)$ is the gamma function, t_0 is the lower limit of the fractional derivative and α is the (noninteger) order [88]. The integer-order limiting cases are

$$\lim_{\alpha\to\nu} {}_{t_0}^{t}D_*^{\alpha} f(t) = f^{(\nu)}(t) \tag{2.28}$$

and

$$\lim_{\alpha\to\nu-1} {}_{t_0}^{t}D_*^{\alpha} f(t) = f^{(\nu-1)}(t) - f^{(\nu-1)}(t_0)\,. \tag{2.29}$$

The lower limit t_0 is usually chosen to be $t_0 = 0$. If we take the Laplace transform

of (2.27) with $t_0 = 0$, then we obtain

$$\mathcal{L}\left({}_0^t D_*^\alpha f(t)\right) = s^\alpha F(s) - \sum_{k=0}^{\nu-1} s^{\alpha-k-1} f^{(k)}(0)\,, \tag{2.30}$$

where $F(s)$ is the Laplace transform of $f(t)$ [88]. Fractional-order differential equations based on the Caputo fractional derivative require integer-order initial values, which can be easily determined using the measured values of physical variables. Moreover, the Caputo fractional derivative of a constant is equal to zero. These properties make this definition favorable in many applications [33].

Other commonly used definitions are the Riemann–Liouville fractional derivative and the Grünwald–Letnikov fractional derivative [88]. The Grünwald–Letnikov fractional derivative is defined as

$${}_{t_0}^t\mathfrak{D}^\alpha x(t) = \lim_{h\to 0} \frac{1}{h^\alpha} \sum_{k=0}^{\frac{t-t_0}{h}} w_k^\alpha x(t-kh)\,, \tag{2.31}$$

where $\alpha \geq 0$, the limit is taken such that $(t-t_0)/h$ is an integer, and the weights in the sum are related to the (generalized) binomial coefficients

$$w_k^\alpha = (-1)^k \binom{\alpha}{k} = (-1)^k \frac{\Gamma(\alpha+1)}{k!\Gamma(\alpha-k+1)}\,. \tag{2.32}$$

These weights can also be obtained by the recurrence relation

$$w_0^\alpha = 1\,, \tag{2.33}$$

$$w_k^\alpha = \left(1 - \frac{\alpha+1}{k}\right) w_{k-1}^\alpha\,, \quad k > 0\,. \tag{2.34}$$

This formulation can easily be combined with other discretization techniques. Therefore, the Grünwald–Letnikov fractional derivative will be used for numerical calculations in this dissertation.

2.4.1 Fractional-order state equation with delayed feedback

Let us consider the multiple-input linear time-invariant state equation of fractional-order

$${}_{t_0}^t D_*^\alpha \mathbf{x}(t) = \mathbf{A}\mathbf{x}(t) + \mathbf{B}\mathbf{u}(t)\,, \tag{2.35}$$

where $\mathbf{A} \in \mathbb{R}^{n\times n}$ and $\mathbf{B} \in \mathbb{R}^{n\times m}$ are constant matrices, $\mathbf{x}(t) : \mathbb{R} \mapsto \mathbb{R}^n$ is the state vector, $\mathbf{u}(t) : \mathbb{R} \mapsto \mathbb{R}^m$ is the input (or control) vector and $0 < \alpha \leq 1$. Applying the multiple-delay state feedback (2.11), we obtain a retarded fractional-order delay differential equation of the form

$$ {}_{t_0}^{t}D_*^{\alpha}\mathbf{x}(t) = \mathbf{A}\mathbf{x}(t) + \sum_{i=1}^{r} \mathbf{B}\mathbf{K}_i\mathbf{x}(t-\tau_i)\,. \tag{2.36} $$

Consider the scalar fractional-order differential equation

$$ {}_{t_0}^{t}D_*^{\alpha_k}x(t) = f\big(t,\, {}_{t_0}^{t}D_*^{\alpha_1}x(t),\, {}_{t_0}^{t}D_*^{\alpha_2}x(t), \dots,\, {}_{t_0}^{t}D_*^{\alpha_{k-1}}x(t)\big) \tag{2.37} $$

of Caputo type with rational derivative orders $0 \leq \alpha_1 < \alpha_2 < \dots < \alpha_k$. By defining $x_1(t) = x(t)$, (2.37) can be written in the form of a system of fractional-order differential equations of order α as

$$ \begin{aligned} {}_{t_0}^{t}D_*^{\alpha}x_1(t) &= x_2(t)\,, \\ {}_{t_0}^{t}D_*^{\alpha}x_2(t) &= x_3(t)\,, \\ &\vdots \\ {}_{t_0}^{t}D_*^{\alpha}x_{n-1}(t) &= x_n(t)\,, \\ {}_{t_0}^{t}D_*^{\alpha}x_n(t) &= f\big(t, x_{\frac{\alpha_1}{\alpha}+1}(t), x_{\frac{\alpha_2}{\alpha}+1}(t), \dots, x_{\frac{\alpha_{k-1}}{\alpha}+1}(t)\big)\,, \end{aligned} \tag{2.38} $$

where $\alpha = 1/q$, $n = q\alpha_k$ and q is the least common multiple of the denominators of α_i [33]. This shows that the elements of the state vector $\mathbf{x}(t)$ are usually fractional derivatives of a scalar function $x(t)$. Therefore, the delayed state feedback can also contain fractional derivatives in equation (2.36).

2.4.2 Stability of fractional-order differential equations

The characteristic function of (2.36) can be written as

$$ D(s) = \det\left(s^{\alpha}\,\mathbf{I} - \mathbf{A} - \sum_{i=1}^{r} \mathbf{B}\mathbf{K}_i \mathrm{e}^{-s\tau_i}\right) \tag{2.39} $$

and takes the form

$$ D(s) = s^{n\alpha} + d_{n-1}(s)s^{(n-1)\alpha} + \dots + d_0(s)\,, \tag{2.40} $$

where each function $d_k(s)$ is a polynomial in $\mathrm{e}^{-s\tau_i}$, $i = 1, 2, \ldots, r$. In (2.39), s^α indicates the principle value of the complex power function, that is, we consider the first Riemann sheet with a branch cut along the negative real axis. The exact relations between the roots of (2.39) and the asymptotic stability of the trivial solution of (2.36) is still not known in the general case; however, some recent results are available for the following special cases.

If $\mathbf{B} = \mathbf{0}$ and $t_0 = 0$ in (2.35), then (2.36) takes the form

$$ {}_0^t D_*^\alpha \mathbf{x}(t) = \mathbf{A}\mathbf{x}(t)\,. \tag{2.41} $$

The trivial solution of (2.41) is asymptotically stable if and only if $|\arg(\lambda_i)| > \alpha\pi/2$, $i = 1, 2, \ldots, n$, where λ_i denotes the eigenvalues of $\mathbf{A}$ [69]. These eigenvalues correspond to the characteristic function (2.39) with $\mathbf{B} = \mathbf{0}$ and $\lambda = s^\alpha$. If we consider directly the roots s_i of (2.39) with $\mathbf{B} = \mathbf{0}$, then asymptotic stability holds if and only if s_i have negative real parts [82]. The solutions of (2.41) can be expressed in terms of the one-parameter Mittag-Leffler function. In the case of asymptotic stability, the solutions decay towards 0 like a power function if $\alpha \neq 1$: $|\mathbf{x}(t)| \sim c\,t^{-\alpha}$ as $t \to \infty$, where c is a positive real constant [69, 33].

The equation

$$ {}_0^t D_*^\alpha \mathbf{x}(t) = \mathbf{A}\mathbf{x}(t-\tau) \tag{2.42} $$

with a single delay (and without a delay-free term on the right-hand side) was considered in [28]. It was found that, for any $\alpha > 0$, the trivial solution is asymptotically stable if and only if the characteristic function of (2.42) has roots with negative real parts only. The same authors investigated the scalar equation

$$ {}_0^t D_*^\alpha x(t) = ax(t) + bx(t-\tau) \tag{2.43} $$

with $0 < \alpha < 1$ [27] and $1 < \alpha < 2$ [29]. In both cases, asymptotic stability holds if and only if the corresponding characteristic function has roots with negative real parts only.

We may also consider bounded-input bounded-output (BIBO) stability of fractional-order time-delay systems of the form

$$ {}_{t_0}^t D_*^\alpha \mathbf{x}(t) = \mathbf{A}\mathbf{x}(t) + \sum_{i=1}^{r} \mathbf{B}\mathbf{K}_i \mathbf{e}(t-\tau_i) \tag{2.44} $$

with an error signal $\mathbf{e}(t) = \mathbf{x}(t) - \mathbf{u}_\mathrm{r}(t)$, where $\mathbf{u}_\mathrm{r}(t)$ is the reference input.

If (2.44) is a single-input system with a controllable pair $(\mathbf{A}, \mathbf{B})$ and $\alpha = 1/q$, $q \in \mathbb{Z}^+$, then it can be written in controllable canonical form such that

$$\mathbf{x}(t) = \left[x(t) \quad {}_{t_0}^{t}D_*^{\alpha} x(t) \quad \dots \quad {}_{t_0}^{t}D_*^{(n-1)\alpha} x(t) \right]^T . \tag{2.45}$$

In accordance with (2.45), let the reference input be

$$\mathbf{u}_{\mathrm{r}}(t) = \left[u_{\mathrm{r}}(t) \quad {}_{t_0}^{t}D_*^{\alpha} u_{\mathrm{r}}(t) \quad \dots \quad {}_{t_0}^{t}D_*^{(n-1)\alpha} u_{\mathrm{r}}(t) \right]^T . \tag{2.46}$$

In this case, (2.44) reduces to a scalar differential equation for $x(t)$ and $u_{\mathrm{r}}(t)$, and the corresponding transfer function has the form

$$\frac{X(s)}{U_{\mathrm{r}}(s)} = \frac{\sum_{i=0}^{r_2} q_i(s) \mathrm{e}^{-\eta_i s}}{\sum_{i=0}^{r_1} p_i(s) \mathrm{e}^{-\vartheta_i s}} , \tag{2.47}$$

where $0 = \vartheta_0 < \vartheta_1 < ... < \vartheta_{r_1}$, $0 \leq \eta_0 < \eta_1 < ... < \eta_{r_2}$, $p_i(s) = \sum_{k=0}^{l_i} c_{i,k} s^{\alpha_{i,k}}$, $\alpha_{i,k} \geq 0$, $q_i(s) = \sum_{k=0}^{m_i} d_{i,k} s^{\beta_{i,k}}$, $\beta_{i,k} \geq 0$ with $\deg p_0 > \deg p_i$, $i = 1, \dots, r_1$ and $\deg p_0 > \deg q_i$, $i = 0, \dots, r_2$. It was shown in [12] that systems with transfer function (2.47) are BIBO stable if and only if (2.47) has no poles in the closed right half of the complex plane. Note that, under the same conditions, the denominator of (2.47) is equal to the characteristic function (2.39).

An example for fractional-order delay differential equations is

$$\ddot{\varphi}(t) + a_0 \varphi(t) = -b_0 e(t-\tau) - b_1 \, {}_{t_0}^{t}D_*^{\mu} e(t-\tau) , \tag{2.48}$$

which is a model for the inverted pendulum subject to delayed fractional-order proportional-derivative (PD^{μ}) feedback with $e(t) = \varphi(t) - u_{\mathrm{r}}(t)$. Stability of (2.48) will be analyzed in Chapter 5.

Chapter 3

Conditions for stabilizability of time-delay systems

In this chapter, we analyze the general nth-order single-input linear time-invariant dynamical system with a single delay. Relying on the multiplicity-induced dominancy (MID) property, we propose a unified methodology to assess the critical delay associated with γ-stabilizability based on the integral representation of quasipolynomials as in the works [21, 17, 20]. Furthermore, we extend the idea of [18] to nth-order setting in exploiting the root location of the open-loop characteristic polynomial in order to have the MID property of the overall system. In particular, we analyze real-rooted open-loop systems. Such systems arise in many biological applications. Trivial cases are given by first-order scalar systems, for example, in the description of the control of blood cell dynamics [68], the pupil light reflex [66] or simple models of human postural sway [34]. Real-rooted systems typically arise when a mechanical system is set to its completely unstable position, that is, the number of unstable characteristic roots is N for an N-degree-of-freedom system. Human balancing can be mentioned as example, where single, double or even multiple-link inverted pendulum models are used to describe human standing, walking or running [77, 103, 83, 119]. Balancing on rolling or pinned balance board is another example where the governing equation resembles that of a double inverted pendulum [30, 81]. The ball-and-beam balancing task can also be mentioned as a special case: actually $s = 0$ is a double root of the open-loops system [24].

The chapter is organized as follows. The problem is stated in Section 3.1. Section 3.2 collects some preliminary results. Subsection 3.2.1 provides the main ingredient of the dominancy proof, which consists in writing a quasipolynomial function

with a multiple ($(n+1)$-fold) real root as an integral operator. Subsection 3.2.2 gives a similar result for an at least n-fold real root. Subsection 3.2.3 reviews a necessary condition for γ-stabilizability. In Section 3.3, sufficient conditions for the dominancy of a multiple real root and necessary conditions for γ-stabilizability are provided for real-rooted plants. The results are illustrated through the stabilization of an N-link inverted pendulum in Section 3.4.

3.1 Problem statement

We consider delayed feedback systems whose characteristic function is a quasipolynomial of the form

$$D(s) = P(s) + \mathrm{e}^{-s\tau}Q(s)\,, \tag{3.1}$$

where $\tau > 0$, and the degrees of polynomials $P(s)$ and $Q(s)$ are n and $n-1$, respectively:

$$\begin{aligned} P(s) &= a_n s^n + a_{n-1}s^{n-1} + ... + a_0\,, \\ Q(s) &= b_{n-1}s^{n-1} + b_{n-2}s^{n-2} + ... + b_0\,. \end{aligned} \tag{3.2}$$

Assume that the plant parameters a_i are known and fixed such that $a_n > 0$. Furthermore, assume that coefficients b_i in $Q(s)$ can be considered as independently adjustable control parameters. The problem we are focusing on can be summarized as follows: for what values of τ is system (3.1) γ-stabilizable (i.e., there exist $b_i(a_0, a_1, ..., a_n, \tau)$, $i = 0, 1, ..., n-1$ for which the real parts of all roots of (3.1) are less than γ for some given γ). To give a sufficient condition for γ-stabilizability, we utilize the MID property: the control parameters b_i are tuned in a way that the characteristic function $D(s)$ has a real root s_0 with multiplicity $n+1$.

3.2 Preliminary results for arbitrary plants

In this section, some preliminary results are discussed for arbitrary plants without restriction to real-rootedness. First, factorization and a sufficient condition for dominancy are derived in the case of a real spectral value with multiplicity at least n and, similarly, with multiplicity at least $n+1$. Then, a necessary condition for stabilizability is given.

3.2.1 Factorization and a sufficient condition for dominancy

Let us define the family of polynomials $R_k(s;\tau)$ as

$$R_k(s;\tau) = \sum_{i=0}^{k} \binom{k}{i} P^{(i)}(s)\tau^{k-i},\ k \in \mathbb{Z}_0^+ . \tag{3.3}$$

Using this notation, we have the following result.

Proposition 3.1. *If the quasipolynomial* (3.1) *has a real root* s_0 *with multiplicity at least* n*, then it can be written as*

$$D(s) = (s-s_0)^n \left(a_n + \int_0^1 \mathrm{e}^{-(s-s_0)\tau t} \frac{\tau R_{n-1}(s_0;\tau t)}{(n-1)!} \mathrm{d}t \right) . \tag{3.4}$$

Proof. The quasipolynomial $D(s)$ has a root s_0 with algebraic multiplicity at least n if and only if $D^{(k)}(s_0) = 0$, $k = 0, 1, ..., n-1$:

$$\left.\begin{aligned} P(s_0) + \mathrm{e}^{-s_0\tau} Q(s_0) &= 0 , \\ P'(s_0) + \mathrm{e}^{-s_0\tau} \left((-\tau) Q(s_0) + Q'(s_0) \right) &= 0 , \\ &\vdots \\ P^{(k)}(s_0) + \mathrm{e}^{-s_0\tau} \sum_{i=0}^{k} \binom{k}{i} Q^{(i)}(s_0)(-\tau)^{k-i} &= 0 , \\ &\vdots \\ P^{(n-1)}(s_0) + \mathrm{e}^{-s_0\tau} \sum_{i=0}^{n-1} \binom{n-1}{i} Q^{(i)}(s_0)(-\tau)^{n-1-i} &= 0 . \end{aligned}\right\} \tag{3.5}$$

Equation (3.5) gives a linear system of equations for the control coefficients. Solving (3.5) for b_i enables the integral factorization of the form (3.4). The system of equations (3.5) is equivalent to the following system of equations:

$$\left.\begin{aligned} \mathrm{e}^{s_0\tau} P(s_0) + Q(s_0) &= 0 , \\ \mathrm{e}^{s_0\tau} \left(\tau P(s_0) + P'(s_0) \right) + Q'(s_0) &= 0 , \\ &\vdots \\ \mathrm{e}^{s_0\tau} \sum_{i=0}^{k} \binom{k}{i} P^{(i)}(s_0)\tau^{k-i} + Q^{(k)}(s_0) &= 0 , \\ &\vdots \\ \mathrm{e}^{s_0\tau} \sum_{i=0}^{n-1} \binom{n-1}{i} P^{(i)}(s_0)\tau^{n-1-i} + Q^{(n-1)}(s_0) &= 0 . \end{aligned}\right\} \tag{3.6}$$

The system of equations (3.6) can be written as

$$\underbrace{\begin{bmatrix} 1 & s_0 & s_0^2 & ... & s_0^{n-1} \\ 0 & 1 & 2s_0 & ... & (n-1)s_0^{n-2} \\ 0 & 0 & 2 & ... & (n-1)(n-2)s_0^{n-3} \\ \vdots & \vdots & \vdots & & \vdots \\ 0 & 0 & 0 & ... & (n-1)! \end{bmatrix}}_{=:\mathbf{S}(s_0)} \underbrace{\begin{bmatrix} b_0 \\ b_1 \\ b_2 \\ \vdots \\ b_{n-1} \end{bmatrix}}_{=:\mathbf{b}} = -\mathrm{e}^{s_0\tau} \underbrace{\begin{bmatrix} R_0(s_0;\tau) \\ R_1(s_0;\tau) \\ R_2(s_0;\tau) \\ \vdots \\ R_{n-1}(s_0;\tau) \end{bmatrix}}_{=:\mathbf{R}(s_0;\tau)} . \tag{3.7}$$

Since $\mathbf{S}(s_0)$ is an upper triangular matrix with nonzero diagonal elements, the unique solution of (3.7) is

$$\mathbf{b} = -\mathrm{e}^{s_0\tau}\mathbf{S}^{-1}(s_0)\mathbf{R}(s_0;\tau)\,. \tag{3.8}$$

With the control coefficients (3.8), the polynomial $Q(s)$ and the characteristic function $D(s)$ in (3.1) have the form

$$Q(s) = \underbrace{\begin{bmatrix} 1 & s & s^2 & \dots & s^{n-1} \end{bmatrix}}_{=:\mathbf{s}^T} \mathbf{b}\,, \tag{3.9}$$

and

$$D(s) = P(s)+Q(s)\mathrm{e}^{-s\tau} = P(s)+\mathbf{s}^T\mathbf{b}\mathrm{e}^{-s\tau} = P(s)-\mathbf{s}^T\mathbf{S}^{-1}(s_0)\mathbf{R}(s_0;\tau)\mathrm{e}^{-(s-s_0)\tau}\,. \tag{3.10}$$

It can be proved by induction that if

$$\mathbf{w}^T = \begin{bmatrix} w_0 & w_1 & \dots & w_{n-1} \end{bmatrix} \coloneqq \mathbf{s}^T\mathbf{S}^{-1}(s_0)\,, \tag{3.11}$$

then

$$w_k = \frac{1}{k!}(s-s_0)^k\,,\ k = 0,1,...,n-1\,. \tag{3.12}$$

Since $R_k(s_0;0) = P^{(k)}(s_0)$,

$$\begin{aligned} \mathbf{s}^T\mathbf{S}^{-1}(s_0)\mathbf{R}(s_0;0) &= \sum_{k=0}^{n-1}\frac{1}{k!}(s-s_0)^k P^{(k)}(s_0) = P(s) - \frac{1}{n!}(s-s_0)^n P^{(n)}(s_0) \\ &= P(s) - a_n(s-s_0)^n\,. \end{aligned} \tag{3.13}$$

From (3.10) and (3.13) it can be seen that

$$\begin{aligned} D(s) =& a_n(s-s_0)^n + \mathbf{s}^T\mathbf{S}^{-1}(s_0)\mathbf{R}(s_0;0) - \mathbf{s}^T\mathbf{S}^{-1}(s_0)\mathbf{R}(s_0;\tau)\mathrm{e}^{-(s-s_0)\tau} \\ =& a_n(s-s_0)^n - \left[\mathbf{s}^T\mathbf{S}^{-1}(s_0)\mathbf{R}(s_0;\tau t)\mathrm{e}^{-(s-s_0)\tau t}\right]_{t=0}^{t=1} . \end{aligned} \tag{3.14}$$

Let

$$F(t) \coloneqq \mathbf{s}^T\mathbf{S}^{-1}(s_0)\mathbf{R}(s_0;\tau t)\mathrm{e}^{-(s-s_0)\tau t} . \tag{3.15}$$

The derivative of the function $F(t)$ can be written in the form

$$\frac{\mathrm{d}F(t)}{\mathrm{d}t} = \mathbf{s}^T\mathbf{S}^{-1}(s_0)\mathbf{G}(t)\mathrm{e}^{-(s-s_0)\tau t} , \tag{3.16}$$

where

$$\mathbf{G}(t) = \frac{\mathrm{d}\mathbf{R}(s_0;\tau t)}{\mathrm{d}t} - (s-s_0)\tau\mathbf{R}(s_0;\tau t) . \tag{3.17}$$

For $k \in \mathbb{Z}^+$, direct calculation gives

$$\frac{\partial R_k(s;\tau)}{\partial\tau} = \sum_{i=0}^{k-1}\binom{k}{i}P^{(i)}(s)(k-i)\tau^{k-i-1} = k\sum_{i=0}^{k-1}\binom{k-1}{i}P^{(i)}(s)\tau^{k-1-i} = kR_{k-1}(s;\tau) . \tag{3.18}$$

Hence, the elements $G_k(t)$, $k = 0, 1, \dots, n-1$ of $\mathbf{G}(t)$ are

$$\begin{aligned} G_0(t) &= -(s-s_0)\tau R_0(s_0;\tau t) , \\ G_k(t) &= k\tau R_{k-1}(s_0;\tau t) - (s-s_0)\tau R_k(s_0;\tau t) , \quad k = 1, 2, \dots, n-1 . \end{aligned} \tag{3.19}$$

Using equations (3.16), (3.12) and (3.19), the derivative of $F(t)$ can be expanded as

$$\begin{aligned} \frac{\mathrm{d}F(t)}{\mathrm{d}t} &= \left(\sum_{k=1}^{n-1}\frac{1}{(k-1)!}(s-s_0)^k\tau R_{k-1}(s_0;\tau t) - \sum_{k=0}^{n-1}\frac{1}{k!}(s-s_0)^{k+1}\tau R_k(s_0;\tau t)\right)\mathrm{e}^{-(s-s_0)\tau t} \\ &= \left(\sum_{k=0}^{n-2}\frac{1}{k!}(s-s_0)^{k+1}\tau R_k(s_0;\tau t) - \sum_{k=0}^{n-1}\frac{1}{k!}(s-s_0)^{k+1}\tau R_k(s_0;\tau t)\right)\mathrm{e}^{-(s-s_0)\tau t} \\ &= -\frac{1}{(n-1)!}(s-s_0)^n\tau R_{n-1}(s_0;\tau t)\mathrm{e}^{-(s-s_0)\tau t} . \end{aligned} \tag{3.20}$$

Finally, using equations (3.14) and (3.20), we arrive at the desired integral factorization

$$\begin{aligned} D(s) &= a_n(s-s_0)^n - \left[F(t)\right]_{t=0}^{t=1} = a_n(s-s_0)^n - \int_0^1 \frac{\mathrm{d}F(t)}{\mathrm{d}t}\mathrm{d}t \\ &= (s-s_0)^n \left(a_n + \int_0^1 \mathrm{e}^{-(s-s_0)\tau t} \frac{\tau R_{n-1}(s_0;\tau t)}{(n-1)!}\mathrm{d}t \right) . \end{aligned} \tag{3.21}$$

□

Remark 3.1. If $D(s)$ has a real root s_0 with multiplicity at least $n+1$, then (3.4) holds and, in addition, $D^{(n)}(s_0) = 0$:

$$D^{(n)}(s_0) = n! \left(a_n + \int_0^1 \frac{\tau R_{n-1}(s_0;\tau t)}{(n-1)!}\mathrm{d}t \right) = R_n(s_0;\tau) = 0 . \tag{3.22}$$

In this case, $D(s)$ can be factorized as

$$D(s) = \frac{1}{n!}(s-s_0)^{n+1} \int_0^1 \mathrm{e}^{-(s-s_0)\tau t} \tau R_n(s_0;\tau t)\mathrm{d}t . \tag{3.23}$$

Proposition 3.2. *Let s_0 be a real root of the quasipolynomial* (3.1) *with multiplicity at least $n+1$. If $R_{n-1}(s_0;\tau t) \leq 0$, $\forall t$, $0 < t \leq 1$, then s_0 is the dominant root of* (3.1).

Proof. Due to Proposition 3.1, (3.1) can be written in the form of (3.4). To prove that there exists no root $s_1 = \gamma_1 + \mathrm{i}\omega_1$ of (3.4) such that $\gamma_1 > s_0$, substitute s_1 into (3.4). Then, since $s_1 - s_0 \neq 0$, $D(s_1) = 0$ gives

$$a_n + \int_0^1 \mathrm{e}^{-(s_1-s_0)\tau t} \frac{\tau}{(n-1)!} R_{n-1}(s_0;\tau t)\mathrm{d}t = 0 . \tag{3.24}$$

Since $a_n > 0$, one can obtain that

$$\begin{aligned} a_n &= \left| \int_0^1 \mathrm{e}^{-(s_1-s_0)\tau t} \frac{\tau}{(n-1)!} R_{n-1}(s_0;\tau t)\mathrm{d}t \right| \leq \int_0^1 \left| \mathrm{e}^{-(s_1-s_0)\tau t} \frac{\tau}{(n-1)!} R_{n-1}(s_0;\tau t) \right| \mathrm{d}t \\ &= \int_0^1 \mathrm{e}^{-(\gamma_1-s_0)\tau t} \frac{\tau}{(n-1)!} \left| R_{n-1}(s_0;\tau t) \right| \mathrm{d}t . \end{aligned} \tag{3.25}$$

Using the condition $R_{n-1}(s_0;\tau t) \leq 0$, $\forall t$, $0 < t \leq 1$, (3.25) can be written as

$$a_n \leq -\int_0^1 \mathrm{e}^{-(\gamma_1-s_0)\tau t} \frac{\tau}{(n-1)!} R_{n-1}(s_0;\tau t)\mathrm{d}t =: f(\gamma_1) . \tag{3.26}$$

For $\gamma_1 = s_0$ the function $f(\gamma_1)$ takes the value

$$\begin{aligned} f(\gamma_1 = s_0) &= -\int_0^1 \frac{\tau}{(n-1)!} R_{n-1}(s_0; \tau t)\mathrm{d}t = -\int_0^1 \frac{1}{n!}\frac{\mathrm{d}R_n(s_0;\tau t)}{\mathrm{d}t}\mathrm{d}t \\ &= -\frac{1}{n!}\left[R_n(s_0;\tau t)\right]_{t=0}^{t=1} = -\frac{1}{n!}\left(\underbrace{R_n(s_0;\tau)}_{=0} - \underbrace{R_n(s_0;0)}_{=a_n n!}\right) = a_n\,. \end{aligned} \tag{3.27}$$

For $\gamma_1 > s_0$ the value of the integral in (3.26) is $f(\gamma_1) < a_n$ since $0 < \mathrm{e}^{-(\gamma_1 - s_0)\tau t} < 1$ for $\gamma_1 > s_0$, $\tau > 0$, $0 < t \leq 1$. Therefore, from (3.26) we obtain $a_n < a_n$, which proves the inconsistency of the hypothesis that the characteristic function (3.4) has a root $s_1 = \gamma_1 + \mathrm{i}\omega_1$ with $\gamma_1 > s_0$. Consequently, (3.1) has no root of the form $s_1 = \gamma_1 + \mathrm{i}\omega_1$ with $\gamma_1 > s_0$. □

3.2.2 Sufficient condition for the dominancy of a real root with multiplicity at least n

Similarly to Proposition 3.2, we can give a sufficient condition for the dominancy of a real root s_0 with multiplicity at least n.

Proposition 3.3. *Let s_0 be a real root of (3.1) with multiplicity at least n, and let $R_{n-1}(s_0;\vartheta)$ have k sign changes in the interval $0 < \vartheta < \tau$ at $\tau_1 < \tau_2 < \ldots < \tau_k$. Furthermore, let us use the notations $\tau_0 = 0$, $\tau_{k+1} = \tau$ and $c(s_0) \coloneqq \operatorname{sgn} R_{n-1}(s_0;\vartheta)$ for $0 < \vartheta < \tau_1$. If*

$$\frac{c(s_0)}{n!}\sum_{i=0}^{k}(-1)^i\left[R_n(s_0;\vartheta)\right]_{\vartheta=\tau_i}^{\vartheta=\tau_{i+1}} \leq a_n\,, \tag{3.28}$$

then s_0 is the dominant root of (3.1).

Proof. Since s_0 is a root with multiplicity at least n, (3.1) can be written as

$$D(s) = (s - s_0)^n\left(a_n + \int_0^\tau \mathrm{e}^{-(s-s_0)\vartheta}\frac{R_{n-1}(s_0;\vartheta)}{(n-1)!}\mathrm{d}\vartheta\right) \tag{3.29}$$

by Proposition 3.1. To prove that there exists no root $s_1 = \gamma_1 + \mathrm{i}\omega_1$ of (3.29) such that

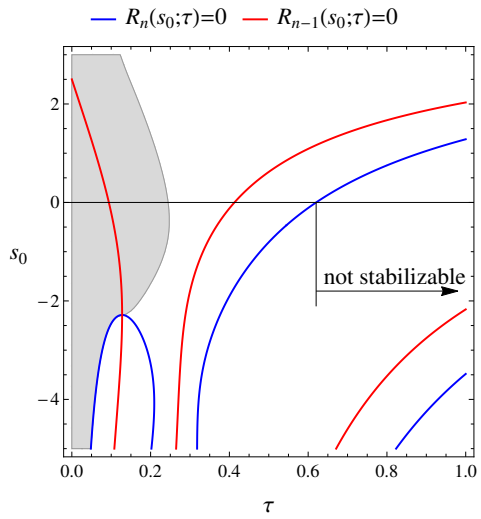

Figure 3.1: Illustration of the sufficient condition for the MID property in the sense of Proposition 3.3 (gray shading) and necessary condition for stabilizability according to Remark 3.4 for the plant $P(s) = (s-2)(s-(2-10\mathrm{i}))(s-(2+10\mathrm{i}))(s-4)$.

$\gamma_1 > s_0$, substitute s_1 into (3.29). Since $a_n > 0$, one can obtain that

$$\begin{aligned} a_n &= \left| \int_0^\tau \mathrm{e}^{-(s_1-s_0)\vartheta} \frac{1}{(n-1)!} R_{n-1}(s_0;\vartheta)\mathrm{d}\vartheta \right| \leq \int_0^\tau \left| \mathrm{e}^{-(s_1-s_0)\vartheta} \frac{1}{(n-1)!} R_{n-1}(s_0;\vartheta) \right| \mathrm{d}\vartheta \\ &= \int_0^\tau \mathrm{e}^{-(\gamma_1-s_0)\vartheta} \frac{1}{(n-1)!} \left| R_{n-1}(s_0;\vartheta) \right| \mathrm{d}\vartheta < \int_0^\tau \frac{1}{(n-1)!} \left| R_{n-1}(s_0;\vartheta) \right| \mathrm{d}\vartheta \\ &= \frac{c(s_0)}{(n-1)!} \sum_{i=0}^{k} (-1)^i \int_{\tau_i}^{\tau_{i+1}} R_{n-1}(s_0;\vartheta)\mathrm{d}\vartheta = \frac{c(s_0)}{n!} \sum_{i=0}^{k} (-1)^i \int_{\tau_i}^{\tau_{i+1}} \frac{\mathrm{d}R_n(s_0;\vartheta)}{\mathrm{d}\vartheta}\mathrm{d}\vartheta \\ &= \frac{c(s_0)}{n!} \sum_{i=0}^{k} (-1)^i \left[R_n(s_0;\vartheta) \right]_{\vartheta=\tau_i}^{\vartheta=\tau_{i+1}} \leq a_n \,. \end{aligned} \tag{3.30}$$

From (3.30) we obtain $a_n < a_n$, which proves the inconsistency of the hypothesis that the characteristic function (3.29) has a root $s_1 = \gamma_1 + \mathrm{i}\omega_1$ with $\gamma_1 > s_0$. Therefore, (3.1) has no root of the form $s_1 = \gamma_1 + \mathrm{i}\omega_1$ with $\gamma_1 > s_0$. □

Remark 3.2. $c(s_0) = 1$ for $s_0 > s_\mathrm{a}$ and $c(s_0) = -1$ for $s_0 < s_\mathrm{a}$, where s_a is the average of the roots of $P(s)$.

Figure 3.1 demonstrates the MID property for a plant of degree $n = 4$. Gray shading indicates the pairs (s_0, τ) that satisfies the sufficient condition of Proposition 3.3. In this region s_0 is the dominant root.

3.2.3 Necessary condition for stabilizability

In this subsection, the necessary condition for the stabilizability of system (3.1) is discussed. We start with a lemma from [53] and [84].

Lemma 3.1. *Consider the quasipolynomial*

$$h(s) = \sum_{i=0}^{n} \sum_{j=1}^{r} h_{ij} s^{n-i} \mathrm{e}^{\tau_j s} \tag{3.31}$$

such that $\tau_1 < \tau_2 < ... < \tau_r$*, with main term* $h_{0r} \neq 0$*, and* $\tau_1 + \tau_r > 0$*. If* $h(s)$ *is stable (i.e., the roots of* $h(s) = 0$ *are located in the open left half of the complex plane), then* $h'(s)$ *is also a stable quasipolynomial.*

Remark 3.3. Lemma 3.1 can be generalized to γ-stability by applying a shift $z = s - s_0$ with $s_0 = \gamma$.

We can give a necessary condition for the γ-stability of (3.1) by the successive application of Lemma 3.1 and Remark 3.3 to the quasipolynomial $P(s)\mathrm{e}^{s\tau} + Q(s)$.

Proposition 3.4. *If the quasipolynomial* (3.1) *is* γ*-stable, then the polynomial* $R_n(s;\tau)$ *is* γ*-stable.*

Proof. If (3.1) is γ-stable, then $P(s)\mathrm{e}^{s\tau} + Q(s)$ is γ-stable, and by Lemma 3.1 and Remark 3.3 the nth derivative of $P(s)\mathrm{e}^{s\tau} + Q(s)$ is also γ-stable. □

Remark 3.4. $R_n(s;\tau)$ is independent of the control coefficients b_i; therefore, Proposition 3.4 also gives a necessary condition for the γ-stabilizability of (3.1).

Figure 3.1 also demonstrates the necessary condition for stabilizability (i.e., $\gamma = 0$). If $\tau > 0.6202$, then the system cannot be stabilized.

3.3 Systems with real-rooted plant

In this section, we assume that the polynomial $P(s)$ corresponding to the open-loop system has only real roots. In this case, $P(s)$ has the form $P(s) = a_n \prod_{i=1}^{n}(s - s_i)$, $s_i \in \mathbb{R}$, $s_n \leq s_{n-1} \leq ... \leq s_1$. To apply the sufficient condition in Proposition 3.2 and the necessary condition in Proposition 3.4, first, we need to characterize the properties of polynomials $R_k(s;\tau)$. These properties are outlined and discussed in the forthcoming subsections.

3.3.1 Interlacing property of polynomials $R_k(s;\tau)$

The two-variable polynomials $R_k(s;\tau)$, $k \in \mathbb{Z}^+$ have the following properties:

$$R_k(s;\tau) = \tau R_{k-1}(s;\tau) + \frac{\partial R_{k-1}(s;\tau)}{\partial s}\,, \tag{3.32}$$

$$\frac{\partial R_k(s;\tau)}{\partial \tau} = k R_{k-1}(s;\tau)\,. \tag{3.33}$$

Property (3.32) allows us to say that, for a fixed τ, the roots of polynomials $R_k(s;\tau)$ and $R_{k-1}(s;\tau)$ interlace and $R_k(s;\tau)$ has only real roots for s, since $R_0(s;\tau) = P(s)$ has only real roots [35]. Polynomials $R_n(s;\tau)$ and $R_{n-1}(s;\tau)$ have n distinct real roots for s if $\tau \neq 0$. Let $s_{0,k}$, $k = 1, 2, ..., n$ denote the roots of $R_n(s;\tau)$, $\tau \neq 0$ with $s_{0,n} < s_{0,n-1} < ... < s_{0,1}$.

It can also be shown that, for a fixed s, the polynomial $R_n(s;\tau)$ has only real roots for τ [91]. Moreover, as direct consequences of property (3.33) and Rolle's theorem, $R_k(s;\tau)$, $k = 1, 2, ..., n-1$ has only real roots for τ, and the roots of $R_k(s;\tau)$ and $R_{k-1}(s;\tau)$ interlace.

3.3.2 Monotonicity

In the (τ, s) plane the algebraic curve $R_n(s;\tau) = 0$ has distinct branches, and every branch is strictly increasing since the derivative of the implicit function $R_n(s;\tau) = 0$ in a point (s,τ) reads

$$\frac{\mathrm{d}s}{\mathrm{d}\tau} = -\frac{\frac{\partial R_n(s;\tau)}{\partial \tau}}{\frac{\partial R_n(s;\tau)}{\partial s}} = -\frac{n R_{n-1}(s;\tau)}{R_{n+1}(s;\tau)} > 0\,. \tag{3.34}$$

The fraction $\frac{R_{n-1}(s;\tau)}{R_{n+1}(s;\tau)}$ is negative since, for a fixed $\tau \neq 0$, at a root s of the polynomial $R_n(s;\tau)$, the function values $R_{n-1}(s;\tau)$ and $R_{n+1}(s;\tau)$ are nonzero and have different signs because of the interlacing property.

A similar property holds for the algebraic curve $R_{n-1}(s;\tau) = 0$. If $P(s)$ has at least two distinct roots, then $R_{n-1}(s;\tau) = 0$ has distinct branches, and every branch is strictly increasing. If $P(s)$ has one root s_1 with multiplicity n (i.e., $P(s) = a_n(s - s_1)^n$), then one branch is constant and all the other branches are strictly increasing as a function of τ.

3.3.3 Asymptotic properties

If $\tau \to \infty$ (or $\tau \to -\infty$), then the roots of $R_k(s;\tau)$ for s approach the roots of $P(s)$ (i.e., $s_n \leq s_{n-1} \leq ... \leq s_1$). Similarly, if $s \to \infty$ or $s \to -\infty$, then the roots of $R_k(s;\tau)$ for τ approach the roots of $\tau^k = 0$ (i.e., 0 with multiplicity k).

3.3.4 Roots of $R_k(s;0)$

If $\tau = 0$, then $R_k(s;\tau) = R_k(s;0) = P^{(k)}(s)$. Therefore, if $k = n$, then $R_n(s;0) = n!a_n$ has no roots for s. If $k = n-1$, then $R_{n-1}(s;0) = \frac{n!}{1!}a_n s + \frac{(n-1)!}{0!}a_{n-1}$ has one root for s:

$$s_{\mathrm{a}} = -\frac{1}{n}\frac{a_{n-1}}{a_n} = \frac{1}{n}\sum_{i=1}^{n} s_i \,, \tag{3.35}$$

which is the average of the roots of $P(s)$ according to Vieta's formulas.

3.3.5 Sufficient and necessary conditions for dominancy and stabilizability

Let τ_0 denote the smallest positive root of $R_n(0;\tau) = 0$ for τ. For $\tau > 0$ the first branch of the algebraic curve $R_n(s;\tau) = 0$ corresponds to the greatest s values and takes values in the interval $]-\infty, s_1[$. Therefore, if $s_1 > 0$, then τ_0 corresponds to the first branch of $R_n(s;\tau) = 0$. If $s_1 \leq 0$, then $R_n(0;\tau) = 0$ has no positive roots: in this case we set $\tau_0 = \infty$.

Furthermore, let τ_{a} denote the smallest positive root of $R_n(s_{\mathrm{a}};\tau) = 0$ for τ. If $P(s) \neq a_n(s-s_1)^n$, that is, $P(s)$ has at least two distinct roots, then τ_{a} corresponds to the first branch of $R_n(s;\tau) = 0$ since $s_n < s_{\mathrm{a}} < s_1$. If $P(s) = a_n(s-s_1)^n$, then $s_{\mathrm{a}} = s_1$ and $R_n(s_{\mathrm{a}};\tau) = 0$ has no roots: in this case we set $\tau_{\mathrm{a}} = \infty$.

The curve $R_n(s;\tau) = 0$ gives a connection between the delay τ and the possible values of the real root s_0 with multiplicity $n+1$, while the curve $R_{n-1}(s;\tau) = 0$ is needed to analyze the sufficient condition given in Proposition 3.2. It is clear that the condition $R_{n-1}(s_{0,k};\tau t) \leq 0$, $\forall t$, $0 < t \leq 1$ can be satisfied if and only if $k = 1$ and $0 < \tau \leq \tau_{\mathrm{a}}$ (i.e., for the greatest s_0 and in a certain delay interval).

These observations are summarized in the following theorems.

Theorem 3.1. *Let $P(s)$ be real-rooted, and consider the case $s_{\mathrm{a}} \geq 0$. Then,*

1. $\tau_0 \leq \tau_{\mathrm{a}}$,

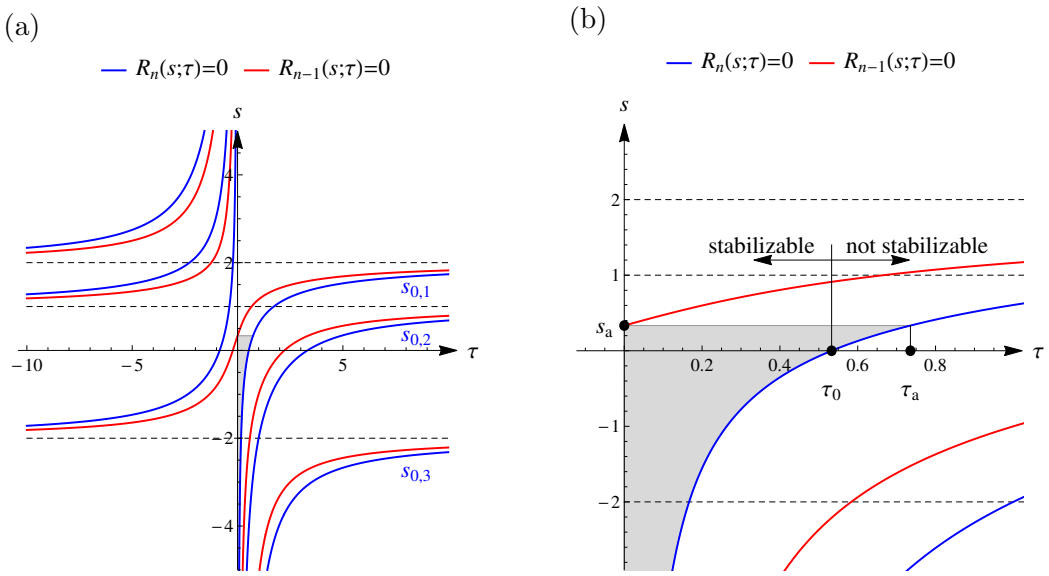

Figure 3.2: Illustration of the sufficient condition for the MID property (gray shading) and the necessary and sufficient condition for stabilizability based on the roots of the polynomials $R_n(s;\tau)$ and $R_{n-1}(s;\tau)$ in the (τ, s) plane for the plant $P(s) = (s-2)(s-1)(s+2)$ according to Theorem 3.1 (case $s_a \geq 0$).

2. *$s_{0,1}$ is the dominant root of system* (3.4) *if* $0 < \tau \leq \tau_a$,

3. *system* (3.1) *is stabilizable if and only if* $0 < \tau < \tau_0$.

Proof. If $s_a > 0$, then there is at least 1 positive root s_1 of $P(s)$; therefore, there is a finite τ_0 corresponding to the first branch of $R_n(s;\tau) = 0$. Then, item 1. follows from the monotonicity of the curve $R_n(s;\tau) = 0$. If $s_a = 0$, then $\tau_0 = \tau_a$. Item 2. follows from the sufficient condition in Proposition 3.2. If $0 < \tau < \tau_0$, then $s_{0,1} < 0$, which gives the sufficient condition for the stabilizability of system (3.1) in item 3. For $\tau \geq \tau_0$, $R_n(s;\tau)$ has a root in the closed right half of the complex plane; therefore, by Propostion 3.4, system (3.1) cannot be stabilized. This gives the necessary condition in item 3. □

Figure 3.2 shows the branches of the algebraic curves $R_n(s;\tau) = 0$ and $R_{n-1}(s;\tau) = 0$ corresponding to the interlacing and asymptotic properties for a plant of degree $n = 3$. The roots of the open-loop system are $s_1 = 2$, $s_2 = 1$, $s_3 = -2$, thus $s_a = 1/3 > 0$ hence Theorem 3.1 applies. The horizontal asymptotes corresponding to the roots of $P(s)$ are indicated with dashed lines. In the gray shaded region $R_{n-1}(s_0;\tau) \leq 0$ hence Proposition 3.2 applies. In this example, the numerical values are $\tau_0 = 0.532$ and $\tau_a = 0.735$ and the critical delay is $\tau_{crit} = \tau_0$.

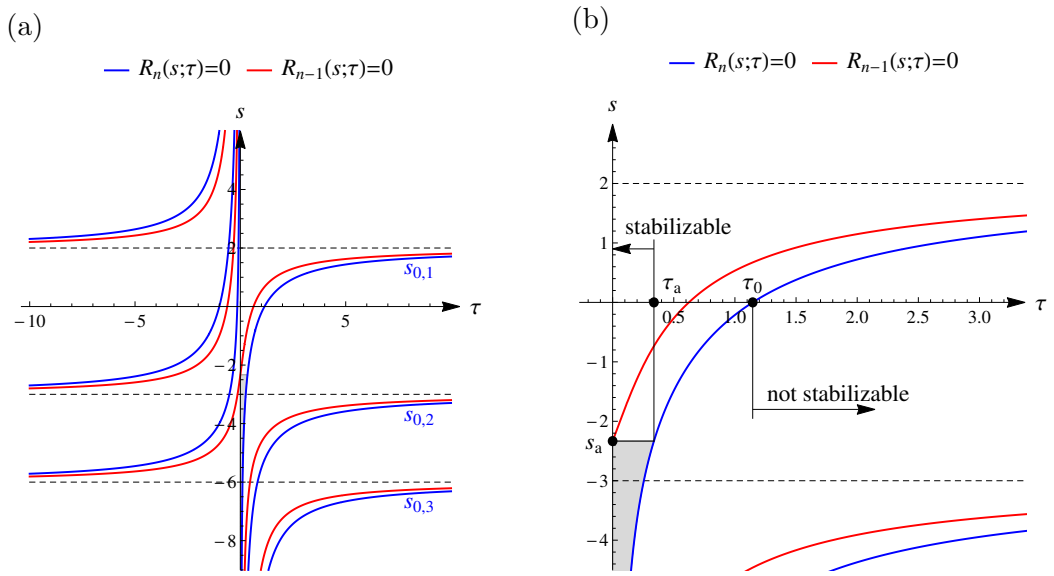

Figure 3.3: Illustration of the sufficient condition for the MID property (gray shading) and the sufficient and necessary conditions for stabilizability based on the roots of the polynomials $R_n(s;\tau)$ and $R_{n-1}(s;\tau)$ in the (τ, s) plane for the plant $P(s) = (s-2)(s+3)(s+6)$ according to Theorem 3.2 (case $s_a < 0$).

Theorem 3.2. *Let $P(s)$ be real-rooted, and consider the case $s_a < 0$. Then,*

1. *$\tau_0 \geq \tau_a$,*
2. *$s_{0,1}$ is the dominant root of system (3.4) if $0 < \tau \leq \tau_a$,*
3. *system (3.1) is stabilizable if $0 < \tau \leq \tau_a$ and cannot be stabilized for $\tau \geq \tau_0$.*

Proof. The proof follows the same lines as the proof of Theorem 3.1. □

Figure 3.3 shows the branches of the algebraic curves $R_n(s;\tau) = 0$ and $R_{n-1}(s;\tau) = 0$ for a plant of degree $n = 3$, when the roots of the open-loop system are $s_1 = 2$, $s_2 = -3$, $s_3 = -6$. In this case $s_a = -7/3 < 0$ hence Theorem 3.2 applies. Again, the horizontal asymptotes corresponding to the roots of $P(s)$ are indicated with dashed lines and in the gray shaded region $R_{n-1}(s_0;\tau) \leq 0$ hence Proposition 3.2 applies. Here, the numerical values are $\tau_a = 0.337$ and $\tau_0 = 1.145$. We may also investigate the proposed controller design (s_0 with multiplicity $n+1$) numerically. For a given τ, the n possible values of the $(n+1)$-fold real characteristic roots can be determined using equation (3.22). Then, the corresponding values of s_0 and τ can be substituted into the factorized characteristic function (3.23). The number of unstable characteristic

roots can be calculated using a numerical testing integral [112, 117]. Using evenly-spaced grid points over the interval $0 < \tau \leq 2$, the numerical analysis shows that we can stabilize the system if $\tau < \hat{\tau} = 0.977$, that is, $\tau_{\mathrm{a}} < \hat{\tau} < \tau_0$. If we apply a shift $s = z + s_0 + \varepsilon$ in (3.23), then the same technique can be used to determine the number of characteristic roots with real part larger than $s_0 + \varepsilon$. Using a sufficiently small value of ε, we can decide if the characteristic root s_0 is dominant. With $\varepsilon = 0.01$, it was found that s_0 is the dominant root if $\tau < 0.831$.

Remark 3.5. Let $P(s)$ be real-rooted, and let s_0 be a real root of (3.1) with multiplicity at least $n+1$. Then, $D^{(n+1)}(s_0) = R_{n+1}(s_0;\tau) \neq 0$ because of the interlacing property; therefore, the maximal multiplicity of a real root s_0 is $n+1$.

Remark 3.6. It can be seen by applying Proposition 3.4 that the real root $s_{0,1}$ gives a lower bound on the spectral abscissa of the quasipolynomial (3.1), and this lower bound is independent of the control parameters b_i. Thus, if $s_{0,1}$ is dominant, then it gives the minimum of the spectral abscissa with respect to the control parameters.

This remark implies the following proposition.

Proposition 3.5. *Let $P(s)$ be real-rooted, and assume that $\gamma \leq s_{\mathrm{a}}$. Then, system (3.1) is γ-stabilizable if and only if $\tau \in]0, \tau_\gamma[$, where τ_γ is the smallest positive real root of $R_n(\gamma;\tau)$ for τ.*

3.4 Multi-degree-of-freedom mechanical example

Consider an N-link inverted pinned pendulum with rods of equal mass m and length l moving in the vertical plane. The control torque is applied at the first (lowest) rod:

$$T_{\mathrm{c}}(t) = -\sum_{i=1}^{N} p_i \varphi_i(t-\tau) - \sum_{i=1}^{N} d_i \dot{\varphi}_i(t-\tau)\,. \tag{3.36}$$

3.4.1 Derivation of the equation of motion

The equation of motion can be determined using the Euler–Lagrange equations. The generalized coordinates are chosen to be the absolute pendulum angles $\varphi_i(t)$ (i.e., angular displacement of the rods from the vertically upward position). The equation of motion linearized around the unstable equilibrium has the form

$$\mathbf{M}\ddot{\mathbf{q}}(t) + \mathbf{S}\mathbf{q}(t) = \mathbf{Q}(t)\,, \tag{3.37}$$

where the mass matrix $\mathbf{M} = [m_{ij}]$ and the stiffness matrix $\mathbf{S} = [s_{ij}]$ can be written as

$$\mathbf{M} = \frac{1}{6}ml^2 \begin{bmatrix} 6(N-1)+2 & 6(N-2)+3 & ... & 21 & 15 & 9 & 3 \\ 6(N-2)+3 & 6(N-2)+2 & ... & 21 & 15 & 9 & 3 \\ \vdots & \vdots & & \vdots & \vdots & \vdots & \vdots \\ 21 & 21 & ... & 20 & 15 & 9 & 3 \\ 15 & 15 & ... & 15 & 14 & 9 & 3 \\ 9 & 9 & ... & 9 & 9 & 8 & 3 \\ 3 & 3 & ... & 3 & 3 & 3 & 2 \end{bmatrix}, \tag{3.38}$$

$$\mathbf{S} = -\frac{1}{2}mgl \begin{bmatrix} 2(N-1)+1 & 0 & ... & 0 & 0 & 0 & 0 \\ 0 & 2(N-2)+1 & ... & 0 & 0 & 0 & 0 \\ \vdots & \vdots & & \vdots & \vdots & \vdots & \vdots \\ 0 & 0 & ... & 7 & 0 & 0 & 0 \\ 0 & 0 & ... & 0 & 5 & 0 & 0 \\ 0 & 0 & ... & 0 & 0 & 3 & 0 \\ 0 & 0 & ... & 0 & 0 & 0 & 1 \end{bmatrix}, \tag{3.39}$$

that is,

$$\begin{aligned} m_{ij} &= \frac{1}{6}ml^2(6(N-j)+3), \quad i < j\,, \\ m_{ij} &= \frac{1}{6}ml^2(6(N-i)+2), \quad i = j\,, \\ m_{ij} &= \frac{1}{6}ml^2(6(N-i)+3), \quad i > j\,, \end{aligned} \tag{3.40}$$

and

$$\begin{aligned} s_{ij} &= -\frac{1}{2}mgl(2(N-i)+1), \quad i = j\,, \\ s_{ij} &= 0, \quad i \neq j\,. \end{aligned} \tag{3.41}$$

For more details, see Appendix A.1. The generalized force $\mathbf{Q}(t)$ reads

$$\mathbf{Q}(t) = -\begin{bmatrix} p_1 & p_2 & ... & p_N \\ 0 & 0 & ... & 0 \\ \vdots & \vdots & & \vdots \\ 0 & 0 & ... & 0 \end{bmatrix} \mathbf{q}(t-\tau) - \begin{bmatrix} d_1 & d_2 & ... & d_N \\ 0 & 0 & ... & 0 \\ \vdots & \vdots & & \vdots \\ 0 & 0 & ... & 0 \end{bmatrix} \dot{\mathbf{q}}(t-\tau)\,. \tag{3.42}$$

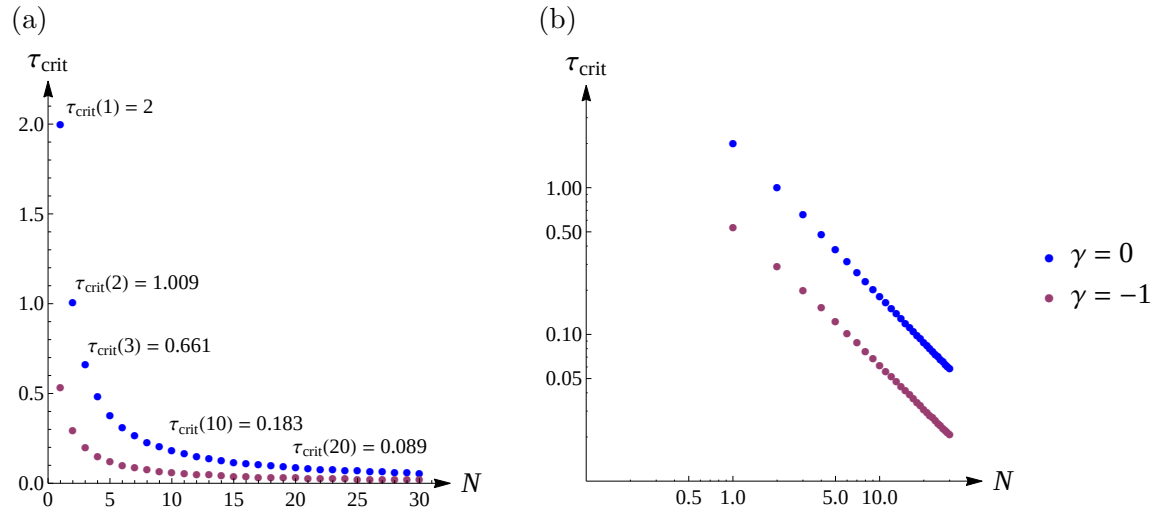

Figure 3.4: Critical delay $\tau_{\text{crit}}(N, \gamma)$ of an N-link inverted pendulum if $3g/l = 1$ (a). Representation of the points (N, τ_{crit}) on a logarithmic scale suggests a hyperbolic convergence of τ_{crit} to 0 as N approaches infinity (b).

Therefore, the characteristic function has the form (3.1) where the open-loop characteristic function $P(s)$ reads

$$P(s) = \det\left(s^2\mathbf{M} + \mathbf{S}\right). \tag{3.43}$$

3.4.2 Stabilizable delay interval

The mass matrix $\mathbf{M}$ is positive definite and the stiffness matrix $\mathbf{S}$ is negative definite; therefore, $P(s)$ has only real roots. Furthermore, the roots occur in real pairs $\pm s_i$, $i = 1, ..., N$; therefore, the average of the roots is $s_{\text{a}} = 0$. Thus, we can apply the results of Theorem 3.1: system (3.37) is stabilizable if and only if $0 < \tau < \tau_0$, where τ_0 can be calculated if the system parameters are known. Figure 3.4 shows the critical delay $\tau_{\text{crit}}(N) = \tau_0$ as a function of N if $3g/l = 1$. The case $N = 1$ gives the single inverted pendulum, when $\tau_{\text{crit}}(1) = 2$ (see Section 2.1). This figure also shows the largest delays for which we can reach a given spectral abscissa γ. That is, we use a slightly generalized notion of the critical delay: $\tau_{\text{crit}}(N, \gamma)$ denotes the critical delay corresponding to a given degree of freedom N and spectral abscissa γ (with $\tau_{\text{crit}}(N) = \tau_{\text{crit}}(N, 0)$ corresponding to stabilizability). An illustration of the root location is shown in Figure 3.5.

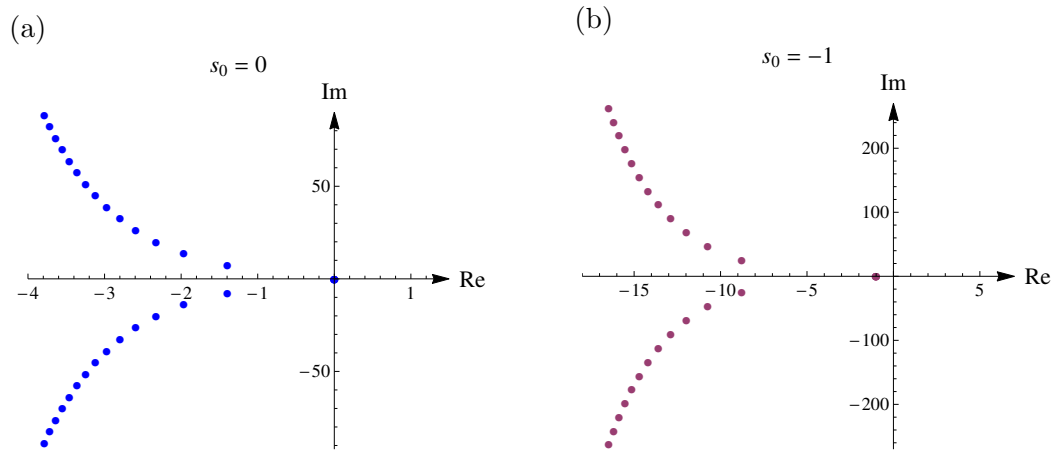

Figure 3.5: Illustration of the root location of the characteristic function if $N = 2$, $3g/l = 1$ and $\tau = \tau_{\text{crit}}(N, s_0)$ with quintuple roots $s_0 = 0$ and $s_0 = -1$ yielding $\gamma = 0$ and $\gamma = -1$, respectively.

3.5 Conclusion

Sufficient conditions were given for the MID property in the case of a real root s_0 with multiplicity at least $n + 1$ and with multiplicity at least n. Necessary condition for γ-stabilizability was investigated based on [53] and [84]. As a main result, sufficient and necessary conditions for the MID property and γ-stabilizability were derived for systems with real-rooted open-loop characteristic function. The results were applied to an N-link inverted pendulum subjected to delayed state feedback. One advantage of the results is that only roots of polynomials should be found in order to check sufficient and necessary conditions for γ-stabilizability.

Although the main results were derived for systems with real-rooted open-loop characteristic function, they can be generalized to systems with $P(s)$ having not only real roots. If $R_n(s;\tau)$ and $R_{n-1}(s;\tau)$ have single dominant real roots $s_{0,1}(\tau)$ and $\tilde{s}_{0,1}(\tau)$ for $\tau > 0$, respectively, such that $\tilde{s}_{0,1}(\tau) > s_{0,1}(\tau)$, and $s_{0,1}(\tau)$ and $\tilde{s}_{0,1}(\tau)$ are increasing as a function of τ and, furthermore, $R_{n-1}(s(\tau);\tau) \neq 0$ for $s_{0,1}(\tau) < s(\tau) < \tilde{s}_{0,1}(\tau)$, then similar statements can be made.

If the coefficients a_i of an arbitrary plant are known, root location of polynomials $R_n(s;\tau)$ and $R_{n-1}(s;\tau)$ can be accessed easily using numerical techniques; hence, the results in Section 3.2 can be applied. Nevertheless, in general, it is difficult to parametrically characterize the root location of these polynomials. However, it could be done by exploiting the structure of the open-loop characteristic polynomial, as we saw in the case of real-rooted plants in Section 3.3.

3.6 Main results

Consider delayed feedback systems whose characteristic function is a quasipolynomial of the form

$$D(s) = P(s) + \mathrm{e}^{-s\tau}Q(s)\,,$$

where $\tau > 0$, and the degrees of polynomials $P(s)$ and $Q(s)$ are n and $n-1$, respectively:

$$P(s) = a_n s^n + a_{n-1}s^{n-1} + ... + a_0\,,$$
$$Q(s) = b_{n-1}s^{n-1} + b_{n-2}s^{n-2} + ... + b_0\,.$$

Assume that the plant parameters a_i are known and fixed such that $a_n > 0$, and assume that coefficients b_i in $Q(s)$ are independently adjustable control parameters. The quasipolynomial $D(s)$ is said to be γ-stabilizable for a given τ if there exists a set of control gains b_i, $i = 0, 1, ..., n-1$ for which the real parts of all roots of $D(s)$ are less than γ. Furthermore, define the family of polynomials $R_k(s;\tau)$ as

$$R_k(s;\tau) = \sum_{i=0}^{k} \binom{k}{i} P^{(i)}(s)\tau^{k-i},\ k \in \mathbb{Z}_0^+\,.$$

Contribution 1

Let s_0 be a real root of $D(s)$ with multiplicity at least n, and let $R_{n-1}(s_0;\vartheta)$ have k sign changes in the interval $0 < \vartheta < \tau$ at $\tau_1 < \tau_2 < ... < \tau_k$. Furthermore, let us use the notations $\tau_0 = 0$, $\tau_{k+1} = \tau$ and $c(s_0) \coloneqq \operatorname{sgn} R_{n-1}(s_0;\vartheta)$ for $0 < \vartheta < \tau_1$. If

$$\frac{c(s_0)}{n!}\sum_{i=0}^{k}(-1)^i \left[R_n(s_0;\vartheta)\right]_{\vartheta=\tau_i}^{\vartheta=\tau_{i+1}} \le a_n\,,$$

then s_0 is the dominant root of $D(s)$.

Related publications: [8, 3].

Contribution 2

Let $P(s)$ be real-rooted, and assume that $\gamma \le s_\mathrm{a}$, where s_a is the average of the roots of $P(s)$. Then, $D(s)$ is γ-stabilizable if and only if $\tau \in]0, \tau_\gamma[$, where τ_γ is the smallest positive real root of $R_n(\gamma;\tau)$ for τ.

Related publications: [8, 80, 3].

Chapter 4

Inverted pendulum subject to detuned PDA feedback

As mentioned in the introduction, constraints of stabilizability of delayed feedback systems can be observed in human stick balancing. Because of the reaction time, human subjects cannot balance a stick shorter than some critical stick length, which is about 40 cm on average. A possible concept for human balancing is the feedback of acceleration in addition to position and velocity feedback [63, 114, 49, 121]. The benefit of acceleration feedback is revealed both in terms of critical delay and robustness to sensory uncertainties [49, 57]. The operation of human sensory system suggests that different terms are fed back with different delays [14, 61]. It is known that additional delay can improve stability properties [2, 46]. The concept of either feeding back the acceleration or employing multiple delays in the feedback loop has been investigated in engineering applications [110, 45, 87]. Different delays can also show up in feedback systems due to the elasticity of the plant [54, 120].

4.1 Problem statement

Motivated by the above applications, in this chapter we analyze a second-order unstable plant with proportional-derivative-acceleration (PDA) feedback governed by

$$\ddot{\varphi}(t) + a_0\varphi(t) = -k_\mathrm{p}\varphi(t-\tau_\mathrm{p}) - k_\mathrm{d}\dot{\varphi}(t-\tau_\mathrm{d}) - k_\mathrm{a}\ddot{\varphi}(t-\tau_\mathrm{a})\,, \tag{4.1}$$

where a_0 is fixed, and $a_0 < 0$, $\tau_\mathrm{p} > 0$, $\tau_\mathrm{d} > 0$, $\tau_\mathrm{a} > 0$. System (4.1) is said to be stabilizable for given delays τ_p, τ_d and τ_a if there exist some k_p, k_d and k_a for which (4.1) is stable.

Following [99] one can also think of (4.1) as a control system with a single control-loop latency τ and some additional delays (or delay detunings) $\delta_\mathrm{p} \geq 0$, $\delta_\mathrm{d} \geq 0$ and $\delta_\mathrm{a} \geq 0$ in all three terms. These additional delays are introduced in hopes of improving the stabilizability of the original system with a single delay τ. This concept leads to

$$\ddot{\varphi}(t) + a_0\varphi(t) = u(t-\tau)\,, \tag{4.2}$$

where

$$u(t) = -k_\mathrm{p}\varphi(t-\delta_\mathrm{p}) - k_\mathrm{d}\dot{\varphi}(t-\delta_\mathrm{d}) - k_\mathrm{a}\ddot{\varphi}(t-\delta_\mathrm{a}) \tag{4.3}$$

with $\delta_\mathrm{p} \geq 0$, $\delta_\mathrm{d} \geq 0$ and $\delta_\mathrm{a} \geq 0$. In this sense, the system is stabilizable for a given τ if there exist some k_p, k_d, k_a and δ_p, δ_d, δ_a for which (4.2) with (4.3) is stable. In the following, we refer to (4.2)–(4.3) as detuned PDA feedback.

The goal of this chapter is to determine the critical delay τ_crit for the detuned PDA feedback (4.2)–(4.3) such that if $\tau < \tau_\mathrm{crit}$, then (4.2) can be stabilized by (4.3) with an appropriate choice of the control parameters k_p, k_d, k_a and δ_p, δ_d, $\delta_\mathrm{a} \geq 0$. The same problem can be posed in terms of parameters in (4.1) as: we are looking for the critical delay τ_crit as the maximum of $\min\{\tau_\mathrm{p}, \tau_\mathrm{d}, \tau_\mathrm{a}\}$ such that (4.1) is still stabilizable. Therefore, the stabilizable region of (4.1) in the $(\tau_\mathrm{p}, \tau_\mathrm{d}, \tau_\mathrm{a})$ space will be investigated. For the sake of simplicity of notation, the analytical and numerical results are derived in terms of τ_p, τ_d and τ_a instead of τ, δ_p, δ_d and δ_a throughout the chapter.

Special cases of (4.1) involve delayed PD feedback ($k_\mathrm{a} = 0$, $\tau_\mathrm{p} = \tau_\mathrm{d}$), detuned PD feedback ($k_\mathrm{a} = 0$) and delayed PDA feedback ($\tau_\mathrm{p} = \tau_\mathrm{d} = \tau_\mathrm{a}$). The critical delay for delayed PD feedback was derived by Schürer [97] as

$$\tau_\mathrm{crit}^\mathrm{PD} = \sqrt{-\frac{2}{a_0}}\,; \tag{4.4}$$

see also Section 2.1. This value is used as reference in this chapter. For detuned PD and delayed PDA feedback, the critical delay was given by Sieber and Krauskopf [99] as

$$\tau_\mathrm{crit}^\mathrm{dPD} = \sqrt{\frac{6+4\sqrt{3}}{3}}\sqrt{-\frac{1}{a_0}} \approx 1.47\;\tau_\mathrm{crit}^\mathrm{PD} \tag{4.5}$$

and

$$\tau_\mathrm{crit}^\mathrm{PDA} = \sqrt{-\frac{4}{a_0}} \approx 1.41\;\tau_\mathrm{crit}^\mathrm{PD}, \tag{4.6}$$

respectively.

The rest of the chapter is organized as follows. In Section 4.2, detuned PDA feed-

back is investigated and the critical point where the region of stabilizability collapses to a single point is determined. In Section 4.3, the location of the characteristic roots is determined at the critical point. Finally, the results are discussed in Section 4.4.

4.2 Stabilization with detuned PDA feedback

The characteristic function of (4.1) reads

$$D(s) = s^2 + a_0 + k_\mathrm{p}\mathrm{e}^{-s\tau_\mathrm{p}} + k_\mathrm{d}s\mathrm{e}^{-s\tau_\mathrm{d}} + k_\mathrm{a}s^2\mathrm{e}^{-s\tau_\mathrm{a}}\,. \tag{4.7}$$

Equation (4.1) is a neutral delay differential equation (NDDE); therefore, strong stability requires that

$$|k_\mathrm{a}| < 1\,. \tag{4.8}$$

Substitution of $s = \mathrm{i}\omega$ into $D(s) = 0$ gives the D-curves

$$\text{if } \omega = 0 \;:\quad k_\mathrm{p} = -a_0\,,\quad k_\mathrm{d} \in \mathbb{R}\,, \tag{4.9}$$

$$\text{if } \omega \neq 0 \;:\quad \begin{cases} k_\mathrm{p}(\omega) = \dfrac{\left(\omega^2 - a_0\right)\cos(\tau_\mathrm{d}\omega) + k_\mathrm{a}\omega^2\cos\left((\tau_\mathrm{a} - \tau_\mathrm{d})\omega\right)}{\cos\left((\tau_\mathrm{d} - \tau_\mathrm{p})\omega\right)}\,, \\ k_\mathrm{d}(\omega) = \dfrac{\left(\omega^2 - a_0\right)\sin(\tau_\mathrm{p}\omega) - k_\mathrm{a}\omega^2\sin\left((\tau_\mathrm{a} - \tau_\mathrm{p})\omega\right)}{\omega\cos\left((\tau_\mathrm{d} - \tau_\mathrm{p})\omega\right)}\,. \end{cases} \tag{4.10}$$

Stable parameter regions in the plane $(k_\mathrm{p}, k_\mathrm{d})$ are bounded by the D-curves. The stable region changes with the control gain k_a and the delays τ_p, τ_d and τ_a. Sample D-curves are shown in Figure 4.1 for some specific parameter combinations. Loss of stabilizability can happen in many different ways corresponding to different root locations of the characteristic function. In the following, the notation $m_{s_0} = k$ will be used to indicate that the characteristic function has a root s_0 with multiplicity k.

In the next subsections, stabilizability of (4.7) is investigated. First, the critical point associated with a zero root with multiplicity 5 and with $k_\mathrm{a} = -1$ is determined in Section 4.2.1. Then, it is shown in Section 4.2.2 that there exists a stabilizable region in the space $(\tau_\mathrm{p}, \tau_\mathrm{d}, \tau_\mathrm{a})$ connecting the critical point and the origin $(\tau_\mathrm{p}, \tau_\mathrm{d}, \tau_\mathrm{a}) = (0, 0, 0)$. Finally, in Section 4.2.3, the stabilizability boundaries in the space $(\tau_\mathrm{p}, \tau_\mathrm{d}, \tau_\mathrm{a})$ are depicted in the neighborhood of the critical point.

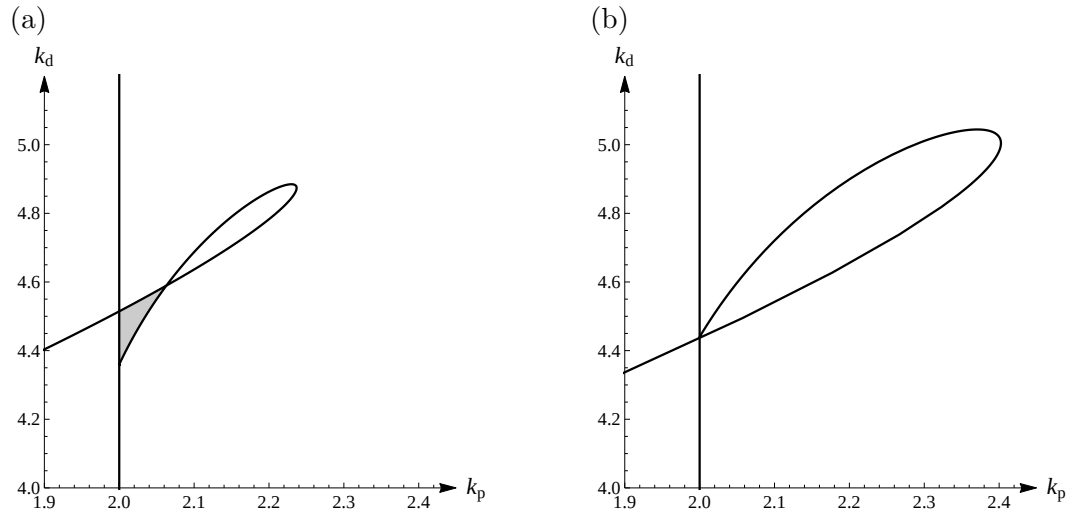

Figure 4.1: Stability charts of (4.1) if $a_0 = -2$, $\tau_d = 1.2$, $\tau_a = 3.4$, $k_a = -0.27$ for $\tau_p = 2.18$ (a) and $\tau_p = 2.22$ (b). The stable region is indicated by gray shading (a). The stable region shrinks to a single point (b).

4.2.1 Critical point: $m_0 = 5, k_a = -1$

Consider the quasipolynomial (4.7) with fixed $a_0 < 0$, and $\tau_p > 0$, $\tau_d > 0$, $\tau_a > 0$. We are looking for the critical delay defined as

$$\tau_{crit} = \sup \left\{ \min\{\tau_p, \tau_d, \tau_a\} | D(s; \tau_p, \tau_d, \tau_a) \text{ is stabilizable} \right\}. \tag{4.11}$$

In order to find the critical parameters corresponding to the critical delay, first, we investigate the maximal multiplicity of the characteristic root $s = 0$. This idea is motivated by the multiplicity-induced dominancy (MID) property [21, 18, 3]. It can be shown that the root $s = 0$ of the quasipolynomial (4.7) cannot have a multiplicity greater than or equal to 6 if $|k_a| < 1$. To see this, the system of equations $D^{(i)}(0) = 0$, $i = 0, 1, ..., 5$ should be solved for $k_p, k_d, k_a, \tau_p, \tau_d$ and τ_a. This gives two solutions for k_a: $k_{a,1} = 12.1362$ and $k_{a,2} = -7.9621$, hence in both cases the strong stability condition $|k_a| < 1$ is violated. Therefore, these parameter combinations cannot be on the stabilizability boundary.

A similar analysis shows that multiplicity 5 of $s = 0$ cannot occur if $0 \leq k_a \leq 1$. However, if $-1 \leq k_a < 0$, then multiplicity 5 can be reached: the corresponding parameters are shown by solid black line in Figure 4.2. The curve $m_0 = 5$ can be parameterized by k_a. When $k_a \to 0$, then the curve approaches an asymptote at $\tau_d = \tau_{crit}^{dPD}$ shown by dashed line. The minimum of the delays is maximal for $k_a = -1$

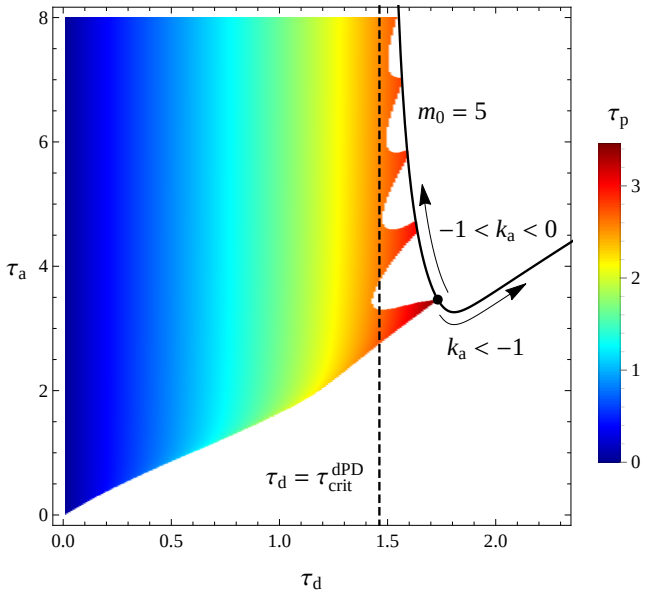

Figure 4.2: The region of feedback delays (τ_p, τ_d, τ_a) that can be stabilized by a real root s_0 with multiplicity $m_{s_0} = 5$ if $a_0 = -2$.

as shown by a black point in Figure 4.2. Therefore, we focus on the case $k_a = -1$. In this case, the control parameters and the delays satisfy the conditions $D^{(i)}(0) = 0$, $i = 0, 1, ..., 4$ and $k_a = -1$. This system of equations gives a unique solution satisfying $\tau_p, \tau_d, \tau_a > 0$:

$$\begin{aligned} &k_p = -a_0\,, \quad k_d = 2\sqrt{-6a_0}\,, \quad k_a = -1\,, \\ &\tau_p = 2\sqrt{-\frac{6}{a_0}}\,, \quad \tau_d = \sqrt{-\frac{6}{a_0}}\,, \quad \tau_a = 2\sqrt{-\frac{6}{a_0}}\,. \end{aligned} \tag{4.12}$$

With parameters (4.12) and $z = \sqrt{6}s/\sqrt{-a_0}$, the quasipolynomial (4.7) has an equivalent form

$$\widetilde{D}(z) = \left(\frac{z^2}{6} - 1\right)\sinh z + z\,. \tag{4.13}$$

In Section 4.3, we will show that (4.13) has only purely imaginary roots (including the zero root with multiplicity 5).

4.2.2 Stabilization for $\tau_d < \sqrt{-6/a_0}$

In order to stabilize (4.7), we choose the control parameters in a way that a real root s_0 has multiplicity 5, i.e. $D^{(i)}(s_0) = 0$, $i = 0, 1, .., 4$. The first three equations ($D^{(i)}(s_0) = 0$, $i = 0, 1, 2$) are linear in k_p, k_d and k_a, and the gains can be given as explicit functions of s_0, τ_p, τ_d and τ_a. Substitution into the remaining two equations

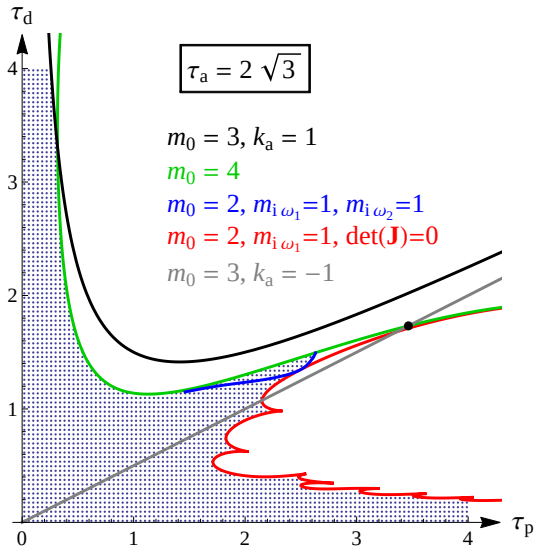

Figure 4.3: Stabilizability boundaries (colored lines) and the region of feedback delays that can be stabilized by a real root $s_0 = -\varepsilon = -0.001$ with multiplicity 2 (blueish dotted region) if $a_0 = -2$ and $\tau_a = 2\sqrt{3}$. The black dot corresponds to $(\tau_p, \tau_d) = (2\sqrt{3}, \sqrt{3})$, i.e., to the critical point $m_0 = 5, k_a = -1$.

$(D^{(i)}(s_0) = 0,\ i = 3, 4)$ gives two polynomial equations for s_0, τ_p, τ_d and τ_a. For a fixed pair $(\tau_d,\ \tau_a)$, one can find s_0 and τ_p numerically. Among the possible solutions only the ones should be considered where $s_0 < 0$ and $\tau_p > 0$. Then, one can check the stability of (4.7) by the condition $|k_a| < 1$ and by calculating the number of unstable roots according to the numerical method [117, 115]. The results are shown in Figure 4.2.

Figure 4.2 shows that for every $0 < \tau_d < \sqrt{-6/a_0}$ we can find $\tau_p, \tau_a > \tau_d$ for which (4.7) is stabilizable. That is, we can use a detuned PDA controller to stabilize the unstable open-loop system $P(s) = s^2 + a_0$ if the control-loop latency τ is smaller than $\sqrt{-6/a_0}$. Thus, we can increase the critical delay by introducing additional delays in the proportional and acceleration terms. The critical delay for detuned PDA feedback is therefore

$$\tau_{\text{crit}}^{\text{dPDA}} = \sqrt{-\frac{6}{a_0}} \approx 1.73\ \tau_{\text{crit}}^{\text{PD}}. \tag{4.14}$$

4.2.3 Stabilizability boundaries in the space (τ_p, τ_d, τ_a)

Stabilizability in the space (τ_p, τ_d, τ_a) is represented by stabilizability diagrams in the plane (τ_p, τ_d) for fixed τ_a, as shown in Figure 4.3 and Figure 4.4. Considering the multiplicity of zero and the multiplicity of purely imaginary roots $i\omega_k, \omega_k > 0$ along with the limits of strong stability $k_a = 1$ and $k_a = -1$, there are 17 algebraically

Table 4.1: Stabilizability boundaries.

	Conditions	Reduced equation
(i)	$m_0 = 4$	$3\tau_\mathrm{a}\left(2 - a_0\tau_\mathrm{p}(\tau_\mathrm{p} - 2\tau_\mathrm{d})\right) + a_0\tau_\mathrm{p}\left(\tau_\mathrm{p}^2 - 3\tau_\mathrm{d}^2\right) = 0$
(ii)	$m_0 = 3,\ k_\mathrm{a} = 1$	$4 + 2a_0\tau_\mathrm{p}\tau_\mathrm{d} - a_0\tau_\mathrm{p}^2 = 0$
(iii)	$m_0 = 3,\ k_\mathrm{a} = -1$	$\tau_\mathrm{p} - 2\tau_\mathrm{d} = 0$
(iv)	$m_0 = 2,\ m_{\mathrm{i}\omega_1} = 1,$ $\det \mathbf{J} = 0$	-
(v)	$m_0 = 2,\ m_{\mathrm{i}\omega_1} = 1,$ $m_{\mathrm{i}\omega_2} = 1$	-

possible (one-dimensional) stabilizability boundaries in a plane $(\tau_\mathrm{p}, \tau_\mathrm{d})$ with fixed τ_a. Out of the 17 cases only 4 are relevant close to the critical parameter combinations, namely cases (i), (ii), (iii) and (v) in Table 4.1, which are shown by green, black, gray and blue lines in Figure 4.3 and Figure 4.4, respectively. Note that other types of stabilizability boundaries out of the 17 ones may be relevant for other τ_a values. Furthermore, additional stabilizability boundaries may arise due to local parameter optimization. Such a boundary is given in case (iv) shown by red line in Figure 4.3 and Figure 4.4.

The conditions and equations corresponding to the stabilizability boundaries are summarized in Table 4.1. Note that stabilizability boundaries (ii) and (iii) are independent of τ_a. In the case of boundary (iv), the conditions are as follows: $D(0) = 0$, $D'(0) = 0$, $\mathrm{Re}D(\mathrm{i}\omega_1) = 0$, $\mathrm{Im}D(\mathrm{i}\omega_1) = 0$ and the Jacobian determinant of the previous four equations with respect to $(k_\mathrm{p}, k_\mathrm{d}, k_\mathrm{a}, \omega_1)$ is zero:

$$\mathbf{J} = \begin{bmatrix} 1 & 0 & 0 & 0 \\ -\tau_\mathrm{p} & 1 & 0 & 0 \\ \cos(\omega_1\tau_\mathrm{p}) & \omega_1\sin(\omega_1\tau_\mathrm{d}) & -\omega_1^2\cos(\omega_1\tau_\mathrm{a}) & \frac{\partial \mathrm{Re}D(\mathrm{i}\omega_1)}{\partial\omega_1} \\ -\sin(\omega_1\tau_\mathrm{p}) & \omega_1\cos(\omega_1\tau_\mathrm{d}) & \omega_1^2\sin(\omega_1\tau_\mathrm{a}) & \frac{\partial \mathrm{Im}D(\mathrm{i}\omega_1)}{\partial\omega_1} \end{bmatrix} \tag{4.15}$$

and

$$\det \mathbf{J} = -\omega_1^2\left(\cos(\omega_1\tau_\mathrm{a})\frac{\partial \mathrm{Im}D(\mathrm{i}\omega_1)}{\partial\omega_1} + \sin(\omega_1\tau_\mathrm{a})\frac{\partial \mathrm{Re}D(\mathrm{i}\omega_1)}{\partial\omega_1}\right). \tag{4.16}$$

The singularity of the Jacobian matrix corresponds to a local maximum or minimum of τ_p (turning point); see [75] for a similar type of stabilizability boundary.

The stabilizability boundaries in Figure 4.3 and Figure 4.4 have been verified nu-

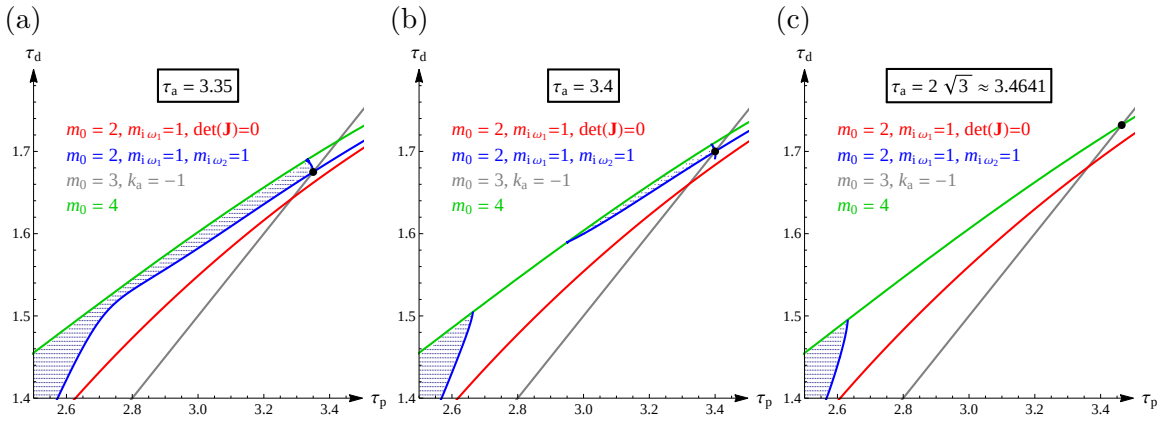

Figure 4.4: Stabilizability boundaries (colored lines) and the region of feedback delays that can be stabilized by a real root $s_0 = -\varepsilon = -0.001$ with multiplicity 2 (blueish dotted region) if $a_0 = -2$ and τ_a is approaching the critical value. The black dot corresponds to the special point $(\tau_p, \tau_d) = (\tau_a, \tau_a/2)$. If $\tau_a < 2\sqrt{3}$, then there is a finite region of stabilizability in the vicinity of the special point in the plane (τ_p, τ_d) (a,b). If $\tau_a = 2\sqrt{3}$, then the region of stabilizability shrinks to the critical point (c).

merically as follows. The equations $D^{(i)}(-\varepsilon) = 0$, $i = 0, 1$ yield unique solutions for k_p and k_d. The control gain k_a is changed between 1 and -1 with step size 0.01 until stability is achieved (if possible). With $a_0 = -2$ and fixed τ_p, τ_d and τ_a, the stability of (4.7) is checked by the numerical method [117, 115]. Stabilizable parameter points are indicated by blueish dotted regions, where each dot corresponds to the numerically investigated parameter combination. Figure 4.4 shows how the region of stabilizability changes with increasing τ_a and how the region of stabilizability disappears at the critical point.

The boundary $\tau_p = 2\tau_d$ associated with $m_0 = 3$ and $k_a = -1$ (gray line in Figure 4.3 and Figure 4.4) includes a special point indicated by black dots where $\tau_p = \tau_a$. In the critical case $\tau_a = 2\sqrt{-6/a_0}$, this special point gives the critical point. The root location at this point is further analyzed in Section 4.3.

4.3 Special points with zero spectral abscissa

In this section, we show that for every $\tau_d < \sqrt{-6/a_0}$ we can choose the control gains k_p, k_d, k_a and delays τ_p, τ_a in a way that the spectral abscissa of (4.7) is equal to zero such that $\tau_p, \tau_a > \tau_d$. This gives another aspect of the stabilizability of (4.2)–(4.3) for $\tau < \sqrt{-6/a_0}$, which was shown numerically in Section 4.2.2. If $D^{(i)}(0) = 0$, $i = 0, 1, 2$,

$k_{\mathrm{a}} = -1$, then $k_{\mathrm{p}} = -a_0$, $k_{\mathrm{d}} = -a_0\tau_{\mathrm{p}}$ and $\tau_{\mathrm{p}} = 2\tau_{\mathrm{d}}$. Assume, in addition, that $\tau_{\mathrm{p}} = \tau_{\mathrm{a}}$. Set $\tau \coloneqq \tau_{\mathrm{d}}$. Then, with $z = s\tau$ and $a = -a_0\tau^2 > 0$, the quasipolynomial (4.7) has an equivalent form

$$\widetilde{D}(z) = \left(\frac{z^2}{a} - 1\right)\sinh z + z\,. \tag{4.17}$$

Proposition 4.1. (4.17) *has roots only on the imaginary axis* ($\widetilde{D}(z_i) = 0 \Rightarrow \operatorname{Re} z_i = 0$) *if* $0 < a \leq 6$.

Proof. After the change of variables $z = u\mathrm{i}$, we analyze

$$\widehat{D}(u) = -\left(\frac{u^2}{a} + 1\right)\sin u + u\,. \tag{4.18}$$

First, we show that (4.18) has the same number of roots (counted with multiplicity) as

$$f \coloneqq -\left(\frac{u^2}{a} + 1\right)\sin u \tag{4.19}$$

in the open disks $C = \{u \in \mathbb{C} : |u| < \left(n + \frac{1}{2}\right)\pi\}$ with closed contours $\partial C = \{u \in \mathbb{C} : |u| = \left(n + \frac{1}{2}\right)\pi\}$, $n \in \mathbb{Z}^+$ if $n > N(a)$ for some $N(a)$. Let us use the notation $r_n \coloneqq \left(n + \frac{1}{2}\right)\pi$. On the closed contours ∂C

$$|f| = \left|\frac{u^2}{a} + 1\right||\sin u| \geq \left|\frac{|u|^2}{a} - 1\right||\sin u| = \left(\frac{r_n^2}{a} - 1\right)|\sin u| \geq \frac{r_n^2}{a} - 1 \tag{4.20}$$

since $|\sin u| \geq 1$ on ∂C (see Lemma 4.1 below). In order to use Rouché's theorem, set $g \coloneqq \widehat{D} - f = u$. On ∂C we have $|g| = r_n$. Therefore f and $\widehat{D}(u) = f + g$ has the same number of roots in C if

$$\frac{r_n^2}{a} - 1 > r_n\,, \tag{4.21}$$

which is true if n is large enough. More precisely if

$$r_n > \frac{a + \sqrt{a^2 + 4a}}{2} \tag{4.22}$$

or equivalently

$$n > \frac{a + \sqrt{a^2 + 4a}}{2\pi} - \frac{1}{2} =: N(a)\,, \tag{4.23}$$

then (4.21) holds. Note that $N(0) = -0.5$, $N(6) \approx 1.6877$, and $N(a)$ is strictly increasing with a.

Next, we show that the number of roots of f is equal to the number of real roots of $\widehat{D}(u)$ in regions C, and therefore $\widehat{D}(u)$ has only real roots. On the one hand, the roots of f are $\pm\mathrm{i}\sqrt{a}$ and the roots of $\sin u$: $k\pi$, $k \in \mathbb{Z}$. Since $\sqrt{a} \leq \sqrt{6} < 3\pi/2$, the number of roots of f in $|u| < r_n$, $n \geq 1$ is $2n+3$. On the other hand, it can be shown that $\widehat{D}(r_{2k}) < 0$ and $\widehat{D}(r_{2k-1}) > 0$ if $0 < a \leq 6$ and $k \geq 1$ (see Lemma 4.2 below). Therefore, $\widehat{D}(u)$ has a root in every interval $]r_n, r_{n+1}[$, $n \geq 1$ by Bolzano's theorem. Moreover, 0 is a root with multiplicity 3 if $0 < a < 6$, and with multiplicity 5 if $a = 6$. If $0 < a < 6$, then there is an additional root in $]0, r_1[$ since $\widehat{D}^{(3)}(0) = 1 - 6/a < 0$. Since $\widehat{D}(u)$ is an odd function, this gives $2n+3$ real roots in $|u| < r_n$, $n \geq 1$. □

We can also show that it is necessary to assume that $a \leq 6$.

Proposition 4.2. *If $a > 6$, then (4.17) has a pair of real roots $\pm\gamma$, $\gamma \neq 0$.*

Proof. If $a > 6$, then $\widetilde{D}^{(3)}(0) = -1+6/a < 0$. Furthermore, $\lim_{x\to\infty} \widetilde{D}(x) = \infty$. Therefore, $\widetilde{D}(z)$ has at least one positive real root γ. Since $\widetilde{D}(z)$ is an odd function, it also has a negative real root $-\gamma$. □

Remark 4.1. In the critical case $a = 6$, (4.17) has infinitely many roots on the imaginary axis (including a real root $\gamma = 0$ with multiplicity 5). Numerical analysis in Section 4.2.3 shows that if $a \leq 6$, then there is a neighborhood of the special point in the space of parameters $(k_\mathrm{p}, k_\mathrm{d}, k_\mathrm{a}, \tau_\mathrm{p}, \tau_\mathrm{d}, \tau_\mathrm{a})$ where all the infinitely many roots of (4.7) have negative real parts (see the blueish dotted regions in Figure 4.4a and Figure 4.4b). In these narrow regions, however, the system may be sensitive to parameter uncertainties.

The following two lemmas have been used in the proof of Proposition 4.1.

Lemma 4.1. $|\sin u| \geq 1$ *on* $\partial C = \{u \in \mathbb{C} : |u| = r_n\}$, $r_n = \left(n + \frac{1}{2}\right)\pi$, $n \in \mathbb{Z}^+$.

Proof. With $z = r\mathrm{e}^{\mathrm{i}\varphi}$ and $r, \varphi \in \mathbb{R}$, $r > 0$

$$|\sin z|^2 = \frac{1}{2}\left(\cosh(2r\sin\varphi) - \cos(2r\cos\varphi)\right) \tag{4.24}$$

and

$$\frac{\partial|\sin z|^2}{\partial\varphi} = r\left(\cos\varphi\sinh(2r\sin\varphi) - \sin\varphi\sin(2r\cos\varphi)\right). \tag{4.25}$$

Since (4.24) is even and π-periodic in φ, it is enough to consider the interval $0 \leq \varphi \leq \pi/2$. If $0 < \varphi < \pi/2$, then $\sin\varphi > 0$ and $\cos\varphi > 0$. Using $\sin x < x$ and $\sinh x > x$ for $x > 0$, $x \in \mathbb{R}$, we have

$$\frac{\partial |\sin z|^2}{\partial \varphi} > 0\,, \quad 0 < \varphi < \pi/2\,. \tag{4.26}$$

Therefore, for a given r, (4.24) has a global minimum at $\varphi = 0$, and the minimum value is $\sin^2 r$. Thus, $|\sin z|^2 \geq \sin^2 r$. With $r = r_n = \left(n + \frac{1}{2}\right)\pi$ we have $|\sin z|^2 \geq 1$. □

Lemma 4.2. *$\widehat{D}(r_{2k}) < 0$ and $\widehat{D}(r_{2k-1}) > 0$ if $0 < a \leq 6$ and $k \geq 1$.*

Proof. If $r_n < \frac{r_n^2}{a} + 1$ and $n = 2k$, then

$$\widehat{D}(r_{2k}) = (-1)^{2k+1}\left(\frac{r_{2k}^2}{a} + 1\right) + r_{2k} < \left(1 + (-1)^{2k+1}\right)\left(\frac{r_{2k}^2}{a} + 1\right) = 0\,. \tag{4.27}$$

The condition $r_n < \frac{r_n^2}{a} + 1$ holds for $0 < a \leq 6$ and $n \geq 2$. For $n = 2k - 1$ we have

$$\widehat{D}(r_{2k-1}) = (-1)^{2k}\left(\frac{r_{2k-1}^2}{a} + 1\right) + r_{2k-1} > 0\,. \tag{4.28}$$

□

4.4 Conclusion

The critical delay and the corresponding critical parameters (feedback delays $\tau_\mathrm{p}, \tau_\mathrm{d}, \tau_\mathrm{a}$ and control gains $k_\mathrm{p}, k_\mathrm{d}, k_\mathrm{a}$) are summarized in Table 4.2 for PD, detuned PD, PDA and detuned PDA feedbacks. Detuning the feedback terms in PD feedback increases the achievable feedback delay by 47% [99]. Adding acceleration feedback increases the critical delay by 41% (by a factor of $\sqrt{2}$) [99]. Here, we have shown that the critical delay can further be increased, up to 73% (by a factor of $\sqrt{3}$) via employing detuned PDA feedback. This improved stabilizability can be exploited by assigning a negative real root with multiplicity 5. That is, this way we can always construct a stabilizing controller for any feedback delay smaller than the critical delay.

Two interesting features can be observed in Table 4.2. First, for both detuned PD and detuned PDA feedback the critical delay is limited by the delay τ_d in the derivative term. This observation suggests that it is more crucial to decrease the feedback delay in the derivative term than in the proportional and the acceleration terms. Second, for detuned PDA feedback, the acceleration control gain at the critical point is $k_\mathrm{a} = -1$,

Table 4.2: Critical parameters for $a_0 = -2$

	PD	detuned PD	PDA	detuned PDA
τ_p	$\sqrt{-\frac{2}{a_0}} = 1$	$\sqrt{6+4\sqrt{3}}\sqrt{-\frac{1}{a_0}} = 2.54$	$\frac{2}{\sqrt{-a_0}} = 1.41$	$2\sqrt{-\frac{6}{a_0}} = 3.46$
τ_d	$\sqrt{-\frac{2}{a_0}} = 1$	$\sqrt{\frac{6+4\sqrt{3}}{3}}\sqrt{-\frac{1}{a_0}} = 1.47$	$\frac{2}{\sqrt{-a_0}} = 1.41$	$\sqrt{-\frac{6}{a_0}} = 1.73$
τ_a	-	-	$\frac{2}{\sqrt{-a_0}} = 1.41$	$2\sqrt{-\frac{6}{a_0}} = 3.46$
k_p	$-a_0 = 2$	$-a_0 = 2$	$-a_0 = 2$	$-a_0 = 2$
k_d	$\sqrt{-2a_0} = 2$	$\sqrt{6+4\sqrt{3}}\sqrt{-a_0} = 5.08$	$2\sqrt{-a_0} = 2.83$	$2\sqrt{-6a_0} = 6.93$
k_a	-	-	1	-1
τ_crit	$\sqrt{-\frac{2}{a_0}} = 1$	$\sqrt{\frac{6+4\sqrt{3}}{3}}\sqrt{-\frac{1}{a_0}} = 1.47$	$\frac{2}{\sqrt{-a_0}} = 1.41$	$\sqrt{-\frac{6}{a_0}} = 1.73$

which is just the opposite of $k_\mathrm{a} = 1$ corresponding to the critical delay for the single-delay PDA feedback. Such an inverse control logic might seem unnatural, still there is a consequent conception behind: the acceleration signal is typically in antiphase to the position; hence, negative feedback of the acceleration contributes as a kind of positive position feedback.

It should be mentioned that $\tau < \tau_\mathrm{crit}^\mathrm{PD}$ and $\tau < \tau_\mathrm{crit}^\mathrm{PDA}$ for PD and PDA feedback both give necessary and sufficient conditions for stabilizability. However, for detuned PD and PDA feedback, the conditions $\tau < \tau_\mathrm{crit}^\mathrm{dPD}$ and $\tau < \tau_\mathrm{crit}^\mathrm{dPDA}$ are "only" sufficient, and necessity has not been proved yet (to the best of the author's knowledge). Hence, further extension of the critical delay might be possible. Complete characterization of the stabilizable region and the stabilizability boundaries in the $(\tau_\mathrm{p}, \tau_\mathrm{d}, \tau_\mathrm{a})$ space is, however, a more complex problem. Here, only some sample stabilizability diagrams were shown for fixed values of τ_a in the neighborhood of the critical point. It was already observed that the special points discussed in Section 4.3 are sources of different types of stabilizability boundaries associated with different root locations.

4.5 Main results

It has been shown that the critical delay for the delayed feedback control of the inverted pendulum can be extended by using detuned proportional-derivative-acceleration feedback. The corresponding critical delay is significantly larger than that of proportional-derivative feedback, proportional-derivative-acceleration feedback and detuned proportional-derivative feedback.

Contribution 3

Consider the delayed feedback system

$$\ddot{\varphi}(t) + a_0\varphi(t) = u(t-\tau)$$

with detuned proportional-derivative-acceleration feedback

$$u(t) = -k_\mathrm{p}\varphi(t-\delta_\mathrm{p}) - k_\mathrm{d}\dot{\varphi}(t-\delta_\mathrm{d}) - k_\mathrm{a}\ddot{\varphi}(t-\delta_\mathrm{a})\,,$$

where $a_0 < 0$ is the fixed plant parameter, $\tau > 0$ is the feedback delay, k_p, k_d, k_a are the control gains, and $\delta_\mathrm{p} \geq 0$, $\delta_\mathrm{d} \geq 0$, $\delta_\mathrm{a} \geq 0$ are delay detunings. The system can be stabilized using an appropriate choice of the control parameters k_p, k_d, k_a and δ_p, δ_d, δ_a if τ is smaller than the critical delay

$$\tau_\mathrm{crit}^\mathrm{dPDA} = \sqrt{-\frac{6}{a_0}}\,.$$

This value is larger by a factor of $\sqrt{3}$ than the critical delay of the proportional-derivative feedback with a single delay.

Related publications: [10].

Chapter 5

Inverted pendulum subject to fractional-order PD feedback

As was shown in Chapter 4, the critical delay for delayed feedback control of the inverted pendulum can be extended by detuning the delays. In this chapter, the effect of delay detuning is investigated for fractional-order proportional-derivative feedback.

Introducing fractional-order derivative in the feedback loop allows us to exploit the time history starting from some initial time to the current time instant. This can be seen from the most frequently used definitions of fractional derivative: the Riemann–Liouville fractional derivative, the Caputo fractional derivative and the Grünwald–Letnikov fractional derivative. All of these definitions of the fractional derivative resembles a distributed delay term. Implementation of fractional-order feedback is, therefore, computationally challenging.

The different delays originate in the different sensory systems used for the perception of position and velocity. In engineering applications, the operation of position and velocity sensors is different; therefore, they typically result in different delays in the feedback loop. In human postural balance, as a biological application, position and velocity information are obtained by the static and dynamic receptors of the inner ear, which induces that the corresponding delays are different. When the velocity is calculated as a discrete difference of the position, then signal processing introduces an extra delay.

5.1 Problem statement

We consider the PD$^\mu$ control of an inverted pendulum with different delays in the proportional and the fractional derivative terms. The characteristic function of the system under investigation reads

$$D(s) = s^2 + a_0 + k_\mathrm{p}\mathrm{e}^{-s\tau_\mathrm{p}} + k_\mathrm{d}s^\mu\mathrm{e}^{-s\tau_\mathrm{d}}\,, \tag{5.1}$$

where $a_0 < 0$ is the plant parameter, $\tau_\mathrm{p} > 0$ and $\tau_\mathrm{d} > 0$ are the feedback delays, and $0 < \mu < 2$ is the order of the fractional derivative term. System (5.1) is said to be stabilizable for given delays τ_p and τ_d if there exist some control gains k_p, k_d and derivative order μ for which (5.1) is stable (i.e., (5.1) has roots with negative real parts only). The goal of this chapter is to determine the critical delay τ_crit as the maximum of $\min\{\tau_\mathrm{p}, \tau_\mathrm{d}\}$ such that (5.1) is still stabilizable.

Similarly to Chapter 4, one can also think of (5.1) as a control system with a single control-loop latency τ and some additional delays (or delay detunings) δ_p and δ_d. This concept leads to

$$D(s) = s^2 + a_0 + k_\mathrm{p}\mathrm{e}^{-s(\tau+\delta_\mathrm{p})} + k_\mathrm{d}s^\mu\mathrm{e}^{-s(\tau+\delta_\mathrm{d})} \tag{5.2}$$

with $\delta_\mathrm{p} \geq 0$ and $\delta_\mathrm{d} \geq 0$. In this sense, the system is stabilizable for a given τ if there exist some k_p, k_d, μ, and δ_p, δ_d for which (5.2) is stable. In the following, we refer to (5.2) as detuned PD$^\mu$ feedback. The goal can be rephrased as follows. We are looking for the critical delay τ_crit for the detuned PD$^\mu$ feedback (5.2) such that if $\tau < \tau_\mathrm{crit}$, then (5.2) can be stabilized with an appropriate choice of k_p, k_d, μ and δ_p, $\delta_\mathrm{d} \geq 0$.

The chapter is organized as follows. After some preliminary thoughts, some special cases are discussed in Section 5.3. In Section 5.4, stabilizability diagrams are constructed and their change is analyzed with respect to the order of the fractional derivative in order to find the critical delay.

5.2 Preliminaries

Stability of controllable single-input linear time-invariant fractional-order time-delay systems can be investigated using their characteristic function: the system is BIBO (bounded-input bounded-output) stable if and only if the roots of the characteristic function have negative real part on the first Riemann sheet [69, 12, 82]. Consequently, the D-subdivision method can be applied to (5.1) as follows.

Substitution of $s = 0$ and $s = \pm \mathrm{i}\omega$, $\omega > 0$ into $D(s) = 0$ gives the D-curves

$$s = 0 : k_\mathrm{p} = -a_0 \,, \quad k_\mathrm{d} \in \mathbb{R} \,, \tag{5.3}$$

$$s = \pm \mathrm{i}\omega : \begin{cases} k_\mathrm{p} = \left(\omega^2 - a_0\right) \dfrac{\sin(\frac{\mu\pi}{2} - \tau_\mathrm{d}\omega)}{\sin\left(\frac{\mu\pi}{2} - (\tau_\mathrm{d} - \tau_\mathrm{p})\omega\right)} \,, \\ k_\mathrm{d} = \left(\omega^2 - a_0\right) \dfrac{\sin(\tau_\mathrm{p}\omega)}{\omega^\mu \sin\left(\frac{\mu\pi}{2} - (\tau_\mathrm{d} - \tau_\mathrm{p})\omega\right)} \,. \end{cases} \tag{5.4}$$

The D-curves bound the parameter regions in the plane $(k_\mathrm{p}, k_\mathrm{d})$ where the number of unstable characteristic roots is constant. Stable regions (zero unstable characteristic roots) can be determined by the argument principle [112, 74]. When the delays increase, then the stable regions typically shrink and disappear. There is a critical delay $\tau_\mathrm{crit}^{\mathrm{dPD}^\mu}$: if $\min\{\tau_\mathrm{p}, \tau_\mathrm{d}\} > \tau_\mathrm{crit}^{\mathrm{dPD}^\mu}$, then the system (5.1) cannot be stabilized by any triplet $(k_\mathrm{p}, k_\mathrm{d}, \mu)$. The goal is to determine the stabilizability boundaries in the plane $(\tau_\mathrm{p}, \tau_\mathrm{d})$ and to find $\tau_\mathrm{crit}^{\mathrm{dPD}^\mu}$.

5.3 Special cases

Special cases can be defined either by setting the fractional order μ to integer or by setting $\tau_\mathrm{p} = \tau_\mathrm{d}$.

5.3.1 Integer-order controllers: $\mu = 0$, $\mu = 1$ and $\mu = 2$

Special cases $\mu = 0$ and $\mu = 1$ were already analyzed in [99]. If $\mu = 0$ and $\tau_\mathrm{p} \neq \tau_\mathrm{d}$ then one gets the proportional minus delay (PMD) controller of [99]. In this case, a non-semisimple triple-zero eigenvalue occurs at the limit of stabilizability, which corresponds to the parameter combinations

$$k_\mathrm{p} = -\frac{a_0\tau_\mathrm{d}}{\tau_\mathrm{d} - \tau_\mathrm{p}} \,, \quad k_\mathrm{d} = \frac{a_0\tau_\mathrm{p}}{\tau_\mathrm{d} - \tau_\mathrm{p}} \,, \quad \tau_\mathrm{d} = -\frac{2}{a_0\tau_\mathrm{p}} \,. \tag{5.5}$$

Equation (5.5) gives a hyperbolic relation between the delays (see Figure 5.1a). Note that τ_d is a strictly decreasing function of τ_p, therefore $\min\{\tau_\mathrm{p}, \tau_\mathrm{d}\}$ is maximal if τ_p approaches τ_d. The limit case $\tau_\mathrm{p} \to \tau_\mathrm{d}$ would give the critical delay $\tau_\mathrm{crit}^{\mathrm{PMD}} = \sqrt{-2/a_0} = \tau_\mathrm{crit}^{\mathrm{PD}}$. However, at the limit case $\tau_\mathrm{p} = \tau_\mathrm{d}$, the control gains k_p and k_d are singular. This limit case corresponds to a proportional feedback with a single delay $\tau = \tau_\mathrm{p} = \tau_\mathrm{d}$, which cannot stabilize the inverted pendulum as explained below. Due to the necessary

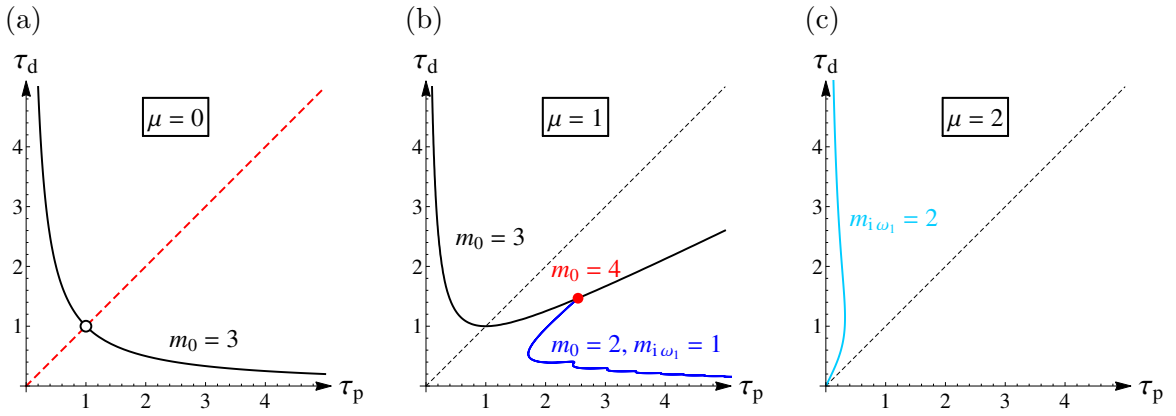

Figure 5.1: The stabilizability boundaries and multiplicity conditions in the plane (τ_p, τ_d) if $\mu = 0$ (a), $\mu = 1$ (b) and $\mu = 2$ (c) with $a_0 = -2$.

condition in [53], if the quasipolynomial $f(s) = e^{s\tau}(s^2 + a_0) + k_p$ is stable, then $f'(s) = e^{s\tau}(\tau s^2 + 2s + a_0\tau)$ should also be stable. However, this is not true, since $a_0 < 0$ and $\tau > 0$. Hence, $f(s)$ cannot be stable. Alternatively, it can be seen that the inverted pendulum cannot be stabilized by delayed PD feedback if $k_d = 0$ since $k_d > -a_0\tau$ is a necessary condition for stabilization [102, 48].

The case $\mu = 1$ corresponds to the detuned PD (dPD) controller in [99], where it was shown that the critical delay can be extended to $\tau_{crit}^{dPD} \approx 1.47\,\tau_{crit}^{PD}$. The stabilizability boundaries for this case were given in [10] and are shown in Figure 5.1b. The critical parameter combination is indicated by a red dot, where there is a root $s = 0$ with multiplicity 4 ($m_0 = 4$). At this point, the ratio of the delays is $\tau_p/\tau_d = \sqrt{3}$. This critical point is given as the intersection of two parametric curves indicated by black and blue lines in Figure 5.1b. The black curve is associated with a triple root $s = 0$ ($m_0 = 3$), and the blue curve is associated with a combination of a double root $s = 0$ ($m_0 = 2$) and a pair of purely imaginary roots ($m_{i\omega_1} = 1$). For further details on this case, see [10].

The case $\mu = 2$ corresponds to a detuned proportional-acceleration (dPA) feedback, i.e., a detuned PDA feedback with $k_d = 0$. If $\tau_p = \tau_d$, then the system cannot be stabilized similarly to the case $\mu = 0$. If delay detuning is allowed, then the system can be stabilized and the critical delay is $\tau_{crit}^{dPA} \approx 0.32\,\tau_{crit}^{PD}$. The stabilizability boundary shown in Figure 5.1c was derived using the methods explained later in Subsection 5.4.1.

A special combination of the cases $\mu = 1$ and $\mu = 2$ gives the detuned PDA feedback, which was investigated in Chapter 4. The idea of integer-order delayed proportional-derivative and derivative-acceleration controllers was also addressed in [113] in the case

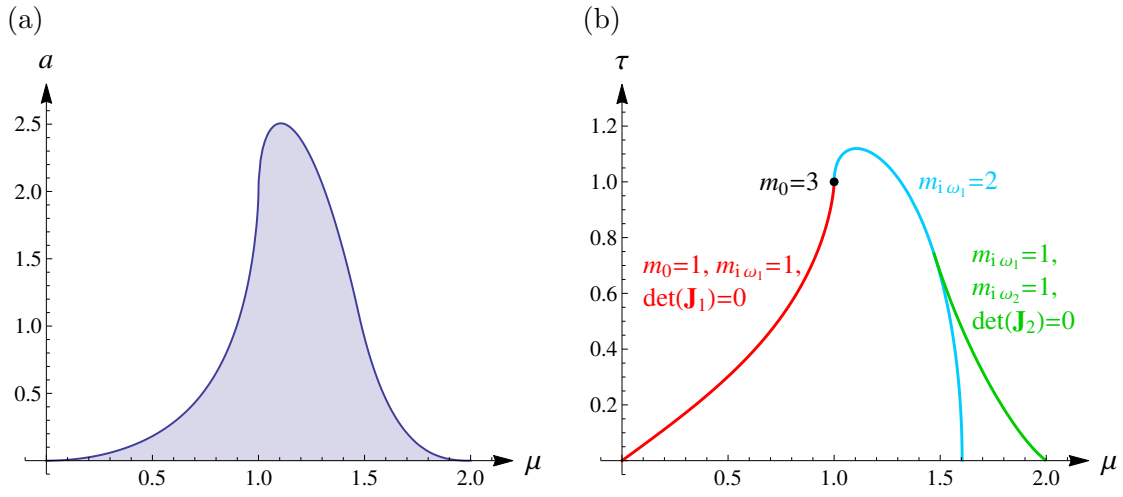

Figure 5.2: Stabilizable region of (5.1) if $\tau_\mathrm{p} = \tau_\mathrm{d} = \tau$ with $a = -a_0\tau^2$ (a). The stabilizability boundaries and multiplicity conditions in the plane (μ, τ) if $a_0 = -2$ (b).

of the damped harmonic oscillator.

5.3.2 PD$^\mu$ controller with a single delay

In the special case $\tau_\mathrm{p} = \tau_\mathrm{d} = \tau$, the stabilizable region can be derived in the plane of the dimensionless parameters $a = -a_0\tau^2$ and μ (see Figure 5.2a). Using the D-subdivision technique, one can observe four types of loss of stabilizability. These geometric conditions can directly be translated into the multiplicity conditions shown in Figure 5.2b. The stabilizability boundary consist of three segments:

1. There is a single zero root ($s = 0$) and a single pair of purely imaginary roots ($s = \pm\mathrm{i}\omega_1$, $\omega_1 > 0$) with an additional condition

$$\det \mathbf{J}_1 = 0\,, \tag{5.6}$$

where $\mathbf{J}_1$ is the Jacobian matrix of equations

$$D(0) = 0, \quad \mathrm{Re}D(\mathrm{i}\omega_1) = 0, \quad \mathrm{Im}D(\mathrm{i}\omega_1) = 0 \tag{5.7}$$

with respect to k_p, k_d, and ω_1 (for more details, see Appendix A.2). Thus, equation (5.6) represents the singularity of the Jacobian matrix $\mathbf{J}_1$. The geometric interpretation of this condition is the tangency of the D-curves at the critical point similarly to the case shown in Figure 5.3a. This segment is indicated by red line

in Figure 5.2b. A similar type of stabilizability boundary can be seen in [75] (where this phenomenon is referred to as a turning point).

2. There is a double pair of purely imaginary roots shown by blue line in Figure 5.2b. The corresponding geometric interpretation is a loop-cusp transition of the stable region similarly to the case shown in Figure 5.3c.

3. There are two pairs of purely imaginary roots ($s = \pm \mathrm{i}\omega_1$, $\omega_1 > 0$ and $s = \pm \mathrm{i}\omega_2$, $\omega_2 > 0$) with an additional condition

$$\det \mathbf{J}_2 = 0\,, \tag{5.8}$$

where $\mathbf{J}_2$ is the Jacobian matrix of equations

$$\begin{aligned} &\mathrm{Re}D(\mathrm{i}\omega_1) = 0\,, \quad \mathrm{Im}D(\mathrm{i}\omega_1) = 0\,, \\ &\mathrm{Re}D(\mathrm{i}\omega_2) = 0\,, \quad \mathrm{Im}D(\mathrm{i}\omega_2) = 0 \end{aligned} \tag{5.9}$$

with respect to k_p, k_d, ω_1, and ω_2. In this case, the stable region disappears as the complex root boundary crosses itself tangentially similarly to the case shown in Figure 5.3f. This stabilitability boundary is shown by green line in Figure 5.2b.

At the connection point of segments 1 and 2, there is a triple zero root ($s = 0$) similarly to the case shown in Figure 5.3b.

5.4 Stabilizability analysis

The main goal is to determine the stabilizable region in the plane $(\tau_\mathrm{p}, \tau_\mathrm{d})$ for the general case ($0 < \mu < 2$). Then, the critical delay for (5.2) can also be obtained by analyzing the changes of the stabilizability boundaries for varying μ.

5.4.1 Constructing stabilizability diagrams in the plane $(\tau_\mathrm{p}, \tau_\mathrm{d})$

Stabilizability can be investigated by observing the change of the stable parameter region with respect to the change of some other parameters. Figure 5.4 shows an example how the stable region in the parameter plane $(k_\mathrm{p}, k_\mathrm{d})$ (bounded by the loop of (5.4)) changes as parameter τ_p is increased if $\mu = 1.2$ and $\tau_\mathrm{d} = 0.58$ with $a_0 = -2$. The stable region shrinks to a single point if $\tau_\mathrm{p} \approx 1.19$. At this critical point, the characteristic function has two distinct pairs of purely imaginary roots since the

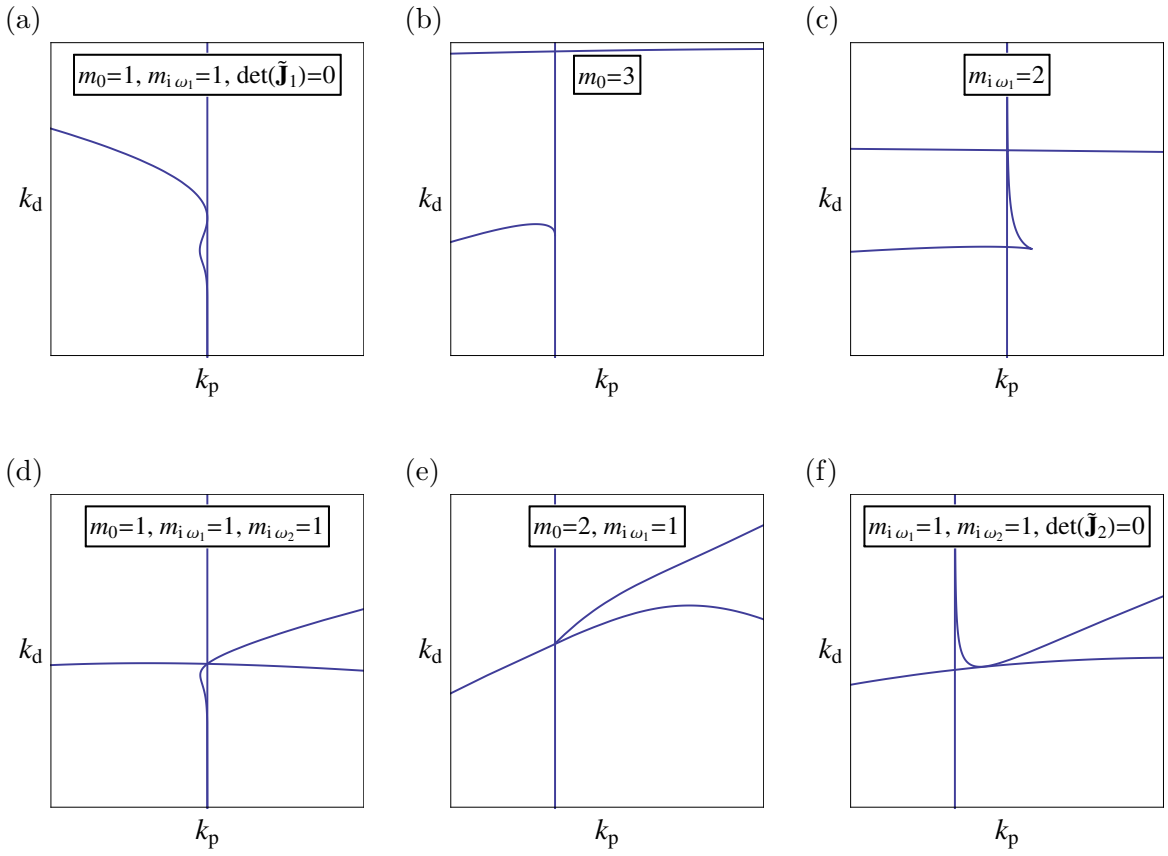

Figure 5.3: Stability charts: types of loss of stabilizability and the corresponding multiplicity conditions. Here, $\tilde{\mathbf{J}}_1$ is the Jacobian matrix of (5.7) with respect to k_{p}, k_{d}, and ω_1.

complex root boundary (5.4) touches itself. The tangency at the critical point imposes another condition, namely, $\det \tilde{\mathbf{J}}_2 = 0$. Here, $\tilde{\mathbf{J}}_2$ is the Jacobian matrix of (5.9) with respect to k_{p}, k_{d}, ω_1, and ω_2.

The multiplicity conditions in Subsection 5.3.2 give a uniform description of the stabilizability boundaries. Furthermore, the techniques in Subsection 5.3.2 can also be applied if $\tau_{\mathrm{p}} \neq \tau_{\mathrm{d}}$. That is, the stabilizability boundaries can be obtained following the steps below.

1. Geometric conditions at the limit of stabilizability should be detected by D-subdivision as shown in Figure 5.4. Different parameter regions exhibit different types of loss of stabilizability. Here, six different geometric conditions are distinguished, which are represented in Figure 5.3.

2. Geometric conditions should be translated into multiplicity conditions. The mul-

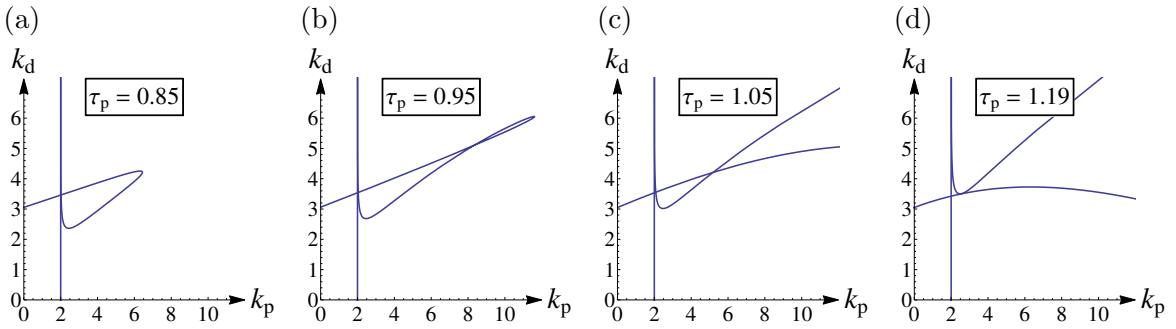

Figure 5.4: Stability charts of (5.1) if $\mu = 1.2$ and $\tau_d = 0.58$ with $a_0 = -2$. The critical point corresponds to $m_{i\omega_1} = 1$, $m_{i\omega_2} = 1$ and $\det \tilde{\mathbf{J}}_2 = 0$.

tiplicity conditions corresponding to the critical points are also shown in Figure 5.3. Note that multiplicity condition $m_{i\omega_1} = 1$, $m_{i\omega_2} = 1$, $m_{i\omega_3} = 1$ is also possible algebraically, but was not found to be relevant.

3. Each multiplicity condition gives a nonlinear system of $M + 3$ equations for variables k_p, k_d, τ_p, τ_d, μ and ω_i, $i = 1, \ldots, M$ for some M that could also be 0. If μ and τ_p or τ_d are fixed, then this system of equations could be solved for the rest of the variables. These nonlinear systems of equations are linear in k_p and k_d, therefore reduced systems of equations can be obtained by solving two of the equations for k_p and k_d. Then, only the remaining equations have to be solved numerically.

4. A solution can be represented by a point in the plane (τ_p, τ_d) for a fixed μ. In order to find an initial solution, a critical point and the corresponding parameter values (obtained by D-subdivision) can be used as an initial guess. If the reduced system of equations consists of less than three equations, then contour plots of these equations also give insight into the possible initial solutions. Then, such an (initial) point can be extended to a curve (that is, to a stabilizability boundary) by using numerical continuation. Pseudo-arclength continuation allows us to follow the solution curve even if the tangent is vertical (or horizontal).

An example for the stabilizability boundaries is shown in Figure 5.5 for $\mu = 1.2$. Two types of loss of stabilizability may show up: a pair of purely imaginary roots with multiplicity two indicated by blue line; and two distinct pairs of purely imaginary roots with and additional condition $\det(\tilde{\mathbf{J}}_2) = 0$ indicated by green line.

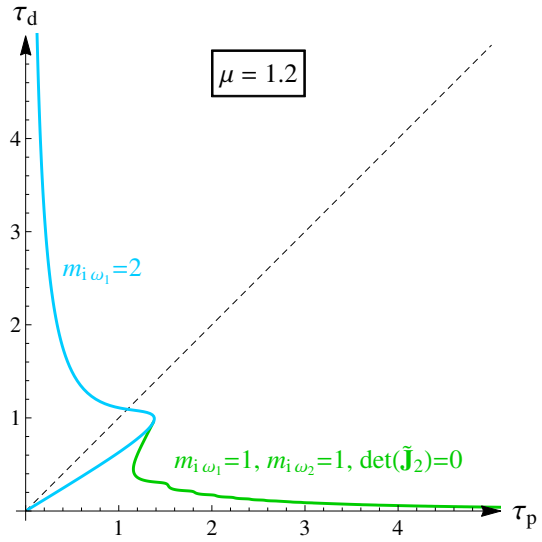

Figure 5.5: The stabilizability boundaries and multiplicity conditions in the plane (τ_p, τ_d) if $\mu = 1.2$ with $a_0 = -2$.

5.4.2 Changes in stabilizability for varying μ

Figure 5.6 shows the stabilizability boundaries in the plane (τ_p, τ_d) for different values of μ in the neighborhood of $\mu = 1$. The stabilizable region can be extended compared to the detuned PD controller ($\mu = 1$) by choosing an appropriate value of the fractional order μ. The line $\tau_d = \tau_p/\sqrt{3}$ passes through the critical point of the case $\mu = 1$ and separates the plane (τ_p, τ_d) into two regions. If $\tau_d < \tau_p/\sqrt{3}$, then it can be beneficial to use a fractional derivative of order less than 1. On the other hand, if $\tau_d > \tau_p/\sqrt{3}$, then the fractional-order derivatives of order greater than 1 may show better stabilizability properties.

5.4.3 Critical delay in the sense of detuned fractional-order PD feedback

We can draw more conclusions from the stabilizability diagrams. For every μ, we can find a point in the stabilizable region where the minimum of τ_p and τ_d is maximal. The path of this point is shown by red line in Figure 5.7a if $\mu \leq 1$. In Figure 5.7b, the critical delay (related to the detuned fractional-order PD feedback (5.2)) is shown as a function of μ in the left neighborhood of $\mu = 1$.

The largest admissible delay is obtained for $\mu = 0.999637$. In this case, the critical delay is

$$\tau_{\text{crit}}^{\text{dPD}^\mu} = 1.479\tau_{\text{crit}}^{\text{PD}}, \tag{5.10}$$

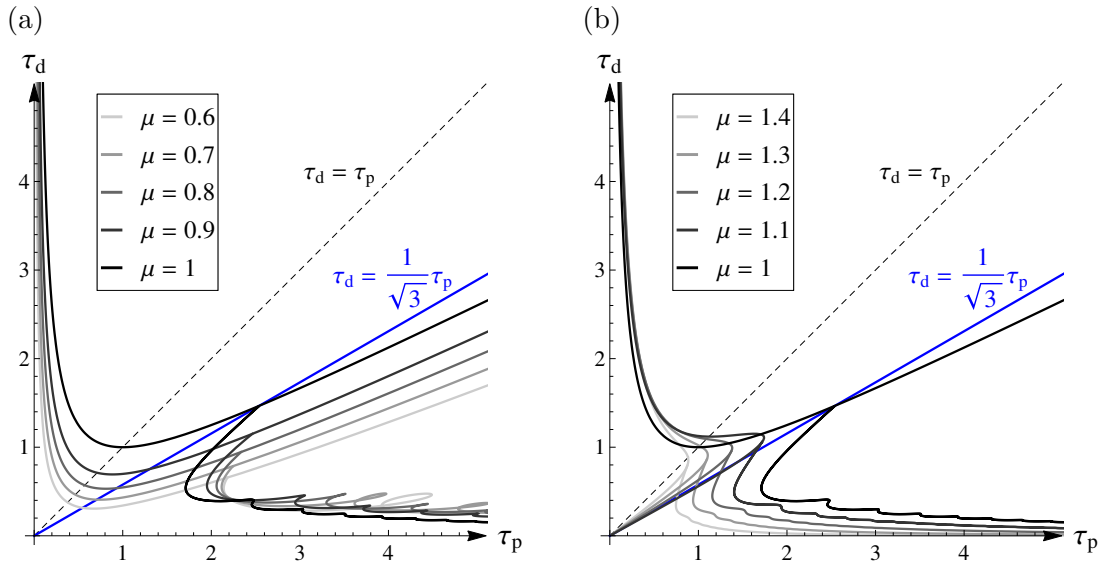

Figure 5.6: The stabilizability boundaries in the plane (τ_p, τ_d) if $\mu \leq 1$ (a) and $\mu \geq 1$ (b) with $a_0 = -2$. Stabilizable regions are to the left of the curves.

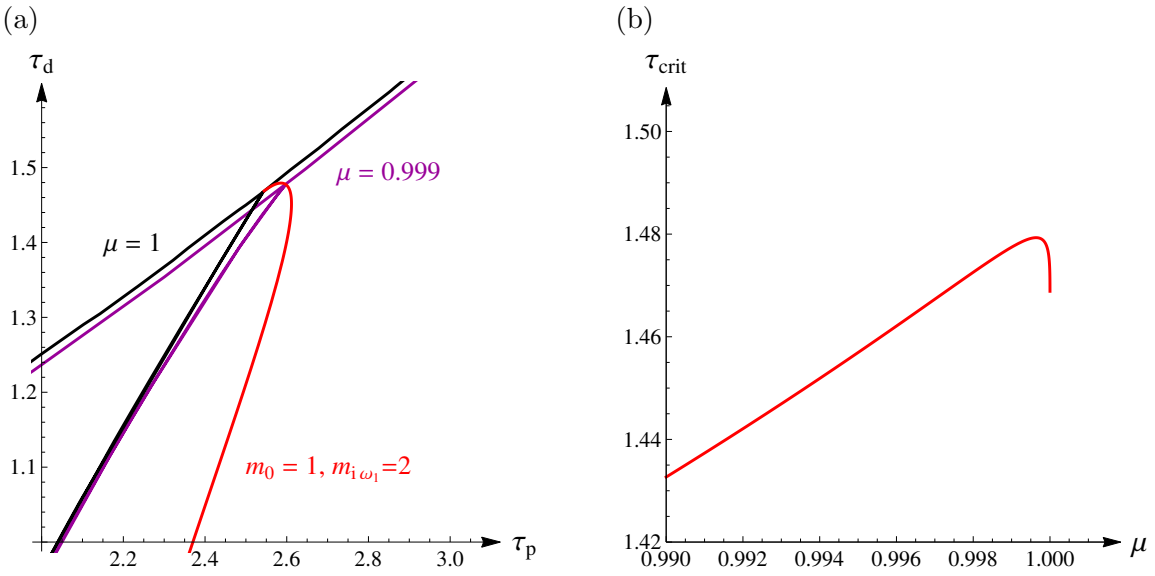

Figure 5.7: The path of the critical point in the plane (τ_p, τ_d) if $\mu \leq 1$ (a) and the critical delay for $0.99 \leq \mu \leq 1$ (b) with $a_0 = -2$.

where τ_{crit}^{PD} is the critical delay for single-delay PD feedback. Since $\tau_{crit}^{dPD} = 1.468\tau_{crit}^{PD}$, the extension caused by employing fractional-order PD feedback is not significant: $\tau_{crit}^{dPD^\mu} = 1.00778\tau_{crit}^{dPD}$.

Table 5.1: Critical delays for $a_0 = -2$.

	PD	detuned PD	PD$^\mu$	detuned PD$^\mu$
τ_{crit}	1	1.468	1.120	1.479

5.5 Conclusion

Table 5.1 shows how the numerical values of the critical delay compare to each other in the case of the PD, detuned PD, fractional-order PD and detuned fractional-order PD controllers. As can be seen, the critical delay for the detuned PD$^\mu$ controller is slightly larger than that of the detuned PD controller, namely, by a factor of 1.00778. Although this gain in the critical delay is practically insignificant, there are some cases when fractional-order feedback may still be beneficial. If there are some constraints on the delays τ_{p} and τ_{d}, then fractional-order feedback may stabilize a system that cannot be stabilized by integer-order feedback. This can be seen by the extended stabilizable region for different derivative orders μ in Figure 5.6.

Stability of fractional-order systems can also be analyzed using numerical techniques. If time delay is also present in the system, then the combination of fractional-order dynamics with the infinite-dimensional state space generated by the delay turns the stability analysis into a more challenging task. The semi-discretization method, which has been established in [50, 51], can be adapted to control systems with delayed fractional-order feedback [6]. Exponential approximation of the weights in the Grünwald–Letnikov derivative allows us to obtain infinite memory effect using a discretization scheme of finite size [95, 6].

5.6 Main results

It has been shown that the critical delay for the delayed feedback control of the inverted pendulum can be extended by using detuned fractional-order proportional-derivative feedback. The corresponding critical delay is slightly larger than that of detuned proportional-derivative feedback.

Contribution 4

Consider the characteristic function

$$D(s) = s^2 + a_0 + k_\mathrm{p}\mathrm{e}^{-s(\tau+\delta_\mathrm{p})} + k_\mathrm{d}s^\mu\mathrm{e}^{-s(\tau+\delta_\mathrm{d})}$$

corresponding to a second-order unstable plant subject to detuned fractional-order proportional-derivative feedback, where $a_0 < 0$ is the fixed plant parameter, $\tau > 0$ is the feedback delay, k_p, k_d are the control gains, $\delta_\mathrm{p} \geq 0$, $\delta_\mathrm{d} \geq 0$ are delay detunings, and $0 < \mu < 2$ is the order of the fractional-order feedback. The system can be stabilized using an appropriate choice of the control parameters k_p, k_d, δ_p, δ_d and μ if τ is smaller than the critical delay

$$\tau_\mathrm{crit}^{\mathrm{dPD}^\mu} \approx \sqrt{-\frac{4.377}{a_0}}\,.$$

Without delay detuning, that is, if $\delta_\mathrm{p} = \delta_\mathrm{d} = 0$, the critical delay is

$$\tau_\mathrm{crit}^{\mathrm{PD}^\mu} \approx \sqrt{-\frac{2.507}{a_0}}\,.$$

Related publications: [5, 4, 7, 6].

Chapter 6

Human performance in virtual stabilization of a fractional-order system with reaction delay

The mechanism of human motion control is still not entirely understood in the sense that the underlying control model is a subject of debate. Whether it is state- or noise-dependent [25, 11], whether it is intermittent-time or continuous-time [38, 47], whether it is direct state feedback or internal-model-based predictor feedback [52, 72, 85], whether it utilizes the stable manifold of the open-loop system [118], whether it is optimal [104, 64], whether it can be described by a single-loop process or within a hierarchical control framework [65, 106, 105]. In any case, the human reaction time plays an important role in cortically-mediated motor control, which is well reflected in human stick balancing [48]. Shorter sticks move faster than longer ones and may fall if the control action is not fast enough. Indeed, human subjects typically cannot balance a stick shorter than 40 cm.

Stick balancing corresponds to the stabilization of the inverted pendulum. An inverted pendulum attached to a linearly driven cart can be stabilized by delayed proportional-derivative (PD) feedback if and only if the length of the pendulum is larger than some critical length. If the mass of the cart is significantly larger than the mass of the pendulum, then the critical length is

$$l_{\text{crit}}^{\text{PD}} = \frac{3}{4} g \tau^2, \tag{6.1}$$

where g is the gravitational acceleration and τ is the feedback delay [102, 48]. Thus, the critical length is proportional to τ^2.

The effect of feedback delay can be investigated in virtual balancing tasks where additional delays can be introduced in the overall control loop by artificially delaying visual feedback on the computer screen [13, 36, 59]. The dynamics can also be altered artificially, i.e., Aristotelian dynamics can be employed instead of the Newtonian one [58], or an artificial coupling can be introduced with an adjustable gain [94, 62]. In [59], it was shown that the length of the shortest stick that human subjects can balance for a given artificially added delay is indeed approximately proportional to τ^2 as equation (6.1) suggests. In [58], Aristotelian dynamics (Peripatetic dynamics, that is, first-order dynamics where force is proportional to velocity) has also been employed in addition to Newtonian dynamics (second-order dynamics where force is proportional to acceleration). It was shown that for Aristotelian dynamics the theoretical critical length is proportional to τ, which was partially verified by measurements. In this chapter, a fractional-order dynamics is employed in the virtual environment, where it is assumed that the force is proportional to the fractional derivative of the displacement with derivative order α, $1 \leq \alpha \leq 2$ [107]. Although fractional dynamics has no clear physical meaning, it can be implemented computationally in virtual environment.

Even though fractional calculus is as old as classical calculus (and hence classical mechanics), there is no universal way of defining fractional mechanics. We may replace the second-order derivative of the position in Newton's second law of motion with a fractional-order derivative, generalize the force (or force field), or use a fractional-order generalization of Euler–Lagrange equations [107, 96]. Furthermore, there are many different definitions for the fractional derivative itself. Here, we use the Caputo fractional derivative defined as (2.27).

In this chapter, the virtual environment is used to assess the shortest stick length that human subjects can balance for a given fractional-order dynamics. The shortest stick length is then compared with the critical length of the underlying theoretical model with different feedback laws. It is assumed that human subjects employ delayed fractional-order control, namely delayed PD$^\mu$ feedback with $0 \leq \mu \leq 1$. The special case $\mu = 1$ gives the traditional delayed PD feedback with critical length (6.1). The special case $\mu = 0$ gives the delayed P feedback. The case $0 < \mu < 1$ gives a transition between P and PD feedback. PD$^\mu$ feedback can be considered a modified PD feedback where the parameter μ is used to fit the feedback model to the experimental data. It is known that fractional-order derivatives can be used to model motor control systems, e.g., the control of eye movement by motor and premotor neurons [1, 88].

The chapter is organized as follows. The problem is stated in Section 6.1. In Section 6.2, the theoretical value of the critical pendulum length is determined in

the case of fractional-order dynamics and delayed PD$^\mu$ feedback. The measurement setup and protocol are detailed in Section 6.3. The theory and the measurements are compared in Section 6.4. Finally, Section 6.5 summarizes the results.

6.1 Problem statement

In this section, the governing equation of the inverted pendulum subject to fractional-order dynamics is derived. Then, we consider the system subject to fractional-order delayed PD feedback and obtain the characteristic function to be investigated throughout this chapter.

6.1.1 The inverted pendulum with fractional-order dynamics

In case of Newtonian dynamics, the equation of motion of an inverted pendulum on a cart (see Figure 6.1) can be given as

$$\frac{1}{3}ml^2\ddot{\varphi}(t) + \frac{1}{2}ml\cos\varphi(t)\,\ddot{x}(t) - \frac{1}{2}mgl\sin\varphi(t) = 0\,, \tag{6.2}$$

$$\frac{1}{2}ml\cos\varphi(t)\,\ddot{\varphi}(t) - \frac{1}{2}ml\left(\dot{\varphi}(t)\right)^2\sin\varphi(t) + (m+m_\mathrm{c})\,\ddot{x}(t) = F(t)\,, \tag{6.3}$$

where $\varphi(t)$ is the angular displacement of the pendulum from the vertically upward position, $x(t)$ is the displacement of the cart, $F(t)$ is the horizontal force acting on the cart, g is the gravitational acceleration, l and m are the length and the mass of the pendulum, and m_c is the mass of the cart. We assume that $m_\mathrm{c} \gg m$ as this is the case for real stick balancing due to the inertia of human subjects' arm. In this case, equation (6.3) simplifies to

$$m_\mathrm{c}\ddot{x}(t) = F(t)\,. \tag{6.4}$$

For more details on the derivation of equations (6.2)–(6.4), see Appendix A.3.

It is assumed that the force acting on a point mass is proportional to the fractional derivative of the point mass's position with derivative order α. The case $\alpha = 2$ gives the second-order Newtonian dynamics, and the case $\alpha = 1$ gives the first-order, so-called Aristotelian dynamics [107, 58]. Here we consider general fractional-order cases with $1 \le \alpha \le 2$. The corresponding fractional-order governing equations can be obtained from (6.2) and (6.4) by formally replacing the second-order derivatives with fractional-

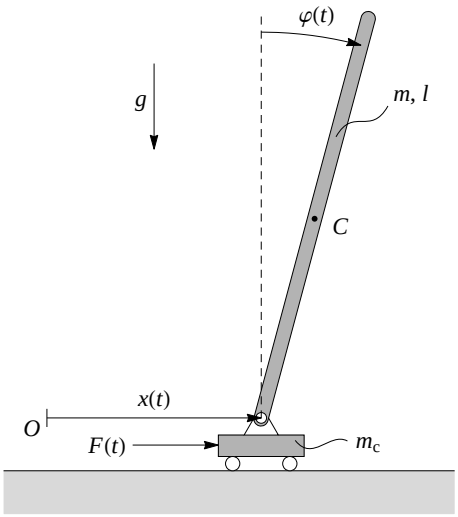

Figure 6.1: Inverted pendulum on a cart.

order ones as

$$\frac{1}{3}ml^2\,{}_0^tD_*^\alpha\varphi(t)+\frac{1}{2}ml\cos\varphi(t)\,{}_0^tD_*^\alpha x(t)-\frac{1}{2}mgl\kappa\sin\varphi(t)=0\,, \tag{6.5}$$

$$m_\mathrm{c}\,{}_0^tD_*^\alpha x(t)=\kappa F(t)\,, \tag{6.6}$$

where ${}_0^tD_*^\alpha$ denotes the Caputo fractional derivative with lower limit 0 according to (2.27), and $\kappa=1\,\mathrm{s}^{2-\alpha}$ is a factor introduced in order to ensure the dimensional correctness of equations (6.5)–(6.6).

6.1.2 Delayed PD$^\mu$ feedback

After eliminating ${}_0^tD_*^\alpha x(t)$, equations (6.5)–(6.6) can be written as

$${}_0^tD_*^\alpha\varphi(t)-\frac{3g\kappa}{2l}\sin\varphi(t)=-\frac{3\kappa}{2lm_\mathrm{c}}\cos\varphi(t)\,F(t)\,. \tag{6.7}$$

If we linearize (6.7) around the unstable equilibrium $\varphi(t)\equiv 0$, then we obtain

$${}_0^tD_*^\alpha\varphi(t)-\frac{3g\kappa}{2l}\varphi(t)=-\frac{3\kappa}{2lm_\mathrm{c}}F(t)\,. \tag{6.8}$$

It should be noted that $F(t)$ is a virtual force within the fractional-order virtual environment that is proportional to ${}_0^tD_*^\alpha x(t)$ according to (6.6). We assume that the virtual force $F(t)$ can be given as a delayed PD$^\mu$ feedback of the angular position of the pendulum $\varphi(t)$. In this case, (6.8) takes the form

$$ {}_0^t D_*^\alpha \varphi(t) + a_0\, \varphi(t) = -k_\mathrm{p}\, e(t-\tau) - k_\mathrm{d}\, {}_0^t D_*^\mu e(t-\tau)\,, \tag{6.9} $$

where $a_0 = -3g\kappa/(2l) < 0$ is the plant parameter, k_p and k_d are the (scaled) proportional and derivative control gains, $\tau > 0$ is the feedback delay, $1 \leq \alpha \leq 2$ is the order of the fractional-order dynamics, and $0 \leq \mu \leq 1$ is the order of the fractional-order feedback. The function $e(t) = \varphi(t) - u_\mathrm{r}(t)$ is the error signal, where $u_\mathrm{r}(t)$ is the reference input. In this chapter, we consider the stability of system (6.9) in the bounded-input bounded-output (BIBO) sense with an input $u_\mathrm{r}(t)$ and an output $\varphi(t)$.

The characteristic function of (6.9) reads

$$ D(s) = s^\alpha + a_0 + \left(k_\mathrm{p} + k_\mathrm{d} s^\mu\right) \mathrm{e}^{-s\tau}\,. \tag{6.10} $$

If we introduce the dimensionless variable $z = s\tau$, we can rewrite (6.10) as

$$ D(z) = z^\alpha - a + (p + dz^\mu)\, \mathrm{e}^{-z} \tag{6.11} $$

with $a = -a_0\tau^\alpha > 0$, $p = k_\mathrm{p}\tau^\alpha$, and $d = k_\mathrm{d}\tau^{\alpha-\mu}$.

System (6.11) is said to be stabilizable for given a, α, and μ if there exist some control gains p and d for which (6.11) is stable (i.e., (6.11) has roots with negative real parts only).

6.2 Stability and stabilizability

In this section, stability and stabilizability analysis is performed in terms of the critical pendulum length that can be compared with the shortest stick lengths that human subjects can balance.

6.2.1 Stability analysis with D-subdivision

The D-subdivision method can be applied to (6.11) as follows. If $0 < \mu \leq 1$, then substitution of $z = 0$ and $z = \pm \mathrm{i}y$, $y > 0$ into $D(z) = 0$ gives the D-curves

$$ z = 0 \;:\quad p = a\,, \quad d \in \mathbb{R}\,, \tag{6.12} $$

$$ z = \pm \mathrm{i}y, y > 0 \;:\quad \begin{cases} p = \dfrac{1}{\sin\left(\mu\frac{\pi}{2}\right)} \left(a \sin\left(\mu\frac{\pi}{2} - y\right) + y^\alpha \sin\left((\alpha-\mu)\,\frac{\pi}{2} + y\right)\right)\,, \\ d = \dfrac{1}{\sin\left(\mu\frac{\pi}{2}\right)} \left(a y^{-\mu} \sin\left(y\right) - y^{\alpha-\mu} \sin\left(\alpha\frac{\pi}{2} + y\right)\right)\,. \end{cases} \tag{6.13} $$

Equations (6.12)–(6.13) give the boundaries of the regions in the space (a, α, μ, p, d) where the number of unstable characteristic roots is constant. These boundaries can be visualized in the two-dimensional (p, d) plane for fixed values of a, α, and μ. The number of unstable characteristic roots can be determined by a testing integral based on the argument principle [112, 74].

In the special case $\mu = 1$, the D-curves are shown in Figure 6.2. In this case, (6.13) gives $(p, d) = (a, a)$ for $1 < \alpha \leq 2$ and $(p, d) = (a, a - 1)$ for $\alpha = 1$ if the dimensionless vibration frequency y approaches 0. This corresponds to a double zero characteristic root of the characteristic function (6.11). Figure 6.2 shows that if α is fixed, then the stable region (with zero unstable roots) shrinks as a increases and it disappears when a reaches a critical value. This implies that if we project the stable region of α, a, p, and d onto the plane (α, a), then we obtain a region bounded by a function $a_{\text{crit}}^{\text{PD}}(\alpha)$. If $0 \leq \mu < 1$, then there is a similar boundary $a_{\text{crit}}^{\text{PD}^\mu}(\alpha)$.

6.2.2 Stabilizability analysis

Stabilizability properties are discussed for the cases $\mu = 1$, $\mu = 0$, and $0 < \mu < 1$ separately.

The case $\mu = 1$.

The critical values $a_{\text{crit}}^{\text{PD}}(\alpha)$ for $\alpha = 1$ and $\alpha = 2$ are already known from the literature. In both cases, the characteristic function (6.11) has a zero root with multiplicity $m_0 = 3$ at the limit of stabilizability. If $\alpha = 1$, then (6.9) is a neutral delay differential equation and the critical value of a was derived as $a_{\text{crit}}^{\text{PD}}(1) = 2$ in [71]. The case $\alpha = 2$ gives a retarded delay differential equation, and $a_{\text{crit}}^{\text{PD}}(2) = 2$ (see, for example, [102]). Thus, Figure 6.2 shows the limit of stabilizability for both $\alpha = 1$ and $\alpha = 2$ with $a = 2$.

If $1 < \alpha < 2$, then the loss of stabilizability occurs at a loop-cusp transition of (6.13) as it is demonstrated in Figure 6.2 with $\alpha = 1.5$. This implies a double pair of purely imaginary roots, that is, the multiplicity of the root $z = \mathrm{i}y$ is $m_{\mathrm{i}y} = 2$. The condition $m_{\mathrm{i}y} = 2$ corresponds to four (real) equations that are linear in a, p, and d and nonlinear in α and y. After the elimination of a, p, and d, a single equation remains for α and y, which can be handled using standard numerical techniques. The obtained function $a_{\text{crit}}^{\text{PD}}(\alpha)$ is shown in Figure 6.3a in the plane (α, a).

The case $\mu = 0$.

In this case, the characteristic function takes the form

$$D(z) = z^\alpha - a + \tilde{p}\mathrm{e}^{-z}\,, \tag{6.14}$$

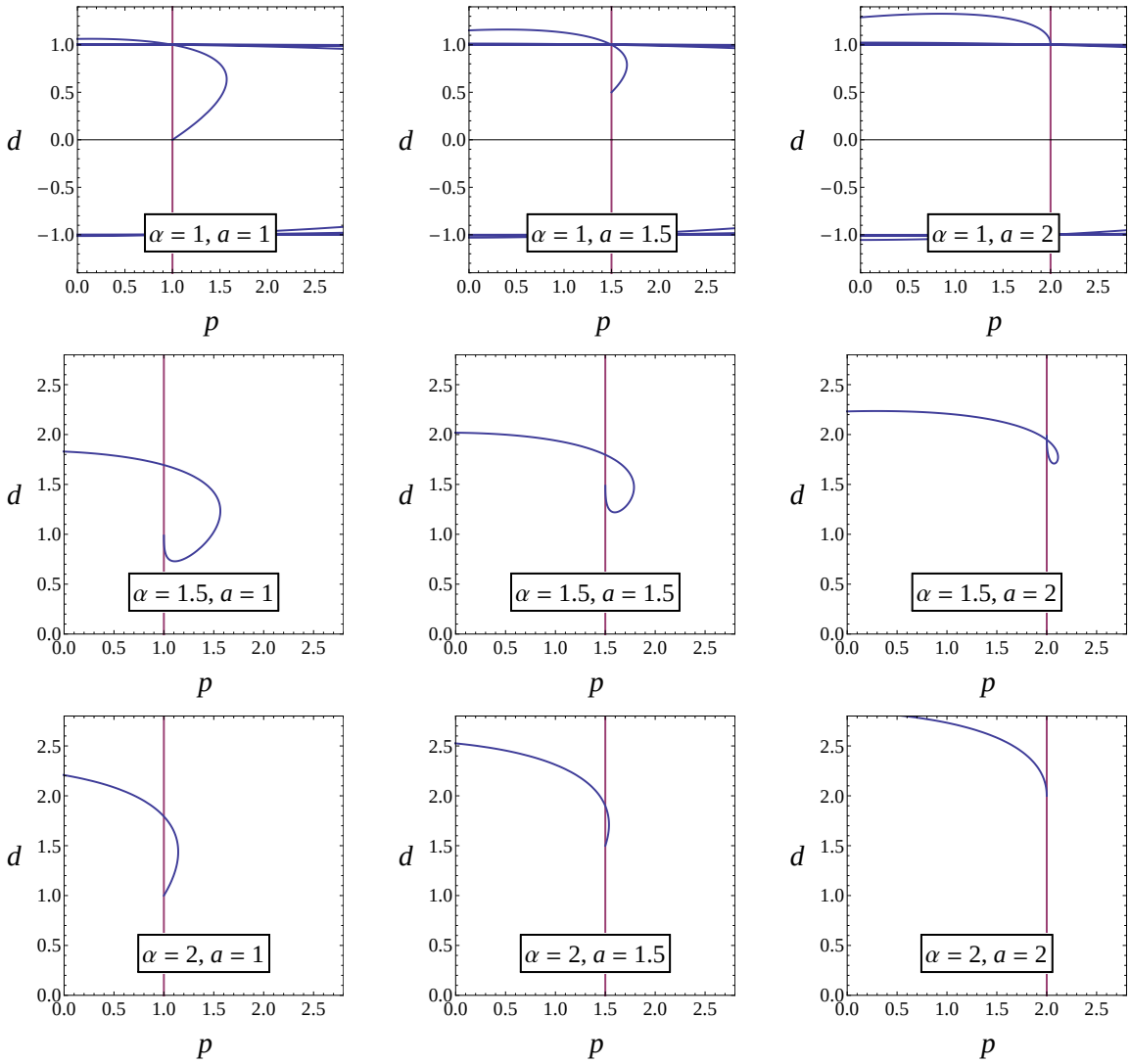

Figure 6.2: Stability charts of (6.11) for $\mu = 1$ and different values of α and a.

where $\tilde{p} = p + d$. This corresponds to a fractional-order generalization of the Hayes equation with $1 \leq \alpha \leq 2$. If $\alpha = 1$, then we get the integer-order Hayes equation, and the critical value of a is $a^{\mathrm{P}}_{\mathrm{crit}}(1) = 1$ [43]. The inverted pendulum ($\alpha = 2$) cannot be stabilized by delayed P feedback [102]; thus, $a^{\mathrm{P}}_{\mathrm{crit}}(2) = 0$. If $1 < \alpha < 2$, then the stability and stabilizability of (6.14) can be investigated using the same techniques as in the case $\mu = 1$ [29]. It was found that the characteristic function has a single pair of purely imaginary roots at the limit of stabilizability ($m_{\mathrm{i}y} = 1$), and an additional condition $\det(\mathbf{J}) = 0$ holds, where $\mathbf{J}$ is the 2-by-2 Jacobian matrix of $\mathrm{Re}D(\mathrm{i}y)$ and $\mathrm{Im}D(\mathrm{i}y)$ with respect to p and y. The corresponding function $a^{\mathrm{P}}_{\mathrm{crit}}(\alpha)$ is shown in Figure 6.3a.

The case $0 < \mu < 1$.

The case $0 < \mu < 1$ and $\alpha = 1$ (that is, a first-order unstable plant with a delayed

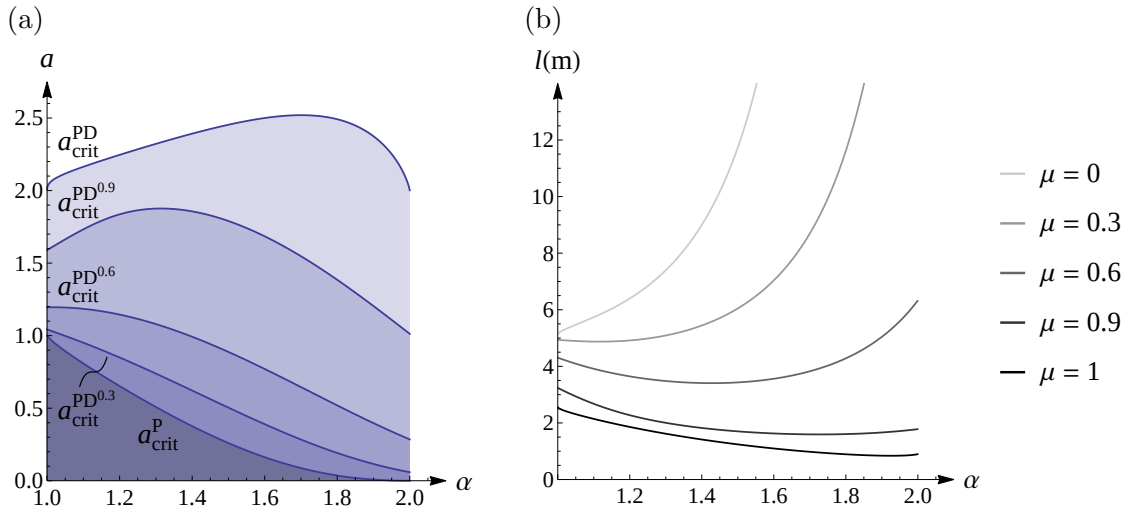

Figure 6.3: Stabilizability diagram of (6.11) in the plane (α, a) (a). The system is stabilizable in the shaded regions. Critical pendulum length according to (6.18) as a function of α for different values of μ in the case $\tau = 0.35$ s (b).

fractional-order PD controller) was investigated in [31] using D-subdivision; however, stabilizability was analyzed in a slightly different sense. The stabilizability limit for the case $0 < \mu < 1$ and $\alpha = 2$ was given in [4].

Loss of stabilizability can be assessed by investigating the D-curves in the (p, d) plane for different a, α, and μ values. Numerical analysis shows that stabilizability is typically lost such that the parametric D-curve (6.13) is tangent to the vertical line $p = a$ (see Figure 6.4). This corresponds to the coexistence of a zero root with multiplicity $m_0 = 1$ and a pair of purely imaginary roots ($m_{\mathrm{i}y} = 1$) such that an additional condition $\det(\mathbf{J}) = 0$ holds, where $\mathbf{J}$ is the 3-by-3 Jacobian matrix of $D(0)$, $\mathrm{Re}D(\mathrm{i}y)$, and $\mathrm{Im}D(\mathrm{i}y)$ with respect to p, d, and y. These conditions correspond to the four (real) equations

$$D(0) = 0, \quad \mathrm{Re}D(\mathrm{i}y) = 0, \quad \mathrm{Im}D(\mathrm{i}y) = 0, \quad \det(\mathbf{J}) = 0\,, \tag{6.15}$$

which can be expanded as

$$\left.\begin{aligned} -a + p &= 0\,,\\ y^{\alpha}\cos\left(\alpha\tfrac{\pi}{2}\right) - a + p\cos(y) + dy^{\mu}\cos\left(\mu\tfrac{\pi}{2} - y\right) &= 0\,,\\ y^{\alpha}\sin\left(\alpha\tfrac{\pi}{2}\right) - p\sin(y) + dy^{\mu}\sin\left(\mu\tfrac{\pi}{2} - y\right) &= 0\,,\\ y^{\mu}\left(\alpha y^{\alpha-1}\sin\left((\alpha-\mu)\tfrac{\pi}{2} + y\right) - p\cos\left(\mu\tfrac{\pi}{2}\right) - dy^{\mu}\right) &= 0\,. \end{aligned}\right\} \tag{6.16}$$

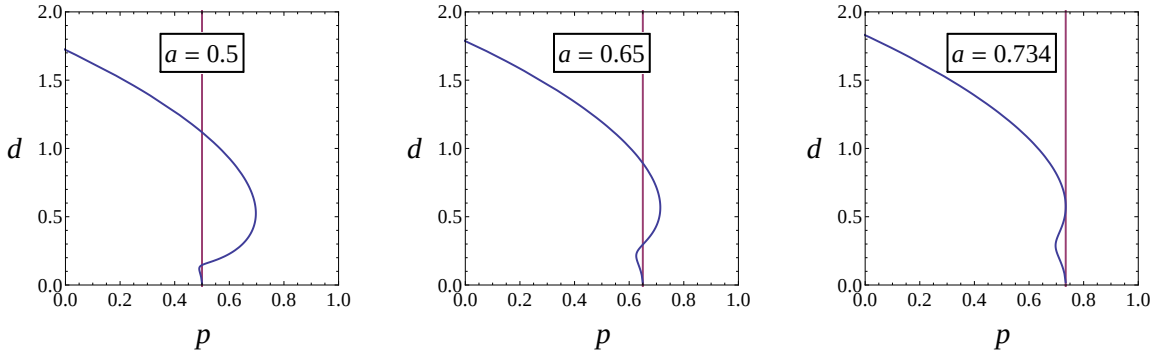

Figure 6.4: Stability charts of (6.11) for $\alpha = 1.5$, $\mu = 0.5$ and different values of a.

Equations (6.16) are linear in a, p, and d and nonlinear in α, μ, and y. After the elimination of a, p, and d, a single equation remains for α, μ, and y. For fixed α and μ, this equation can be solved numerically and the critical dimensionless plant parameter can be determined.

For certain μ values, other types of loss of stabilizability may occur. Namely, the stable region may disappear at a loop-cusp transition if μ is close to 1. The condition for a loop-cusp transition is that there exists a double pair of purely imaginary roots ($m_{\mathrm{i}y} = 2$), that is,

$$\mathrm{Re}D(\mathrm{i}y) = 0, \quad \mathrm{Im}D(\mathrm{i}y) = 0, \quad \mathrm{Re}D'(\mathrm{i}y) = 0, \quad \mathrm{Im}D'(\mathrm{i}y) = 0\,. \tag{6.17}$$

This system of equations is also linear in a, p, and d and nonlinear in α, μ, and y. A loop-cusp transition occurs for some fixed α and μ if (6.17) has a solution for a, p, d and y with $a > 0$ and $y > 0$. Furthermore, it can represent a loss of stabilizability only if $p \geq a$. Numerical analysis shows that such a solution exists only if μ is greater than some $\mu_0(\alpha)$. At the limit case, when $p = a$, the system of equations (6.17) should be extended with an additional equation $D(0) = 0$. Solving $D(0) = 0$ together with (6.17) gives the function $\mu_0(\alpha)$, which is shown in Figure 6.5. The function $\mu_0(\alpha)$ is minimal for $\tilde{\alpha} = 1.215$, and the minimum value is $\tilde{\mu} = 0.940$. If $0 < \mu < \mu_0(\alpha)$, then the stable region disappears such that the parametric D-curve (6.13) is tangent to the vertical line $p = a$, that is, equation (6.15) holds. If $\mu_0(\alpha) < \mu < 1$, then a loop-cusp transition occurs for a smaller a value than the one obtained from (6.15); hence, the loop-cusp transition may correspond to the loss of stabilizability. However, other types of loss of stabilizability also occur, which are not investigated here in detail. If $\mu = 1$, then the stable region disappears at a loop-cusp transition for any $1 < \alpha < 2$ as it was shown above. Figure 6.3a shows some sample stabilizability boundaries: the critical dimensionless plant parameter is shown as a function of α for different μ values.

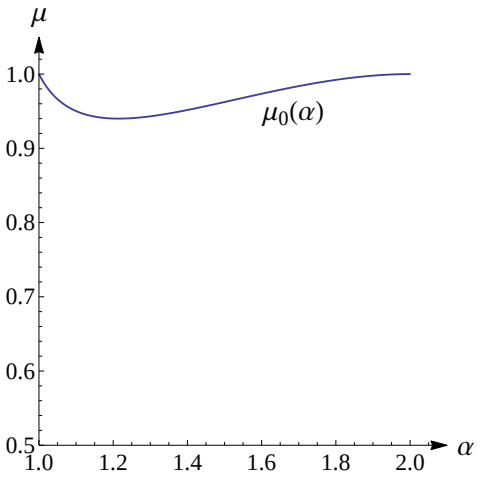

Figure 6.5: Set of points $(\alpha, \mu_0(\alpha))$ corresponding to a zero root and a double pair of purely imaginary roots of the characteristic function (6.11). If $0 < \mu < \mu_0(\alpha)$, then the stable region disappears such that the two D-curves (6.12)–(6.13) are tangent to each other. Note that $\mu_0(1) = \mu_0(2) = 1$.

Using the relation between the pendulum length l and the dimensionless plant parameter a, the critical pendulum length for a given delay τ and fractional derivative orders α and μ can be given as

$$l_{\text{crit}}^{\text{PD}^\mu} = \frac{3g\kappa}{2a_{\text{crit}}^{\text{PD}^\mu}(\alpha)}\tau^\alpha\,, \tag{6.18}$$

where the critical dimensionless plant parameter $a_{\text{crit}}^{\text{PD}^\mu}(\alpha)$ is illustrated in Figure 6.3a. If $\alpha = 2$ and $\mu = 1$, then (6.18) gives (6.1). Note that the critical length is proportional to τ^α for any control law that can be written as a linear combination of integer- or fractional-order derivatives of $\varphi(t-\tau)$. This property is originated from the dimensionless parameter $a = -a_0\tau^\alpha$ in (6.11). The critical length is shown in Figure 6.3b as a function of α.

6.3 Measurement setup

The critical length of the stick was measured experimentally using the virtual balancing environment [58] with governing equation (6.5). In the framework of a student project, eighteen subjects were recruited. All the participants provided consent for all research testing and were given the opportunity to withdraw from the study at any time. The research was carried out following the Declaration of Helsinki. Human subjects performed balancing tests as described below.

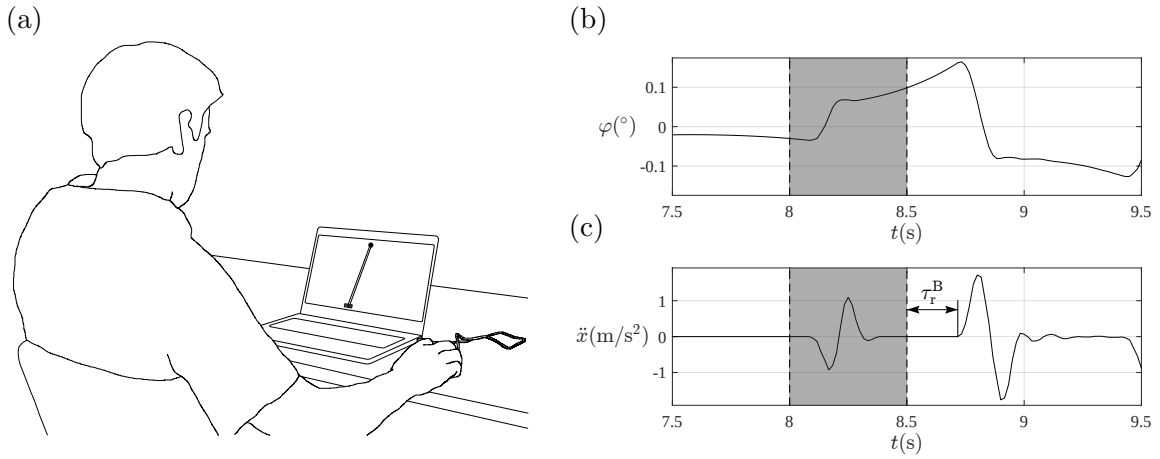

Figure 6.6: Virtual balancing environment (a). Time signals from blank-out tests (b)–(c).

6.3.1 Virtual balancing tests

Virtual balancing tests were implemented in Java. The computer program developed originally for Newtonian dynamics [59, 56, 58] was modified to accommodate fractional-order dynamics. The actual position of the stick is displayed on the screen, and only this visual feedback is available for the subjects (see Figure 6.6a). The horizontal position of the lower endpoint of the stick can be changed by moving the computer mouse. In this way, human input affects directly the displacement of the cart $x(t)$. This is related to the control force $F(t)$ in the theoretical model according to equation (6.6).

6.3.2 Implementing the fractional-order governing equation

The fractional-order governing equation (6.5) was implemented using the discretization scheme developed in [73]. This numerical method assumes that the initial values apart from $y(0)$ are equal to zero, i.e., $y^{(i)}(0) = 0$, $i = 1, 2, ..., \lceil \alpha \rceil - 1$. During the virtual balancing tests, the pendulum starts from rest, so the discretization scheme in [73] can be applied and provides an adequately fast solution of the fractional-order differential equation (6.5).

When applying this method, we also need to take the fractional derivative of displacement of the cart $x(t)$ in equation (6.5). To this end, the Grünwald–Letnikov definition of the fractional derivative was used. If we assume continuity of $x(t)$, i.e., $x(t) \in C^{\lceil \alpha \rceil}[t]$, then the Grünwald–Letnikov and the Riemann–Liouville definitions are equivalent. Furthermore, the Riemann–Liouville and Caputo fractional derivatives are also equal since $x^{(i)}(0) = 0$, $i = 0, 1, 2, ..., \lceil \alpha \rceil - 1$ [88].

6.3.3 Measuring the delay

In order to determine the delay parameter in the model, human reaction time was assessed by two different approaches: instant reaction time tests and blank-out tests.

During the instant reaction time tests, the subjects were asked to click on a button after 10 randomly occurring red flashes on the screen as fast as possible. In this way, the reaction time could be measured independently of the balancing task. A feasible time delay interval of 0.1–0.7 s was used during the evaluation of the instant reaction time tests to eliminate extreme outliers. The remaining data were averaged to get the reaction time τ_{r}.

During the blank-out tests, the subjects chose a constant stick length with which they could comfortably balance. Then, after they started to balance, the stick disappeared from the screen at a random time instant for 0.5 s (see the shaded period in Figure 6.6b and Figure 6.6c). The subjects were asked to keep on balancing despite the loss of visual feedback. After the return of the visual feedback, subjects typically employed a sudden corrective action in order to prevent the stick from falling.

Blank-out tests require the estimation of reaction times by detecting sudden jumps in the time signals preceded by a resting period. In order to eliminate erroneous detection of jumps by automatic processing, the plots of the pendulum angle and cart acceleration were inspected visually. If there were any jumps in the cart acceleration within 0.1 to 0.7 s after the end of the blank-out period, then the time elapsed between the end of the blank-out period and the start of the jump was recorded (see Figure 6.6c). Otherwise, no time delay was recorded. Subjects performed 10 blank-out tests during a session. Time delays from the evaluable blank-out tests were averaged to get the reaction time $\tau_{\mathrm{r}}^{\mathrm{B}}$.

6.3.4 Measurement protocol

The goal of the virtual balancing tests was to determine the shortest pendulum that a subject could balance for a given fractional derivative order α. Subjects performed a series of balancing sessions with $\alpha = 1, 1.2, 1.4, 1.6, 1.8$, and 2. The order of the six values of α was randomized under the condition that the absolute difference of the fractional derivative orders is greater than or equal to 0.4 between successive sessions. Randomized orders allow us to separate the effects of different dynamics and learning throughout the sessions. Each subject was assigned a unique order of the six α values. A single balancing session was constructed as follows.

1. At the beginning of each session, an instant reaction time test was performed.

2. The fractional derivative order was set to a constant value of α_k during the kth session according to the assigned order.

3. The measured critical stick length $l_{\text{crit}}^{\text{meas}}(\alpha_k)$ was determined as follows. Subjects started with an initial length l_1 that they were able to balance for 10 s during preliminary practice without any difficulty. For the first trial, the stick length was gradually decreased by a given step size $\Delta l_1 = 0.2$ m in every second, which resulted in an increasing difficulty in the task. Subjects were allowed to perform the trial with the same l_1 and $\Delta l_1 = 0.2$ m a maximum number of five times. If the balancing time was longer than 10 s for any of the five trials, then the falling length $l_{1,\text{fall}}$ was assessed as the length at the time instant when $|\varphi|$ just exceeded 20°. If none of the five trials lasted at least 10 s, then the falling length was set to $l_{1,\text{fall}} = l_1$. After the first round of trials, the initial stick length was set to $l_2 = l_{1,\text{fall}} + 10\Delta l_1$. The second round of (maximum five) balancing trials was started with a step size $\Delta l_2 = \Delta l_1/2$, and the falling length was recorded as $l_{2,\text{fall}}$. The round of trails was repeated with $l_{i+1} = l_{i,\text{fall}} + 10\Delta l_i$ and $\Delta l_{i+1} = \Delta l_i/2$ for $i = 2, 3, 4, 5$. The critical length associated with α_k was assessed as the falling length in the 6th round of trials: $l_{\text{crit}}^{\text{meas}}(\alpha_k) = l_{6,\text{fall}}$.

4. Finally, the subjects were instructed to perform 10 blank-out tests.

The overall session took approximately 15 min to complete. The above session was repeated a total of 6 times with different fractional orders $\alpha = \alpha_k$, $k = 1, 2, \ldots, 6$ on different days. Instant reaction time tests and blank-out tests were performed during every session. Since the instant reaction time test does not depend on the value of α (and therefore did not change throughout the sessions), the measured delays τ_{r} can serve as a control for the delays $\tau_{\text{r}}^{\text{B}}$ from blank-out tests.

6.4 Measurement results

In this section, we evaluate the instant reaction time and blank out tests and compare the measured critical lengths with the theoretical ones.

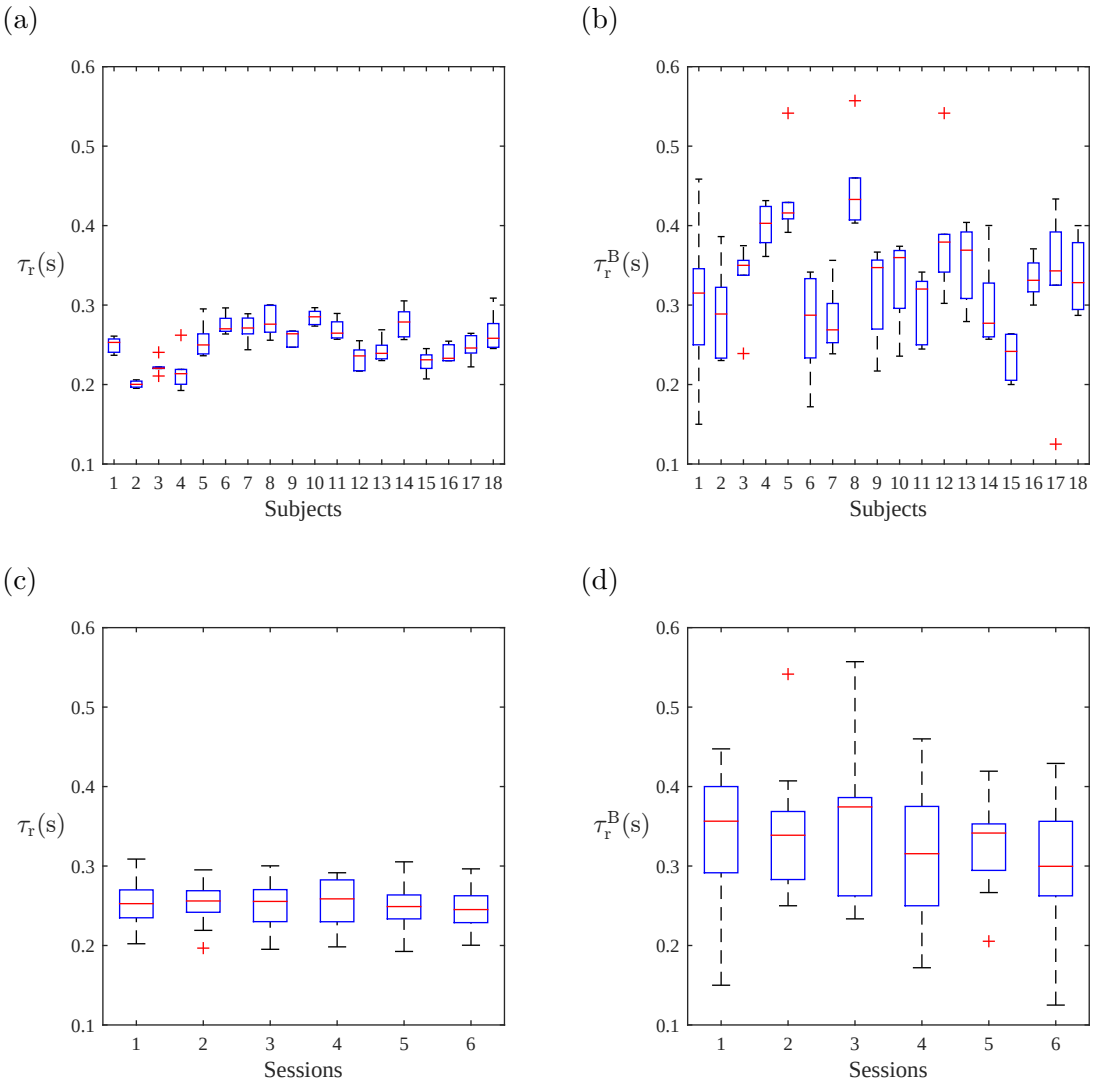

Figure 6.7: Instant reaction time τ_r for the subjects (a) and for the sessions (c). Reaction time obtained from the blank-out tests τ_r^B for the subjects (b) and for the sessions (d). Red central mark: median; blue box: interquartile range (IQR); black dashed whiskers: min–max values not considered outliers; red + marks: outliers.

6.4.1 Instant reaction time and blank-out tests

The box plots of the instant reaction time and blank-out tests are shown in Figure 6.7 for individual subjects and for different sessions. As can be seen, the variation of the median of the reaction times among the subjects is larger than that among the sessions. The delays τ_r^B show a slightly decreasing tendency during the sessions (see Figure 6.7d), which suggests that learning may have a small but still negligible effect. The instant reaction time test measures the response time to a visual input, while

the blank-out test measures the response time to a perturbation during virtual stick balancing, which gives the overall closed-loop delay including the machine processing delay and the time of human decision-making. Therefore, we estimate the delay for a subject as the average of delays from the blank-out tests over the different sessions (or different fractional derivative orders), i.e., $\tau = \bar{\tau}_{\mathrm{r}}^{\mathrm{B}}$.

6.4.2 Measured critical lengths and comparison with theoretical limits

Critical stick lengths for a given fractional derivative order α were recorded during the virtual balancing tests (see Subsection 6.3.1 and Subsection 6.3.4). The results for each subject (S1, S2, ... , S18) and each α (blue dots or crosses) are shown in Figure 6.8. As it was shown in Subsection 6.2.2, the critical stick length can be expressed as a power function of the delay. If we substitute $\tau = \bar{\tau}_{\mathrm{r}}^{\mathrm{B}}$ into equation (6.18), then we obtain the theoretical limit corresponding to a given subject as a function of α. These theoretical limits of l are also shown by solid gray and black lines for $\mu = 0$ and $\mu = 1$, respectively. Most of the measured critical lengths $l_{\mathrm{crit}}^{\mathrm{meas}}$ are between the theoretical limits $l_{\mathrm{crit}}^{\mathrm{P}}$ and $l_{\mathrm{crit}}^{\mathrm{PD}}$.

The results for all the subjects can be summarized in a single diagram with dimensionless parameters. Figure 6.9a shows the critical dimensionless plant parameters determined as

$$a_{\mathrm{crit}}^{\mathrm{meas}} = \frac{3g\kappa\tau^{\alpha}}{2l_{\mathrm{crit}}^{\mathrm{meas}}}\,, \tag{6.19}$$

where $\tau = \bar{\tau}_{\mathrm{r}}^{\mathrm{B}}$ is substituted for each subject. Theoretical stabilizability limits for different μ values are also shown.

Comparison of the data points and the theoretical curves in Figure 6.9a suggests that a feedback law with a fractional derivative of fixed order μ may have been employed for all plant orders α. This is also supported by the observation that the biological processes behind human motion control can be described by fractional-order models of neurons and muscles corresponding to fractional differentiators and integrators [1]. Hence, the order of the fractional-order feedback might be determined by these biological processes. Furthermore, we assume that the control gains k_{p}, k_{d} (or p, d) can be set to their optimal values precisely and quickly. Under these assumptions, the best-fitting fractional order μ can be determined by comparing the measured and the theoretical critical dimensionless plant parameters. Root mean square error (RMSE) analysis gives that PD$^{\mu}$ feedback with $\mu = 0.475$ is the best-fitting control law. This μ

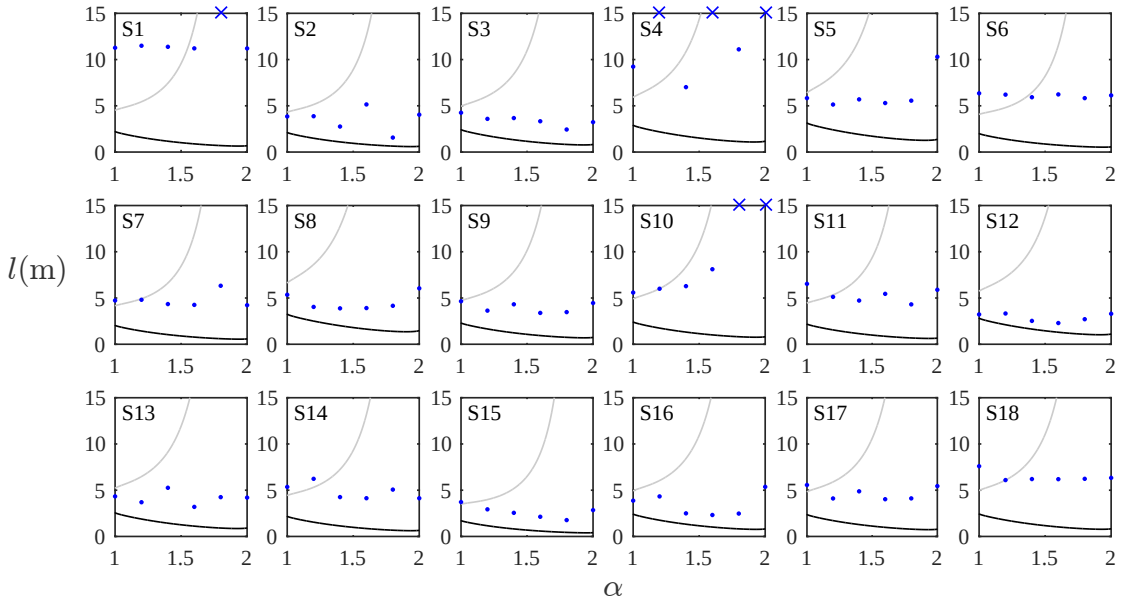

Figure 6.8: Measured critical lengths for different fractional derivative orders α. Data points that lie outside of the range of the plot are indicated by crosses. The theoretical limits are also shown for delayed PD (solid black line) and delayed P (solid gray line) feedback for reference. The theoretical limits are different for each individual subject because of the different delays.

value describes the typical behavior of a human subject.

The RMSE analysis can also be applied to the individual subjects separately. For the best-fitting μ values, the RMSE is minimal and the coefficient of determination R^2 is maximal. For six out of the eighteen subjects (S1, S4, S6, S11, S14, S18), the maximal coefficient of determination is negative, which reflects that these subjects cannot be modeled well with PD$^\mu$ feedback. For the remaining twelve subjects, the best-fitting fractional order is $\mu = 0.542 \pm 0.191$ (mean $\pm$ standard deviation). The corresponding coefficient of determination for these twelve subjects is $R^2 = 0.674 \pm 0.233$.

6.5 Conclusion

Virtual balancing tasks were performed by eighteen human subjects such that the virtual dynamics was of fractional order α. The critical stick length that subjects were able to balance for different α values was experimentally determined and used as a measure of human balancing performance. As opposed to [59, 58], no artificial delay was added. The overall closed-loop delay was measured by blank-out tests for each

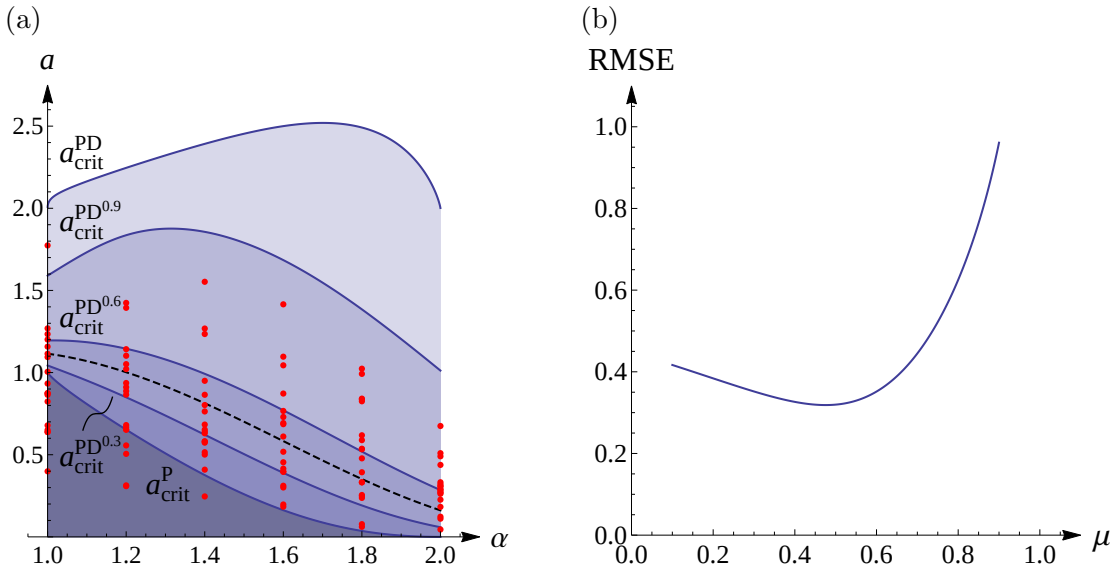

Figure 6.9: Stabilizability limits of (6.11) for different μ values (blue lines), measured $(\alpha, a_{\text{crit}})$ pairs (red dots) for all the subjects, and the best-fitting stabilizability limit (dashed black line) obtained for $\mu = 0.475$ (a). Root mean square error (RMSE) as a function of μ (b).

subject. Theoretical stabilizability limits for the delayed PD$^\mu$ controller with different μ values were fitted to the measured data points. The best fit was obtained for $\mu = 0.475$, which is surprisingly close to $\mu = 1/2$. Half-order fractional derivatives naturally arise in mechanical optimization problems. A generalized version of the tautochrone problem leads to Abel's integral equation which contains a Caputo fractional derivative of order $1/2$ [89, 88]. In [108], the Riemann–Liouville fractional derivative of order $3/2$ was used to construct an initial value problem in order to find the shapes of neutrally floating objects.

While stabilizability limits for fixed $0 \leq \mu \leq 1$ can be fitted to the measured data points, they cannot directly explain data points that lie under the limit $a_{\text{crit}}^{\text{P}}(\alpha)$. These data points can appear because subjects may not tune the control gains to their optimal values. If a is smaller than $a_{\text{crit}}^{\text{PD}^\mu}(\alpha)$ corresponding to a given μ, then there is a finite region of stabilizing control gains. Practical loss of stabilizability might be related to a finite stable region rather than the disappearance of the stable region. This implies a kind of robust stabilizability condition which is related to the size of the stable region. Note that only a single data point lies above the limit $a_{\text{crit}}^{\text{PD}^{0.9}}(\alpha)$, and none of them is above $a_{\text{crit}}^{\text{PD}}(\alpha)$. Therefore, in terms of robust stabilitability, simple PD feedback can still be a good model for the human feedback mechanism.

In this chapter, we considered fractional derivative orders $0 \leq \mu \leq 1$ and $1 \leq \alpha \leq 2$. We may also consider PD$^\mu$ feedback with $1 < \mu \leq 2$. In [4], it was shown that the critical dimensionless plant parameter a_{crit} can be slightly increased for $\alpha = 2$ if $1 < \mu < 2$; however, a_{crit} approaches 0 as μ approaches 2. Furthermore, fractional-order dynamics with orders $2 < \alpha \leq 3$ could be investigated as in [107]. This would result in a higher-order dynamics and a motion that is more difficult to control. In the computer environment, we may also change the value of the gravitational acceleration, which would change the critical length according to (6.1).

6.6 Main results

The dynamics of human stick balancing can be generalized using fractional-order derivatives, which can be implemented in a virtual environment. Reaction delay sets a strong limitation on the length of the shortest stick that human subjects can balance. Human processing of visual input also exhibits a memory effect that can be modeled by fractional-order derivatives. Therefore, a delayed fractional-order proportional-derivative control of the unstable fractional-order plant was hypothesized. The resulting equation of motion was investigated in a dimensionless framework, and stabilizability limits were determined as a function of the dynamics's order α.

Contribution 5

Consider the fractional-order inverted pendulum subject to delayed fractional-order proportional-derivative feedback described by the dimensionless characteristic function

$$D(z) = z^{\alpha} - a + (p + dz^{\mu})\,\mathrm{e}^{-z}\,,$$

where $a > 0$ is the plant parameter, p and d are the proportional and derivative control gains, $1 < \alpha < 2$ is the order of the fractional-order dynamics, and $0 < \mu \leq 1$ is the order of the fractional-order feedback. For $0 < \mu < \tilde{\mu} \approx 0.940$, the loss of stabilizability occurs such that the characteristic function has a zero root $z = 0$ and a pair of purely imaginary roots $z = \pm \mathrm{i}y$, and an additional condition $\det(\mathbf{J}) = 0$ holds, where $\mathbf{J}$ is the 3-by-3 Jacobian matrix of $D(0)$, $\mathrm{Re}D(\mathrm{i}y)$, and $\mathrm{Im}D(\mathrm{i}y)$ with respect to p, d, and y. For $\mu = 1$, which corresponds to integer-order proportional-derivative feedback, the loss of

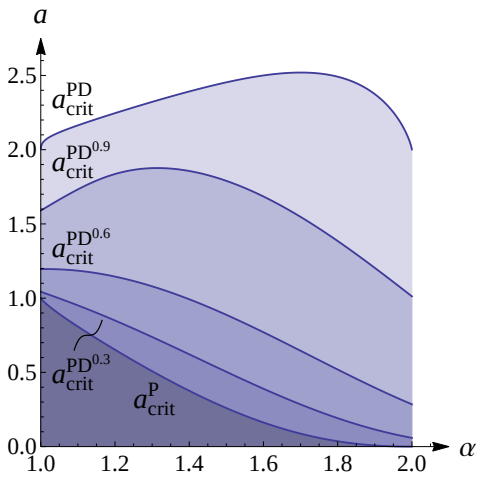

Stabilizability diagram in the plane (α, a).

stabilizability occurs at a loop-cusp transition of one of the D-curves, which implies a pair of purely imaginary roots with multiplicity 2. In both cases, the system can be stabilized using an appropriate choice of the control parameters p and d if a is smaller than the critical value $a_{\text{crit}}^{\text{PD}^\mu}(\alpha)$ that is shown in the figure.

Related publications: [9].

The theoretical limits were compared with the results of a systematic series of virtual balancing tests performed by eighteen subjects. The critical stick lengths that subjects were able to balance for different α values were experimentally determined. The overall closed-loop delay was measured by blank-out tests for each subject. The comparison showed that the theoretical stabilizability limits for controllers with fixed fractional order correspond to the measured data points $(\alpha, a_{\text{crit}})$, where a_{crit} is the critical dimensionless plant parameter that can be calculated from the critical stick length, the overall closed-loop delay and the fractional order of the dynamics.

Contribution 6

Virtual stick balancing tasks were performed by eighteen human subjects such that the virtual dynamics was of fractional order $1 \leq \alpha \leq 2$. Human control action was modeled by delayed fractional-order proportional-derivative feedback of order $0 \leq \mu \leq 1$, and the fractional order μ was assumed to be fixed for a given subject. The corresponding theoretical stabilizability limits for fixed μ values describe the decreasing tendency and order of magnitude of the measured critical dimensionless plant parameters well as a function of α. Nonlinear regression of the measured data points showed that the coefficient of determination R^2 for the best fit was positive for twelve of the eighteen subjects with $R^2 = 0.674 \pm 0.233$ (mean $\pm$ standard deviation for these twelve subjects). For these twelve subjects, the corresponding fractional order was $\mu = 0.542 \pm 0.191$.

Related publications: [9].

Chapter 7

Summary

The critical delay of time-delay systems can be investigated through the more general concept of stabilizability. In the case of single-input linear time-invariant dynamical systems with a single-delay state feedback, the stablizable delay intervals can be assessed using sufficient conditions for the dominancy of a multiple real root and a necessary condition for stability. These polynomial conditions can be evaluated numerically if the coefficients of the plant are known. However, it might be enough to know the structure of the open-loop characteristic polynomial: if the plant has only real roots and the average of the roots is nonnegative, then the critical delay can be expressed as the smallest positive real root of a polynomial. Such a structure occurs in the case of the inverted pendulum subject to delayed proportional-derivative feedback and in many other applications related to balancing.

The critical delay of the inverted pendulum depends on the associated control law. The critical delay can be extended by applying acceleration feedback, detuning the delays, or including fractional derivative terms. The greatest increase was obtained for detuned proportional-derivative-acceleration feedback; hence, this control strategy might be favorable in engineering applications. However, despite the smaller increase in the critical delay and the higher complexity of the controller, delayed fractional-order proportional-derivative feedback can be used to model human motion control in case of visual sensory input.

Human stick balancing measurements were performed in a virtual environment such that the stick followed fractional-order dynamics. The critical lengths and reaction times of the eighteen subjects were analyzed in a dimensionless framework. It was found that delayed fractional-order proportional-derivative feedback with a fixed fractional order describes the human control action well for most of the subjects. That is, such a

fractional-order control law was found to be independent of the fractional order of the dynamics. The best-fitting fractional order of the control law showed only a moderate variation between different subjects.

The presented research might be continued in many different directions. As for single-input linear time-invariant dynamical systems with a single-delay state feedback, it would be worth investigating the connection between the root location of the plant and the root location of the characteristic function at the limit of stabilizability. Recent articles covered the case of the general second-order plant [76]. It might also be possible to approach such a problem using the advanced algebraic tools of computer algebra systems. A software package exploiting the results of Chapter 3 and other recent works was developed in [15]. Stability of fractional-order time-delay systems could also be investigated numerically. The semi-discretization method can be applied along with the exponential approximation of the weights in the Grünwald–Letnikov fractional derivative [6]. It could be worth developing the theory behind [6] such that it could be applicable to the general fractional-order state equation of Caputo type. Finally, it was found in Chapter 6 that the human control action can be modeled as fractional-order proportional-derivative feedback with a fixed order during virtual stick balancing. Further measurements could help us decide if the same holds true for other types of balancing tasks or if the fixed fractional order is related to the biological processing of visual input.

Appendices

A.1 *N*-link inverted pendulum: equation of motion

The position and the velocity of the center of mass of the kth rod ($k = 1, 2, ..., N$) can be written as

$$\mathbf{r}_{C_k} = \begin{bmatrix} l\sum_{i=1}^{k}\sin\varphi_i - \frac{l}{2}\sin\varphi_k \\ l\sum_{i=1}^{k}\cos\varphi_i - \frac{l}{2}\cos\varphi_k \\ 0 \end{bmatrix}, \tag{A.1}$$

$$\mathbf{v}_{C_k} = l\begin{bmatrix} \sum_{i=1}^{k}\cos\varphi_i\dot{\varphi}_i - \frac{1}{2}\cos\varphi_k\dot{\varphi}_k \\ -\sum_{i=1}^{k}\sin\varphi_i\dot{\varphi}_i + \frac{1}{2}\sin\varphi_k\dot{\varphi}_k \\ 0 \end{bmatrix}. \tag{A.2}$$

Using (A.1) and (A.2) the kinetic energy is

$$T = \sum_{k=1}^{N}\left(\frac{1}{2}m\mathbf{v}_{C_k}^2 + \frac{1}{2}\left(\frac{1}{12}ml^2\right)\dot{\varphi}_k^2\right) = \frac{1}{2}ml^2\sum_{k=1}^{N}\left(\frac{\dot{\varphi}_k^2}{3} + \sum_{j=1}^{k-1}\sum_{i=1}^{k}\cos(\varphi_i - \varphi_j)\dot{\varphi}_i\dot{\varphi}_j\right), \tag{A.3}$$

and the potential energy is

$$U = \sum_{k=1}^{N}mgr_{C_k,y} = mgl\left(\sum_{k=1}^{N}\sum_{i=1}^{k}\cos\varphi_i - \frac{1}{2}\sum_{k=1}^{N}\cos\varphi_k\right). \tag{A.4}$$

From (A.3) and (A.4) we obtain the matrix elements (3.40) and (3.41) by

$$\begin{aligned} m_{\alpha\beta} &= \frac{\partial^2 T}{\partial\dot{\varphi}_\alpha\dot{\varphi}_\beta}(\varphi_i = 0, \dot{\varphi}_i = 0), \\ s_{\alpha\beta} &= \frac{\partial^2 U}{\partial\varphi_\alpha\varphi_\beta}(\varphi_i = 0, \dot{\varphi}_i = 0). \end{aligned} \tag{A.5}$$

A.2 Jacobian matrices and determinants

The Jacobian matrix of (5.7) with respect to k_p, k_d, ω_1 can be given as

$$\tilde{\mathbf{J}}_1 = \begin{bmatrix} 1 & 0 & 0 \\ \cos(\tau_\mathrm{p}\omega_1) & \omega_1^\mu \cos(\frac{\mu\pi}{2} - \tau_\mathrm{d}\omega_1) & \frac{\partial \mathrm{Re}D(\mathrm{i}\omega_1)}{\partial\omega_1} \\ -\sin(\tau_\mathrm{p}\omega_1) & \omega_1^\mu \sin(\frac{\mu\pi}{2} - \tau_\mathrm{d}\omega_1) & \frac{\partial \mathrm{Im}D(\mathrm{i}\omega_1)}{\partial\omega_1} \end{bmatrix}, \tag{A.6}$$

where

$$\begin{aligned} \frac{\partial \mathrm{Re}D(\mathrm{i}\omega_1)}{\partial\omega_1} =& -2\omega_1 - k_\mathrm{p}\tau_\mathrm{p}\sin\left(\tau_\mathrm{p}\omega_1\right) + k_\mathrm{d}\mu\omega_1^{\mu-1}\cos\left(\frac{\mu\pi}{2} - \tau_\mathrm{d}\omega_1\right) \\ &+ k_\mathrm{d}\tau_\mathrm{d}\omega_1^\mu \sin\left(\frac{\mu\pi}{2} - \tau_\mathrm{d}\omega_1\right), \end{aligned} \tag{A.7}$$

$$\begin{aligned} \frac{\partial \mathrm{Im}D(\mathrm{i}\omega_1)}{\partial\omega_1} =& -k_\mathrm{p}\tau_\mathrm{p}\cos\left(\tau_\mathrm{p}\omega_1\right) - k_\mathrm{d}\tau_\mathrm{d}\omega_1^\mu\cos\left(\frac{\mu\pi}{2} - \tau_\mathrm{d}\omega_1\right) \\ &+ k_\mathrm{d}\mu\omega_1^{\mu-1}\sin\left(\frac{\mu\pi}{2} - \tau_\mathrm{d}\omega_1\right). \end{aligned} \tag{A.8}$$

Taking the determinant of (A.6) gives

$$\det(\tilde{\mathbf{J}}_1) = -\omega_1^\mu\left(k_\mathrm{p}\tau_\mathrm{p}\cos\left(\frac{\mu\pi}{2} + \omega_1\left(\tau_\mathrm{p} - \tau_\mathrm{d}\right)\right) + k_\mathrm{d}\omega_1^\mu\tau_\mathrm{d} - 2\omega_1\sin\left(\frac{\mu\pi}{2} - \omega_1\tau_\mathrm{d}\right)\right). \tag{A.9}$$

By setting $\tau_\mathrm{p} = \tau_\mathrm{d} = \tau$, we obtain $\det(\mathbf{J}_1)$ from (A.9) as

$$\det(\mathbf{J}_1) = -\omega_1^\mu\left(k_\mathrm{p}\tau\cos\left(\frac{\mu\pi}{2}\right) + k_\mathrm{d}\omega_1^\mu\tau - 2\omega_1\sin\left(\frac{\mu\pi}{2} - \omega_1\tau\right)\right). \tag{A.10}$$

Determinants $\det(\tilde{\mathbf{J}}_2)$ and $\det(\mathbf{J}_2)$ can be derived similarly.

A.3 Inverted pendulum on a cart: equation of motion

The inverted pendulum on a cart is shown in Figure 6.1. The position and the velocity of the center of mass of the pendulum are

$$\mathbf{r}_C = \begin{bmatrix} x + \frac{l}{2}\sin\varphi \\ \frac{l}{2}\cos\varphi \\ 0 \end{bmatrix}, \tag{A.11}$$

$$\mathbf{v}_C = \begin{bmatrix} \dot{x} + \frac{l}{2}\dot{\varphi}\cos\varphi \\ -\frac{l}{2}\dot{\varphi}\sin\varphi \\ 0 \end{bmatrix}. \tag{A.12}$$

Using equations (A.11)–(A.12), the kinetic energy

$$\begin{aligned} T &= \frac{1}{2}m\mathbf{v}_C^2 + \frac{1}{2}J_C\dot{\varphi}^2 + \frac{1}{2}m_\mathrm{c}\dot{x}^2 \\ &= \frac{1}{2}m\left(\frac{l^2}{4}\dot{\varphi}^2 + l\dot{\varphi}\dot{x}\cos\varphi + \dot{x}^2\right) + \frac{1}{2}\frac{1}{12}ml^2\dot{\varphi}^2 + \frac{1}{2}m_\mathrm{c}\dot{x}^2 \\ &= \frac{1}{6}ml^2\dot{\varphi}^2 + \frac{1}{2}ml\dot{\varphi}\dot{x}\cos\varphi + \frac{1}{2}\left(m + m_\mathrm{c}\right)\dot{x}^2 \end{aligned} \tag{A.13}$$

and the potential energy

$$U = mgr_{C,y} = mg\frac{l}{2}\cos\varphi \tag{A.14}$$

can be calculated. Then, equations (6.2)–(6.3) can be obtained using Lagrange's equations of the second kind.

Bibliography

[1] T. J. Anastasio. The fractional-order dynamics of brainstem vestibulo-oculomotor neurons. *Biological Cybernetics*, 72(1):69–79, 1994.

[2] F. M. Atay. Balancing the inverted pendulum using position feedback. *Applied Mathematics Letters*, 12(5):51–56, 1999.

[3] T. Balogh, I. Boussaada, T. Insperger, and S.-I. Niculescu. Conditions for stabilizability of time-delay systems with real-rooted plant. *International Journal of Robust and Nonlinear Control*, 32(6):3206–3224, 2022.

[4] T. Balogh and T. Insperger. Extending the limits of stabilizability of systems with feedback delay via fractional-order PD controllers. *IFAC-PapersOnLine*, 51(14):265–270, 2018.

[5] T. Balogh and T. Insperger. Inverz inga stabilizálása tört rendű késleltetett PD szabályozóval. In *XXVI. Nemzetközi Gépészeti Konferencia, Marosvásárhely, Románia, 2018. 04. 26-29.*, pages 31–34, 2018.

[6] T. Balogh and T. Insperger. Semi-discretization for fractional-order feedback systems with input delay. *IFAC-PapersOnLine*, 55(36):198–203, 2022.

[7] T. Balogh and T. Insperger. Extending the admissible control-loop delays for the inverted pendulum by fractional-order proportional-derivative controller. *Journal of Vibration and Control*, pages 1–9, published online in 2023.

[8] T. Balogh, T. Insperger, I. Boussaada, and S.-I. Niculescu. Towards an MID-based delayed design for arbitrary-order dynamical systems with a mechanical application. *IFAC-PapersOnLine*, 53(2):4375–4380, 2020.

[9] T. Balogh, B. A. Kovacs, and T. Insperger. Human performance in virtual stabilization of a fractional-order system with reaction delay. *Journal of the Royal Society Interface*, pages 1–13, accepted in 2024.

[10] T. Balogh, B. Varszegi, and T. Insperger. On the admissible control-loop delay for the inverted pendulum subject to detuned PDA feedback. *Journal of Sound and Vibration*, 529:116898, 2022.

[11] S. Bazzi, J. Ebert, N. Hogan, and D. Sternad. Stability and predictability in human control of complex objects. *Chaos: An Interdisciplinary Journal of Nonlinear Science*, 28(10):103103, 2018.

[12] C. Bonnet and J. R. Partington. Analysis of fractional delay systems of retarded and neutral type. *Automatica*, 38(7):1133–1138, 2002.

[13] R. Bormann, J.-L. Cabrera, J. G. Milton, and C. W. Eurich. Visuomotor tracking on a computer screen—an experimental paradigm to study the dynamics of motor control. *Neurocomputing*, 58–60:517–523, 2004.

[14] J. Boulet, R. Balasubramaniam, A. Daffertshofer, and A. Longtin. Stochastic two-delay differential model of delayed visual feedback effects on postural dynamics. *Philosophical Transactions of the Royal Society A: Mathematical, Physical and Engineering Sciences*, 368(1911):423–438, 2010.

[15] I. Boussaada, G. Mazanti, S.-I. Niculescu, J. Huynh, F. Sim, and M. Thomas. Partial pole placement via delay action: a Python software for delayed feedback stabilizing design. In *Proceedings of the 24th International Conference on System Theory, Control and Computing*, pages 196–201, Sinaia, Romania, 2020.

[16] I. Boussaada and S.-I. Niculescu. Characterizing the codimension of zero singularities for time-delay systems: a link with Vandermonde and Birkhoff incidence matrices. *Acta Applicandae Mathematicae*, 145:47–88, 2016.

[17] I. Boussaada and S.-I. Niculescu. On the dominancy of multiple spectral values for time-delay systems with applications. *IFAC-PapersOnLine*, 51(14):55–60, 2018.

[18] I. Boussaada, S.-I. Niculescu, A. El-Ati, R. Pérez-Ramos, and K. Trabelsi. Multiplicity-induced-dominancy in parametric second-order delay differential equations: analysis and application in control design. *ESAIM: Control, Optimisation and Calculus of Variations*, 26:57, 2020.

[19] I. Boussaada, S.-I. Niculescu, and K. Trabelsi. Towards a decay rate assignment based design for time-delay systems with multiple spectral values. In *Proceedings*

of the 23rd International Symposium on Mathematical Theory of Networks and Systems, pages 864–871, Hong Kong, China, 2018.

[20] I. Boussaada, S. Tliba, S.-I. Niculescu, H. U. Ünal, and T. Vyhlídal. Further remarks on the effect of multiple spectral values on the dynamics of time-delay systems. Application to the control of a mechanical system. *Linear Algebra and its Applications*, 542:589–604, 2018.

[21] I. Boussaada, H. U. Ünal, and S.-I. Niculescu. Multiplicity and stable varieties of time-delay systems: a missing link. In *Proceedings of the 22nd International Symposium on Mathematical Theory of Networks and Systems*, pages 188–194, Minneapolis, MN, USA, 2016.

[22] D. Breda, S. Maset, and R. Vermiglio. *Stability of linear delay differential equations: A numerical approach with MATLAB*. Springer, 2014.

[23] J. V. Burke, A. S. Lewis, and M. L. Overton. A robust gradient sampling algorithm for nonsmooth, nonconvex optimization. *SIAM Journal on Optimization*, 15(3):751–779, 2005.

[24] G. Buza, J. Milton, L. Bencsik, and T. Insperger. Establishing metrics and control laws for the learning process: ball and beam balancing. *Biological Cybernetics*, 114(1):83–93, 2020.

[25] J. L. Cabrera, R. Bormann, C. Eurich, T. Ohira, and J. Milton. State-dependent noise and human balance control. *Fluctuation and Noise Letters*, 4(1):L107–L117, 2004.

[26] J. L. Cabrera and J. G. Milton. On-off intermittency in a human balancing task. *Physical Review Letters*, 89(15):158702, 2002.

[27] J. Čermák, Z. Došlá, and T. Kisela. Fractional differential equations with a constant delay: stability and asymptotics of solutions. *Applied Mathematics and Computation*, 298:336–350, 2017.

[28] J. Čermák and T. Kisela. Oscillatory and asymptotic properties of fractional delay differential equations. *Electronic Journal of Differential Equations*, 2019(33):1–15, 2019.

[29] J. Čermák and T. Kisela. Stabilization and destabilization of fractional oscillators via a delayed feedback control. *Communications in Nonlinear Science and Numerical Simulation*, 117:106960, 2023.

[30] J. R. Chagdes, S. Rietdyk, M. H. Jeffrey, N. Z. Howard, and A. Raman. Dynamic stability of a human standing on a balance board. *Journal of Biomechanics*, 46(15):2593–2602, 2013.

[31] Y.-C. Cheng and C. Hwang. Stabilization of unstable first-order time-delay systems using fractional-order PD controllers. *Journal of the Chinese Institute of Engineers*, 29(2):241–249, 2006.

[32] K. L. Cooke and P. van den Driessche. On zeroes of some transcendental equations. *Funkcialaj Ekvacioj*, 29(1):77–90, 1986.

[33] K. Diethelm. *The analysis of fractional differential equations: An application-oriented exposition using differential operators of Caputo type*. Springer, 2010.

[34] C. W. Eurich and J. G. Milton. Noise-induced transitions in human postural sway. *Physical Review E*, 54(6):6681–6684, 1996.

[35] D. K. Faddeev and I. S. Sominskii. *Problems in higher algebra*. W. H. Freeman, 1965.

[36] S. Franklin, J. Česonis, R. Leib, and D. W. Franklin. Feedback delay changes the control of an inverted pendulum. In *Proceedings of the 41st Annual International Conference of the IEEE Engineering in Medicine and Biology Society*, pages 1517–1520, Berlin, Germany, 2019.

[37] P. Freitas and P. Lancaster. On the optimal value of the spectral abscissa for a system of linear oscillators. *SIAM Journal on Matrix Analysis and Applications*, 21(1):195–208, 1999.

[38] P. Gawthrop, K.-Y. Lee, M. Halaki, and N. O'Dwyer. Human stick balancing: an intermittent control explanation. *Biological Cybernetics*, 107(6):637–652, 2013.

[39] G. Habib, A. Miklós, E. T. Enikov, G. Stépán, and G. Rega. Nonlinear model-based parameter estimation and stability analysis of an aero-pendulum subject to digital delayed control. *International Journal of Dynamics and Control*, 5(3):629–643, 2017.

[40] J. K. Hale. *Theory of functional differential equations*. Springer, 1977.

[41] J. K. Hale and S. M. V. Lunel. Strong stabilization of neutral functional differential equations. *IMA Journal of Mathematical Control and Information*, 19(1–2):5–23, 2002.

[42] B. D. Hassard. Counting roots of the characteristic equation for linear delay-differential systems. *Journal of Differential Equations*, 136(2):222–235, 1997.

[43] N. D. Hayes. Roots of the transcendental equation associated with a certain difference-differential equation. *Journal of the London Mathematical Society*, s1-25(3):226–232, 1950.

[44] R. A. Horn and C. R. Johnson. *Matrix analysis*. Cambridge University Press, 2012.

[45] H. Hu and Z. Wang. Stability analysis of damped SDOF systems with two time delays in state feedback. *Journal of Sound and Vibration*, 214(2):213–225, 1998.

[46] H. Hu and Z. Wang. *Dynamics of controlled mechanical systems with delayed feedback*. Springer, 2002.

[47] T. Insperger and J. Milton. Sensory uncertainty and stick balancing at the fingertip. *Biological Cybernetics*, 108(1):85–101, 2014.

[48] T. Insperger and J. Milton. *Delay and uncertainty in human balancing tasks*. Springer, 2021.

[49] T. Insperger, J. Milton, and G. Stepan. Acceleration feedback improves balancing against reflex delay. *Journal of the Royal Society Interface*, 10(79):20120763, 2013.

[50] T. Insperger and G. Stépán. Semi-discretization method for delayed systems. *International Journal for Numerical Methods in Engineering*, 55(5):503–518, 2002.

[51] T. Insperger and G. Stépán. *Semi-discretization for time-delay systems: Stability and engineering applications*. Springer, 2011.

[52] M. I. Jordan. Computational aspects of motor control and motor learning. In H. Heuer and S. W. Keele, editors, *Motor skills*, volume 2 of *Handbook of Perception and Action*, pages 71–120. Academic Press, New York, 1996.

[53] V. L. Kharitonov, S.-I. Niculescu, J. Moreno, and W. Michiels. Static output feedback stabilization: necessary conditions for multiple delay controllers. *IEEE Transactions on Automatic Control*, 50(1):82–86, 2005.

[54] M. Kidd and G. Stepan. Delayed control of an elastic beam. *International Journal of Dynamics and Control*, 2(1):68–76, 2014.

[55] V. B. Kolmanovskii and V. R. Nosov. *Stability of functional differential equations*. Academic Press, 1986.

[56] B. A. Kovacs and T. Insperger. Comparison of pixel-based position input and direct acceleration input for virtual stick balancing tests. *Periodica Polytechnica Mechanical Engineering*, 64(2):120–127, 2020.

[57] B. A. Kovacs and T. Insperger. Critical parameters for the robust stabilization of the inverted pendulum with reaction delay: state feedback versus predictor feedback. *International Journal of Robust and Nonlinear Control*, 32(18):9710–9722, 2022.

[58] B. A. Kovacs and T. Insperger. Virtual stick balancing: skill development in Newtonian and Aristotelian dynamics. *Journal of the Royal Society Interface*, 19(188):20210854, 2022.

[59] B. A. Kovacs, J. Milton, and T. Insperger. Virtual stick balancing: sensorimotor uncertainties related to angular displacement and velocity. *Royal Society Open Science*, 6(11):191006, 2019.

[60] R. M. Lewis, V. Torczon, and M. W. Trosset. Direct search methods: then and now. *Journal of Computational and Applied Mathematics*, 124(1–2):191–207, 2000.

[61] Y. Li, W. S. Levine, and G. E. Loeb. A two-joint human posture control model with realistic neural delays. *IEEE Transactions on Neural Systems and Rehabilitation Engineering*, 20(5):738–748, 2012.

[62] Y. Liu, R. Leib, and D. W. Franklin. Follow the force: haptic communication enhances coordination in physical human-robot interaction when humans are followers. *IEEE Robotics and Automation Letters*, 8(10):6459–6466, 2023.

[63] D. B. Lockhart and L. H. Ting. Optimal sensorimotor transformations for balance. *Nature Neuroscience*, 10(10):1329–1336, 2007.

[64] G. E. Loeb. Optimal isn't good enough. *Biological Cybernetics*, 106(11–12):757–765, 2012.

[65] G. E. Loeb, I. E. Brown, and E. J. Cheng. A hierarchical foundation for models of sensorimotor control. *Experimental Brain Research*, 126(1):1–18, 1999.

[66] A. Longtin and J. G. Milton. Modelling autonomous oscillations in the human pupil light reflex using non-linear delay-differential equations. *Bulletin of Mathematical Biology*, 51(5):605–624, 1989.

[67] D. Ma and J. Chen. Delay margin of low-order systems achievable by PID controllers. *IEEE Transactions on Automatic Control*, 64(5):1958–1973, 2018.

[68] M. C. Mackey and L. Glass. Oscillation and chaos in physiological control systems. *Science*, 197(4300):287–289, 1977.

[69] D. Matignon. Stability results for fractional differential equations with applications to control processing. In *Proceedings of the IMACS Multiconference on Computational Engineering in Systems Applications*, volume 2, pages 963–968, Lille, France, 1996.

[70] C. Maurer and R. J. Peterka. A new interpretation of spontaneous sway measures based on a simple model of human postural control. *Journal of Neurophysiology*, 93(1):189–200, 2005.

[71] G. Mazanti, I. Boussaada, S.-I. Niculescu, and Y. Chitour. Effects of roots of maximal multiplicity on the stability of some classes of delay differential-algebraic systems: the lossless propagation case. *IFAC-PapersOnLine*, 54(9):764–769, 2021.

[72] B. Mehta and S. Schaal. Forward models in visuomotor control. *Journal of Neurophysiology*, 88(2):942–953, 2002.

[73] E. M. A. M. Mendes, G. H. O. Salgado, and L. A. Aguirre. Numerical solution of Caputo fractional differential equations with infinity memory effect at initial condition. *Communications in Nonlinear Science and Numerical Simulation*, 69:237–247, 2019.

[74] F. Merrikh-Bayat. General formula for stability testing of linear systems with fractional-delay characteristic equation. *Central European Journal of Physics*, 11(6):855–862, 2013.

[75] W. Michiels and S.-I. Niculescu. *Stability and stabilization of time-delay systems: An eigenvalue-based approach*. Society for Industrial and Applied Mathematics, Philadelphia, 2007.

[76] W. Michiels, S.-I. Niculescu, and I. Boussaada. A complete characterization of minima of the spectral abscissa and rightmost roots of second-order systems with input delay. *IMA Journal of Mathematical Control and Information*, 40(3):403–428, 2023.

[77] J. Milton, J. L. Cabrera, T. Ohira, S. Tajima, Y. Tonosaki, C. W. Eurich, and S. A. Campbell. The time-delayed inverted pendulum: implications for human balance control. *Chaos: An Interdisciplinary Journal of Nonlinear Science*, 19(2):026110, 2009.

[78] J. Milton and T. Insperger. Acting together, destabilizing influences can stabilize human balance. *Philosophical Transactions of the Royal Society A: Mathematical, Physical and Engineering Sciences*, 377(2153):20180126, 2019.

[79] J. Milton, R. Meyer, M. Zhvanetsky, S. Ridge, and T. Insperger. Control at stability's edge minimizes energetic costs: expert stick balancing. *Journal of the Royal Society Interface*, 13(119):20160212, 2016.

[80] C. A. Molnar, T. Balogh, I. Boussaada, and T. Insperger. Calculation of the critical delay for the double inverted pendulum. *Journal of Vibration and Control*, 27(3–4):356–364, 2021.

[81] C. A. Molnar, A. Zelei, and T. Insperger. Estimation of human reaction time delay during balancing on balance board. In *Proceedings of the 13th IASTED International Conference on Biomedical Engineering*, pages 176–180, Innsbruck, Austria, 2017.

[82] C. A. Monje, Y. Chen, B. M. Vinagre, D. Xue, and V. Feliu-Batlle. *Fractional-order systems and controls: Fundamentals and applications*. Springer, 2010.

[83] P. Morasso, A. Cherif, and J. Zenzeri. Quiet standing: the single inverted pendulum model is not so bad after all. *PLoS ONE*, 14(3):e0213870, 2019.

[84] J. Moreno. An extension of Lucas theorem to entire functions. *IFAC Proceedings Volumes*, 31(19):141–145, 1998.

[85] D. J. Nagy, J. G. Milton, and T. Insperger. Controlling stick balancing on a linear track: delayed state feedback or delay-compensating predictor feedback? *Biological Cybernetics*, 117(1–2):113–127, 2023.

[86] J. I. Neimark. D-decomposition of the space of quasi-polynomials (On the stability of linearized distributive systems). *Prikladnaya Matematika i Mekhanika*, 13(4):349–380, 1949.

[87] P. M. Nia and R. Sipahi. Controller design for delay-independent stability of linear time-invariant vibration systems with multiple delays. *Journal of Sound and Vibration*, 332(14):3589–3604, 2013.

[88] I. Podlubny. *Fractional differential equations*. Academic Press, San Diego, 1999.

[89] I. Podlubny, R. L. Magin, and I. Trymorush. Niels Henrik Abel and the birth of fractional calculus. *Fractional Calculus and Applied Analysis*, 20(5):1068–1075, 2017.

[90] G. Pólya and G. Szegő. *Problems and theorems in analysis I: Series, integral calculus, theory of functions*. Springer, 1972.

[91] G. Pólya and G. Szegő. *Problems and theorems in analysis II: Theory of functions, zeros, polynomials, determinants, number theory, geometry*. Springer, 1976.

[92] Z. Qi, Q. Shi, and H. Zhang. Tuning of digital PID controllers using particle swarm optimization algorithm for a CAN-based DC motor subject to stochastic delays. *IEEE Transactions on Industrial Electronics*, 67(7):5637–5646, 2020.

[93] Z.-C. Qin, X. Li, S. Zhong, and J.-Q. Sun. Control experiments on time-delayed dynamical systems. *Journal of Vibration and Control*, 20(6):827–837, 2014.

[94] R. S. Razavian, M. Sadeghi, S. Bazzi, R. Nayeem, and D. Sternad. Body mechanics, optimality, and sensory feedback in the human control of complex objects. *Neural Computation*, 35(5):853–895, 2023.

[95] I. T. Rekanos and T. V. Yioultsis. Approximation of Grünwald–Letnikov fractional derivative for FDTD modeling of Cole–Cole media. *IEEE Transactions on Magnetics*, 50(2):181–184, 2014.

[96] F. Riewe. Nonconservative Lagrangian and Hamiltonian mechanics. *Physical Review E*, 53(2):1890–1899, 1996.

[97] F. Schürer. Zur Theorie des Balancierens. *Mathematische Nachrichten*, 1(5):295–331, 1948.

[98] J. Sieber and B. Krauskopf. Bifurcation analysis of an inverted pendulum with delayed feedback control near a triple-zero eigenvalue singularity. *Nonlinearity*, 17(1):85–103, 2004.

[99] J. Sieber and B. Krauskopf. Extending the permissible control loop latency for the controlled inverted pendulum. *Dynamical Systems*, 20(2):189–199, 2005.

[100] R. Sipahi, S.-I. Niculescu, C. T. Abdallah, W. Michiels, and K. Gu. Stability and stabilization of systems with time delay. *IEEE Control Systems Magazine*, 31(1):38–65, 2011.

[101] G. Stépán. *Retarded dynamical systems: Stability and characteristic functions*. Longman, Harlow, 1989.

[102] G. Stepan. Delay effects in the human sensory system during balancing. *Philosophical Transactions of the Royal Society A: Mathematical, Physical and Engineering Sciences*, 367(1891):1195–1212, 2009.

[103] Y. Suzuki, T. Nomura, M. Casadio, and P. Morasso. Intermittent control with ankle, hip, and mixed strategies during quiet standing: a theoretical proposal based on a double inverted pendulum model. *Journal of Theoretical Biology*, 310:55–79, 2012.

[104] E. Todorov and M. I. Jordan. Optimal feedback control as a theory of motor coordination. *Nature Neuroscience*, 5(11):1226–1235, 2002.

[105] F. J. Valero-Cuevas. *Fundamentals of neuromechanics*. Springer, 2016.

[106] F. J. Valero-Cuevas, H. Hoffmann, M. U. Kurse, J. J. Kutch, and E. A. Theodorou. Computational models for neuromuscular function. *IEEE Reviews in Biomedical Engineering*, 2:110–135, 2009.

[107] G. U. Varieschi. Applications of fractional calculus to Newtonian mechanics. *Journal of Applied Mathematics and Physics*, 6(6):1247–1257, 2018.

[108] P. L. Várkonyi. Neutrally floating objects of density 1/2 in three dimensions. *Studies in Applied Mathematics*, 130(3):295–315, 2013.

[109] R. Vrabel. A note on the matrix determinant lemma. *International Journal of Pure and Applied Mathematics*, 111(4):643–646, 2016.

[110] T. Vyhlídal, D. Pilbauer, B. Alikoç, and W. Michiels. Analysis and design aspects of delayed resonator absorber with position, velocity or acceleration feedback. *Journal of Sound and Vibration*, 459:114831, 2019.

[111] K. Walton and J. E. Marshall. Direct method for TDS stability analysis. *IEE Proceedings D (Control Theory and Applications)*, 134(2):101–107, 1987.

[112] Z. Wang, M. Du, and M. Shi. Stability test of fractional-delay systems via integration. *Science China Physics, Mechanics and Astronomy*, 54(10):1839–1846, 2011.

[113] Z. Wang and Q. Xu. Sway reduction of a pendulum on a movable support using a delayed proportional-derivative or derivative-acceleration feedback. *Procedia IUTAM*, 22:176–183, 2017.

[114] T. D. J. Welch and L. H. Ting. A feedback model reproduces muscle activity during human postural responses to support-surface translations. *Journal of Neurophysiology*, 99(2):1032–1038, 2008.

[115] Q. Xu, G. Stepan, and Z. Wang. Delay-dependent stability analysis by using delay-independent integral evaluation. *Automatica*, 70:153–157, 2016.

[116] Q. Xu, G. Stépán, and Z. Wang. Balancing a wheeled inverted pendulum with a single accelerometer in the presence of time delay. *Journal of Vibration and Control*, 23(4):604–614, 2017.

[117] Q. Xu and Z. Wang. Exact stability test of neutral delay differential equations via a rough estimation of the testing integral. *International Journal of Dynamics and Control*, 2(2):154–163, 2014.

[118] N. Yoshikawa, Y. Suzuki, K. Kiyono, and T. Nomura. Intermittent feedback-control strategy for stabilizing inverted pendulum on manually controlled cart as analogy to human stick balancing. *Frontiers in Computational Neuroscience*, 10:34, 2016.

[119] A. Zelei, B. Krauskopf, P. T. Piiroinen, and T. Insperger. Stable periodic motion of a controlled segmented leg model of pedal locomotion with inelastic ground-foot collision. *Nonlinear Dynamics*, 97(3):1945–1958, 2019.

[120] L. Zhang and G. Stepan. Exact stability chart of an elastic beam subjected to delayed feedback. *Journal of Sound and Vibration*, 367:219–232, 2016.

[121] L. Zhang, G. Stepan, and T. Insperger. Saturation limits the contribution of acceleration feedback to balancing against reaction delay. *Journal of the Royal Society Interface*, 15(138):20170771, 2018.